ANL-7763

TECHNIQUES AND ANALYSES OF FAST-REACTOR NEUTRON SPECTROSCOPY WITH PROTON-RECOIL PROPORTIONAL COUNTERS

E. F. Bennett and T. J. Yule

U of C-AUA-USAEC

ARGONNE NATIONAL LABORATORY, ARGONNE, ILLINOIS

The facilities of Argonne National Laboratory are owned by the United States Government. Under the terms of a contract (W-31-109-Eng-38) between the U. S. Atomic Energy Commission, Argonne Universities Association and The University of Chicago, the University employs the staff and operates the Laboratory in accordance with policies and programs formulated, approved and reviewed by the Association.

MEMBERS OF ARGONNE UNIVERSITIES ASSOCIATION

The University of Arizona
Carnegie-Mellon University
Case Western Reserve University
The University of Chicago
University of Cincinnati
Illinois Institute of Technology
University of Illinois
Indiana University
Iowa State University
The University of Iowa
Kansas State University
The University of Kansas
Loyola University
Marquette University
Michigan State University
The University of Michigan
University of Minnesota
University of Missouri
Northwestern University
University of Notre Dame
The Ohio State University
Ohio University
The Pennsylvania State University
Purdue University
Saint Louis University
Southern Illinois University
The University of Texas at Austin
Washington University
Wayne State University
The University of Wisconsin

Printed in the United States of America
Available from
National Technical Information Service
U.S. Department of Commerce
5285 Port Royal Road
Springfield, Virginia 22151
Price: Printed Copy $3.00; Microfiche $0.95

ANL-7763
Mathematics and Computers

ARGONNE NATIONAL LABORATORY
9700 South Cass Avenue
Argonne, Illinois 60439

TECHNIQUES AND ANALYSES OF FAST-REACTOR NEUTRON SPECTROSCOPY WITH PROTON-RECOIL PROPORTIONAL COUNTERS

by

E. F. Bennett and T. J. Yule

Applied Physics Division

August 1971

TABLE OF CONTENTS

TABLE OF CONTENTS

LIST OF FIGURES

LIST OF FIGURES

LIST OF TABLES

TECHNIQUES AND ANALYSES OF FAST-REACTOR NEUTRON SPECTROSCOPY WITH PROTON-RECOIL PROPORTIONAL COUNTERS

by

E. F. Bennett and T. J. Yule

ABSTRACT

Techniques and analyses are described for fast-neutron spectroscopy with proton-recoil proportional counters. Small, nonperturbing cylindrical counters filled with hydrogen or methane are used in an isotropic flux environment to measure degraded fission spectra in the energy range from 1 keV to 2 MeV. Electronic pulse-shape discrimination distinguishes between gamma-ray induced events and proton recoils. Correction schemes are employed that remove systematic errors inherent in this method of neutron spectroscopy. Sources of error are the nonlinear relationship between energy and ionization at low energies, wall-and-end distortion at higher energies, and distortion of internal field lines at the ends of the counter. The extent of these corrections is assessed for a representative fast-reactor spectrum.

I. INTRODUCTION

The special character of neutron-proton scattering below 10 MeV, together with other favorable circumstances, makes it possible to build simple spectrometers with extended energy response for measurement of degraded fission-type neutron spectra [1–3]. Neutron-proton scattering has a large, well-known elastic scattering cross section, which is isotropic below 10 MeV and initiates no reactions in the energy range of interest [4]. These characteristics of n-p scattering permit one to relate in a simple manner the proton-recoil spectrum D(E), to the neutron spectrum $\phi(E)$:

$$\phi(E) = -\frac{1}{NT}\frac{E}{\sigma(E)}\frac{dD(E)}{dE}, \qquad (1)$$

where $\sigma(E)$ is the n-p scattering cross section and NT is the product of the hydrogen atom number in the effective counter volume by the time duration of the measurement.

It is fortunate that hydrogen gas is a suitable proportional-counter filling. In proportional counters the gas multiplication process is almost noiseless and with care to minimize space-charge saturation is linear. One can produce a pulse proportional to ionization, even for a single ion pair created in the gas [5]. Thus, even low-energy elastically scattered proton recoils can be detected with good resolution. Moreover, the ratio between energy loss and ionization, W, is remarkably insensitive to the proton energy for protons stopping in hydrogen gas. The onset of any detectable W variation is well below 10 keV, and no more than about a 10% change in W occurs down to 1 keV [6]. Thus, it is straightforward to relate the proton-recoil ionization to energy over an extensive energy range.

The physical bases for proton recoil spectrometers, both in gaseous electronics and in an understanding of features of n-p scattering, have been well known for a long time [7]. Initial applications of this method were directed toward use of proportional counters as flux monitors. The work of Ref. 8, for example, describes studies of the response of counters to monoenergetic neutrons and compares this response to a calculated one which takes into account wall-and-end distortion.

It is hardly surprising that these detectors have been of limited value in accelerator experiments—the inherent time jitter is too large (>50 nsec) to be satisfactory for timing purposes. Also, it is difficult to make an efficient detector, since the maximum pressure is limited by contaminants in the gas and high-voltage requirements.

Another obstacle to the use of proton-recoil counters as neutron spectrometers can be traced to the limitations of available electronics prior to the introduction of computers. Classical pulse-height analyzers available since the early 1950's were most effectively used with a reaction that linearly relates neutron energy to pulse height, such as the familiar ^{3}He(n,p)t reaction [9]. Here, a pulse-height spectrum leads directly to the neutron spectrum. The proton-recoil reaction, on the other hand, requires that the measured result be differentiated. This is easily accomplished with a computer but cumbersome to perform "long hand." Probably, more than any other factor, the introduction of computers has made it feasible to consider proton-recoil proportional counters for certain neutron-spectroscopy applications with due allowance for inherent limitations in these counters.

The early applications of proton-recoil proportional counters to neutron spectroscopy had a limited low-energy range. Gamma fluxes, which invariably accompany neutrons, introduce sufficient ionization in the lower-energy region to mask clear identification of the proton-recoil distribution in this range. The initial approach to the problem of gamma-induced background was to reduce gas pressure. As the pressure is decreased, the maximum ionization a fast electron can create as it traverses the counter decreases. Recoil protons of ionization above this limit can be safely counted. The difficulty with the extension of this approach to very low energies is that a reduction to pressures too low to be practical for proportional counting occurs. (Stable detection at high gain requires a minimal ultraviolet quenching cross section and therefore an adequate gas pressure.) The practical energy limit for low-pressure hydrogen counters used for neutron spectroscopy appears to be about 20 keV. In addition to loss of response at low energies, low-pressure counters with little stopping power will also be severely limited at high energy by wall-and-end effects in which proton-recoil events with substantial range leave the effective counting volume before stopping. The simple relationship between proton energy and ionization breaks down. Pulse-shape discrimination, in which events of low and high specific ionization are recognized electronically and separated, affords a way of distinguishing proton-recoil events from gamma-induced, fast-electron events without compromising pressure [10]. The technique is simple. Low-energy proton-recoil tracks with small spatial extension induce a pulse whose initial rate of rise is substantially greater than that for a track of large spatial extension which contains the same total number of ion pairs. An example of this shape-discrimination effect is seen in Fig. 1. The distribution shown is of the ratio of initial rise to fully integrated amplitude for proton recoils and gamma-induced electron events that create the same given ionization. That part of the distribution shown to the left, which was produced by fast electron pulses with low rate of rise, is clearly separable from that part of the distribution to the right, which was produced by proton-recoil pulses with high rate of rise. The distribution from a pure gamma source is also shown in Fig. 1 and it, of course, does not exhibit the fast-rising component.

In any radiation environment in which all the ionizing events can be counted and the relative number of gamma-induced events to neutron-induced events is not inordinately high, shape discrimination can be used to extend the low-energy response to a kilovolt or less. Equally important, the best results are obtained by operating a counter of given size at as high a gas pressure as is consistent with good

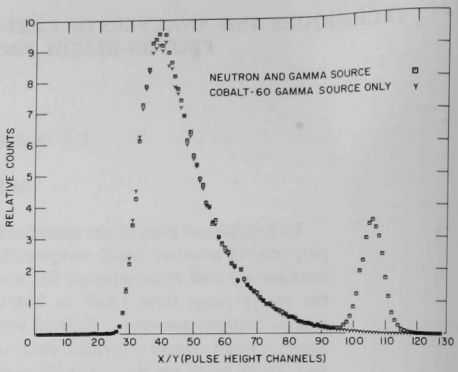

Fig. 1. Specific Ionization Spectrum Illustrating Gamma-Neutron Shape Discrimination in Proportional Counter. ANL Neg. No. 113-16.

energy resolution. This follows since the gamma sensitivity is proportional to the counter wall-and-end area, whereas neutron sensitivity is proportional to the pressure. Not only is the neutron-to-gamma ratio improved at higher pressures, but the onset of wall-and-end truncation is deferred.

While a hydrogen-gas-filled counter with gamma-ray discrimination works well down to low energies of the order of 1 keV, its useful high-energy limit is a few hundred keV. It is necessary to use a gas filling with higher stopping power to extend the energy range to a few MeV. Methane is used to obtain increased containment. More complicated hydrocarbon gases liquify at too low a pressure to be useful. Methane counters using gamma-ray discrimination have a low-energy limit of about 100 keV, below which carbon recoils from elastic scattering of neutrons on carbon compromise the usefulness of methane as a filling gas.

Both the hydrogen-filled and methane-filled counters contain a small amount of nitrogen gas, which permits energy calibration. Placing the counters in a thermal flux and observing the 585-keV protons from the $^{14}N(n,p)^{14}C$ reaction permit an absolute relationship between pulse height and proton energy to be established.

An attractive feature of the technique of using proton-recoil counters for neutron spectroscopy is flexibility in size and efficiency. Where circumstances permit, cylinders of large length and diameter may be used to increase efficiency. On the other hand, rather small detectors work quite well; a 1-cm-dia hydrogen-filled counter has been used for in-core neutron spectroscopy. The structural material required is minimal, and the macroscopic scattering of the whole detector can easily be reduced to the point where no significant perturbation of an incident neutron flux occurs.

II. DETECTORS

A. CONSTRUCTION

Figure 2 shows the construction details of the hydrogen- and methane-filled detectors used for in-core spectroscopy measurements. The methane-filled detector is the larger one. Detector bodies are of thin-walled stainless steel and anodes are of fine stainless steel wire. Field tubes are used to define the sensitive volume of the detector. The detectors shown in Fig. 2 are rather small with a correspondingly short internal effective length. It is somewhat easier to build larger detectors. They permit better separation between gamma-induced events and proton recoils and reduced influence of distortion introduced by the end regions. Detectors with diameters as large as 5 cm and with effective lengths as long as several meters have been used for some special tests and measurements [11]. Some of the intermediate-size detectors are described in later sections, where tests made with these detectors are discussed. The smaller detectors are, however, necessary for compatibility with the requirements of counting inside large plutonium-fueled fast reactors. Invariably, spontaneous fission neutrons from ^{240}Pu in the fuel will provide a high-neutron-flux environment inside the cores, even for far subcritical operation. To approach reasonably near ($k > 0.98$) critical and still maintain the total event rate within acceptable limits (less than 20,000 counts per second), small chambers must be used. A buffer gas cannot be used to desensitize the counters, since the neutron-to-gamma ratio would then become unacceptable.

Both detectors shown in Fig. 2 were filled to as high a pressure as possible before the resolution began to worsen from electron capture by contaminants in the gas—notably oxygen and water vapor. Using tank methane and hydrogen without provision for baking or for cold traps, about 10 atm of predominantly hydrogen gas could be put in the smaller counter and about 8 atm of predominantly methane gas in the larger counter before the resolution exceeded 10%. Note that, to first approximation, if the gain is kept constant, the resolution is unchanged for a given product of pressure times counter diameter. Since the figure of merit for containment of recoils is proportional to this product, going to larger counters will not significantly change the high-energy limit.

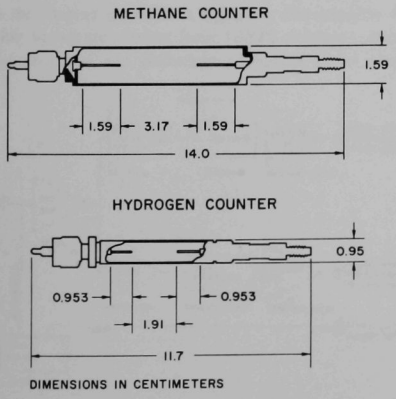

Fig. 2. Proton-recoil Proportional Counters for Use in Fast Reactors. Anodes are 9 μ in radius, and the field tubes 64 μ in radius. ANL Neg. No. 116-28.

B. OPERATING RANGE

Proper operation of proportional counters is only attained at intermediate values of gas multiplication. Ionization created in an end region over field tubes may contribute events of significant amplitude relative to events over the normal anode unless the multiplication over the anode is substantially greater than unity. The acceptable value of multiplication depends upon the spectrum of events and the energy region under observation. It is usually not desirable to operate at an anode gas multiplication much less than about 10; the field tube must be sufficiently larger than the anode to preclude any multiplication upon it over the working voltage range.

Space-charge saturation, on the other hand, will preclude an excessively high multiplication since the attendant nonlinear relationship between ionization and energy degrades the quality of spectra. The onset of nonlinearities relating to space charge is not easily recognized and conservative operating multiplication limits for a given type of detector should be established before its use. One sensitive method of testing is by observation of spectra following successive complementary changes in voltage (gas gain) and amplifier gain—these altered so as to maintain a fixed energy region under surveillance. (Methods of determining the gas gain are considered in Sec. V.) Ordinarily it will not be possible to operate at gas gains sufficiently high that electronics noise will be completely negligible, and a high premium must be placed on low-noise preamplifiers for proportional counter spectroscopy. Thus, in practice, one has a limited range of suitable gas multiplications for viewing a particular proton-recoil energy range. Table I contains the voltage settings with the corresponding gas gains and ionization per channel used in a typical measurement of the proton-recoil distribution from 0.5 keV to 3 MeV. Data are only used from channel 29 to channel 128, which is full scale. Below channel 29 broadening by electronic noise becomes comparable to counter resolution and gamma discrimination becomes more difficult. Data are only taken to about 150 keV with the hydrogen counter. Problems associated with the use of a hydrogen counter

TABLE I. Voltage, Gas Gain, and Ionization per Channel Used in Measuring Proton-recoil Distributions from About 0.5 keV to 3 MeV

Voltage	Gas Gain	Ionization/Channel, keV/channel
3250-Methane	0.893E 01	0.237E 02
3550	0.172E 02	0.123E 02
3750	0.285E 02	0.372E 01
3350-Hydrogen	0.326E 02	0.130E 01
3650	0.868E 02	0.488E 00
3950	0.254E 03	0.167E 00
4250	0.804E 03	0.527E-01
4500	0.224E 04	0.189E-01

when the track length becomes long introduce this rather low high-energy limit (see Sec. V). Gamma discrimination is used for all the hydrogen-filled-counter voltage settings and for the highest methane-filled-counter setting.

C. REDUCTION OF BACKGROUND ELECTRON RESPONSE

A counter set to view the low-energy region of the proton-recoil distribution responds readily to fast electrons traversing the tube. If pulse-shape discrimination against electron background is to be successful, the relative number of proton-recoil events to fast-electron events must be favorable. Measurements near alpha emitters may have an especially high background, independent of the neutron level. Alpha decay in fertile and fissile isotopes will produce a very strong photon and electron component resulting from deexcitation of decay-product nuclei and probably to a lesser extent from ionization during stopping of the alpha particles. Most of this component is readily absorbed in the material itself, but a substantial surface emission will nevertheless exist.

To estimate the magnitude of this background a simple shielding experiment was done. Successively thicker sleeves of gold or lead were wrapped around a stainless steel hydrogen-filled counter with 0.4-mm walls. The counter was placed in a block of depleted uranium and set to register all events in excess of 0.5 keV. The results are shown in Table II. By interpolation, it is seen that only 0.25 mm of lead will significantly reduce this background. Lead shielding, to this extent, will have no observable effect on the neutron spectrum and is recommended in any experience in which chambers are placed near uranium or plutonium metal.

TABLE II. Effectiveness of Various Shielding in Reducing Background Electron Response

Shielding	Detection Rate, counts/min	Shielding	Detection Rate, counts/min
None	333,000	0.10-mm lead	53,000
0.05-mm gold	97,000	0.5-mm lead	44,000

III. ELECTRONICS SYSTEM

A. AMPLIFIER SYSTEM

One problem immediately encountered in measuring neutron spectra with proportional counters is that the electronics system must operate satisfactorily under severe amplifier overloads. When the proton spectra are being recorded in the low-keV range with the counter voltage set at high gas multiplication, protons with several MeV of energy are creating large overloads. These overloads should not be allowed to cause saturation in the preamplifier and should be handled appropriately by the slow ionization amplifier, such that at moderate count rates undistorted spectra can be obtained.

A block diagram of the amplifier system is shown in Fig. 3. The preamplifier, besides not saturating under heavy overloads, must have a moderately fast rise time and low noise. A rise time less than 15 nsec is adequate, since diffusion of the electron bunch makes using time constants of less than 20 nsec meaningless, even for a fast gas like methane. At shorter time constants, the separation of proton-recoils and gamma-induced electrons does not improve, while the resolution of the peaks worsens because of increased noise. A charge-sensitive preamplifier specifically designed for proton-recoil proportional counting is used [12,13]. The preamplifier may be operated with gas amplifications greater than 3000 without saturating. The output pulse from this preamplifier decays with a single time constant of 250 μsec.

The slow side of the amplifier system, which produces a pulse whose height is proportional to the ionization, consists of a pole-zero-compensated linear amplifier, a base-line restorer, and an inverter amplifier. Preamplifier noise dominates the noise in the slow channel; the noise from the shaping amplifier is negligible. The amplifier must be able to rapidly recover from 1000X overloads. Because of the shape of the collection profile, it is not obvious whether using unipolar or bipolar pulse shaping is superior in high-count-rate applications. The shape of the pulse for a point event is given by [14]

$$P(t) = -\frac{e}{C} \ln \left[\frac{2VKt}{a^2 \ln (b/a)} + 1 \right], \qquad (2)$$

until $P = -e/C$, at which time all charge is collected. Here, e is the charge of the electron, C the input capacitance of the counter-preamplifier combination, V the voltage on the counter, K the positive-ion mobility, and a and b the radii of the anode and cathode, respectively. A sketch of the pulse profile is shown in Fig. 4A. The slow component of the pulse persists until positive ion collection. The time scale is chosen so that one unit corresponds to complete collection. For a hydrogen-filled counter, complete collection can take several milliseconds. Using reasonable time constants of a few microseconds in the amplifier, a sizable pedestal results for large overloads with unipolar pulse shaping, as shown in Fig. 4B. This pedestal may be

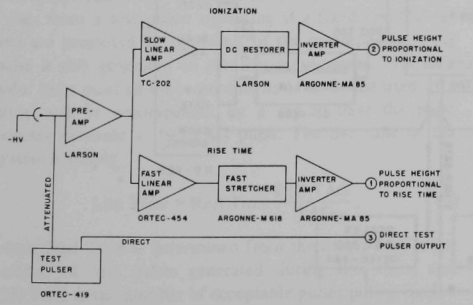

Fig. 3. Block Diagram of Amplifier System Used for Neutron Spectroscopy with Proton-recoil Proportional Counters. ANL Neg. No. 116-316.

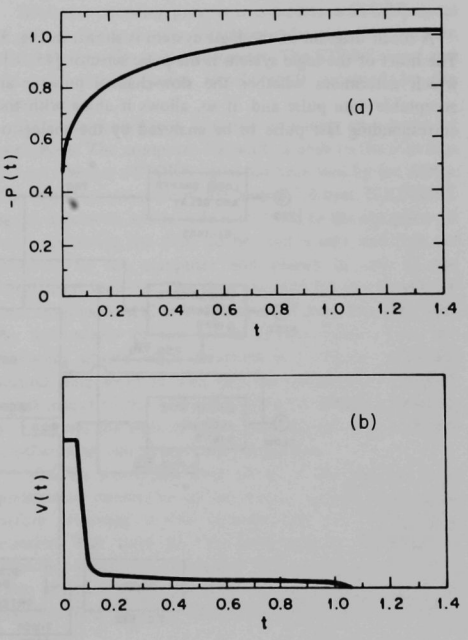

Fig. 4. Pulse Profiles. (a) Pulse profile at input of preamplifier; (b) overload profile at output of slow amplifier without pole zero correction for undershoot. ANL Neg. No. 116-315 Rev. 1.

removed, so that reasonable count-rate capability can be obtained, by using the pole-zero correction adjusted so that a slight negative undershoot is observed that just exceeds the amplitude of the pedestal [13]. The pulse is then restored by using a fast-restoring base-line restorer. In the bipolar mode, the pedestal is strongly attenuated and the dc restorer is not used. For both the unipolar and the bipolar mode, time constants of 2.4 μsec are used. The inverter amplifier inverts the pulse and for the bipolar pulses clips the second node to be compatible with the pulse selector and linear gate, which are described in Sec. B below.

The fast side of the amplifier system, which produces a pulse whose height is proportional to the rise time of the pulse from the preamplifier, consists of a fast linear amplifier, a fast stretcher, and an inverter amplifier. The fast-amplifier system must have pulse-shaping constants in the 20- to 100-nsec range for proton-recoil spectroscopy. A fast amplifier with RC integration and differentiation is used for fast-pulse shaping. The amplifier was designed for timing with Ge(Li) detectors, surface barrier detectors, or photomultipliers. The pulse stretcher and inverter condition the pulse for the linear gate.

B. LOGIC SYSTEM

A block diagram of the logic system is shown in Fig. 5. The heart of the logic system is the pulse selector [15,16], which determines whether the slow-channel pulse is an acceptable data pulse and, if so, allows it along with the corresponding fast pulse to be analyzed by the analog-to-digital converters (ADCs). A number of requirements must be met before the pulse is regarded as acceptable. The pulse must be within a window set by an upper-level and a lower-level discriminator. The ADC-computer combination must not be busy. The pulse must be a data pulse and not a pulser pulse. Pulser pulses are used for live timing. The timer must be on. The base line must have been down for a set period of time. This function is performed by a base-line discriminator and a paralysis circuit. For a given pulse or combination of overlapping pulses, the length of time the base-line discriminator is exceeded is determined. This time may be referred to as the pulse width. The pulse selector will deem unacceptable any pulse that comes within a preset number of pulse widths of a previous pulse. The preset number of dead widths may be 1, 2, or 3. The logic outputs from the pulse selector are: one that indicates that the base-line discriminator has been exceeded–BLD; one that indicates the pulse is an acceptable data pulse–PSO.$\overline{\text{TAG}}$; and one that indicates that the pulse is an acceptable pulser pulse–PSO.TAG. An acceptable pulser pulse must meet all the requirements that an acceptable data pulse must meet. A test pulser pulse is distinguished from a data pulse at the pulse selector by a coincident tag pulse–TAG.

The pulse selector also contains an option for pileup rejection. The pileup rejection circuit differentiates the pulse with a short time constant and checks to see that the zero crossing of the pulse appears at the proper time with respect to the time mark generated by the differentiation.

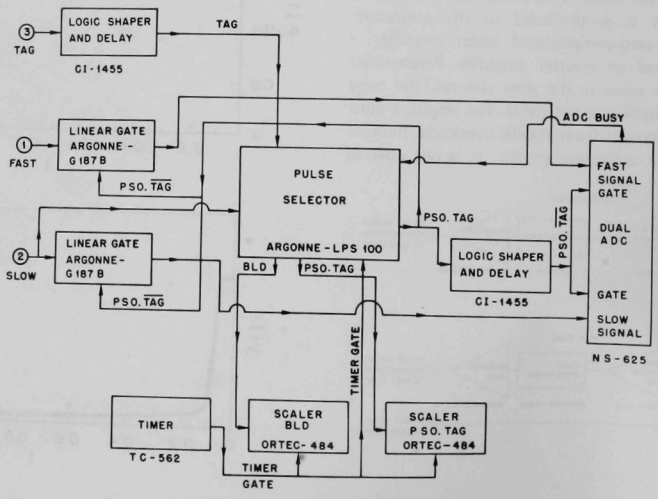

Fig. 5. Block Diagram of Logic System and Data-storage System Used for Neutron Spectroscopy with Proton-recoil Proportional Counters. ANL Neg. No. 116-314.

We have chosen not to use the option in two-parameter analysis for two reasons. First, the two-parameter analysis already contains a fast differentiation, whose magnitude is stored with the pulse height. If a proton pulse is distorted because of pileup, the division of the fast pulse height by the slow pulse height for a given slow pulse height will be such that the event will appear to be a gamma-ray-induced event and not be counted as a proton recoil. Second, the large range of rise times for pulses from a hydrogen counter (where electron drift velocities are low) are such that if the pileup sensor is to be effective for detecting proton-event pileup, some legitimate single gamma-ray-induced events will appear to be pileup events and thus rejected. The shape of the peak of the gamma-ray-induced events will depend on the count rate. An uncertainty results when one makes a background subtraction using background generated at some different count rate, because the backgrounds will not match. There are ways around this problem by employing additional circuits, but unless one wants to increase the count rates far in excess of 20,000 counts/sec, such measures are not called for. However, when gamma-ray discrimination is not being employed, pileup rejection may be effective in limiting distortion. Care must be taken not to set the pileup rejection for too short a pulse width, since even in a fast gas like methane, long track lengths along the diameter have a considerably different rise time than tracks along the axis.

The linear gates delay and stretch the pulses from the slow and fast sides of the system and allow the pulses to be strobed through to the ADCs, only if the appropriate PSO.$\overline{\text{TAG}}$ logic pulses are present. Scalers record BLD and PSO.TAG.

C. COUNTING-LOSS DETERMINATION

Because of the presence of the pulse selector, it is not possible to determine counting losses by simply monitoring the amount of time that the ADC-computer combination is busy [16]. The whole system must be taken into account. Pulses from a test pulser operating at a fixed rate (60 per sec) are presented to the input of the preamplifier. A tag pulse is also generated to identify pulser pulses. The test pulse must meet all the requirements of an undistorted data pulse and be accompanied by a tag to have the pulse selector generate a PSO.TAG pulse. The live time of the system is simply

$$\text{Live Time} = \text{Real Time} \frac{\text{PSO.TAG}}{\text{TAG}}, \qquad (3)$$

where Real Time is determined from the timer, TAG is the number of test pulses generated during this time, and PSO.TAG is the number of acceptable pulser pulses. Such a live-timing system is only suitable for constant count rates [16].

Such a counting-loss determination system may be applied as a rapid method of determining distortion as a function of count rate. In this mode one allows only pulser pulses to be analyzed in the presence of counter-generated pulses. PSO.TAG is used to strobe the linear gates and ADCs instead of PSO.$\overline{\text{TAG}}$. The resulting distribution of pulser pulses indicates the extent of distortion. Results of such tests are considered in Sec. IV.B.

D. STORAGE OF INFORMATION

The ADCs* are interfaced to a Varian Data Machines** 622 computer [17,18]. There are two proton-recoil spectroscopy systems in operation at Argonne, Illinois: one with a discrete-component 622A computer, and one with an integrated-circuit 622/i computer. The computers have an 8k memory and an 18-bit word length and are identical in speed and instruction repertoire.

Analog-to-digital conversion is performed at a 40 MHz digitizing rate. Both the fast and slow pulses are converted to 512 channels. Analyzer dead time per event is approximately 3 + 0.025N μsec, where N is the channel number of the larger analyzed input. Once encoding begins until a RESET signal is received, the ADCs present a BUSY signal to the pulse selector.

After the encoding process is complete, a STORE signal is sent to the computer interface, indicating that data are ready for transfer to the computer. The STORE signal and the two nine-bit codes remain until accepted by the computer.

Data are transferred into the computer in a series of operations. The computer transmits a code to the interface to test whether a STORE signal has been sent by the ADCs. The time for one cycle in the loop is 7.8 μsec. If a STORE signal is present, a true code is returned to the computer. A code containing the ADC to be read is sent, and data are returned to the computer and placed in one of the operational registers. The time required for the transfer of data from each ADC to a register is 3.8 μsec. The total time for the transfer of two words to two registers from the beginning of the sense operation is 11.2 μsec. After the second data word is read into the computer, a RESET signal is sent to the ADCs to remove the STORE command and to reset the address scalers and all logic circuits so that another input can be accepted for analysis.

After the words have been placed in the registers, some preliminary operations are performed and the data stored before returning to the sensing cycle for further data transfer. The ratio of the fast-to-slow pulse height is formed, i.e., the radial specific ionization of the event. This ratio is scaled to 32 channels, and the ionization data are scaled to 100 channels. Checks are made that the ratio and

*Northern Scientific Model NS-625, Northern Scientific, 2551 West Beltine, P.O. Box 66, Middleton, Wisconsin.

**Varian Data Machines, 2722 Michelson Drive, Irvine, California.

ionization are within preset bounds. The data are then stored in a 100 × 32-channel array. The time required for the preliminary data reduction and storage is approximately 110 μsec.

The stored array may be output from the computer in a number of ways. For a given ionization, one may display counts versus specific radial ionization on an oscilloscope. Figure 6 contains a representation of such an output. The region at high values of the specific radial ionization corresponds to proton-recoil events and at low values to electrons. The whole array may be punched on paper tape or printed on a teletype.

Some data reduction and analysis can also be performed with the computer. The analysis and corresponding codes are discussed later. As is evident from Fig. 6, the distribution of gamma-ray events is quite broad and thus some form of background subtraction is necessary. The shape of the spectrum may be approximated by out-of-reactor gamma fields. Using a suitable gamma background, corrections can be made for the projection of the gamma-ray-induced event tail under the proton-recoil peak. For a given voltage the integrated proton-recoil number is determined and printed or punched for each of the 100 energy channels.

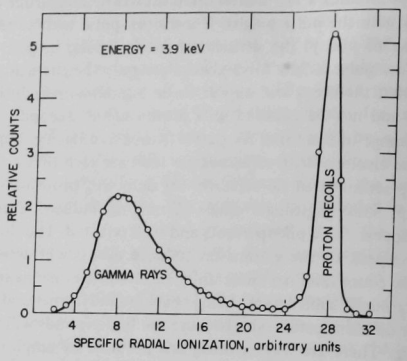

Fig. 6. Typical Specific Ionization Spectrum. ANL Neg. No. 113-848 Rev. 1.

IV. TESTING THE ELECTRONICS SYSTEM

A. STATIC TESTS OF SYSTEM

Certain static tests were made of the system to test the integral and differential linearity of the system. The integral linearity was checked by varying the pulse height from a test pulser. The differential linearity was checked by using a ramp generator as the voltage reference for the test pulser. Although a system may show the proper degree of differential and integral linearity under the static condition, tests must also be performed with various count-rate and overload conditions.

B. DYNAMIC TEST-PULSER TEST OF SYSTEM

The count-rate capability of the system was checked using the test pulser method described in Sec. A above. A 2.54-cm-dia counter with a 16.5-cm sensitive length filled with 5.4 atm of predominantly hydrogen gas was placed 13 cm from the graphite-uranium interface of the Snell block [19]. The spectrum in this position is quite hard, and the long sensitive length of the counter means that proton recoils of several MeV can be stopped in the counter. The counter was operated at 4400 V, which corresponds to a gas gain of about 3300. The electronics were such that full-scale ionization would be a few keV. This represents about the most unfavorable condition with respect to severe overloads. The undistorted pulse-height distribution, i.e., no voltage on the counter, is shown in Fig. 7. The effect of various pulse-shaping and dead-width combinations at a dead-time-corrected, base-line-discriminator rate of 22,000 counts/sec are shown in Figs. 8-11. Note that the ordinate is a logarithmic scale. The cleanest peak is obtained with unipolar shaping using the base-line restorer and a dead-width setting of 3 pulse widths, as shown in Fig. 8. Figure 9 indicates that when the dead-width setting is reduced to 1, unacceptable distortion occurs. There is some fast undershoot associated with the large overloads that the base line restorer is not able to smooth out. Figure 10 indicates the effect of using bipolar pulse shaping and a dead-width setting of 3. The pulse width is that associated with only the first node of the bipolar pulse. The amount of distortion is acceptable—only about 3% of the counts fall in channels less than 90 and greater than 100. Figure 11 shows the effect of using unipolar pulse shaping and a dead-width setting of 2. When unipolar pulse shaping and bipolar pulse shaping are compared, it is most useful to consider Figs. 10 and 11. The pulse width times the dead-width settings are approximately equal for the two cases—only the width of the first node is taken for the bipolar pulse. It is seen that unipolar shaping produces slightly less of a low-energy tail, whereas there is no difference in the high-energy tails. For a given live time, the unipolar and bipolar modes are almost equivalent.

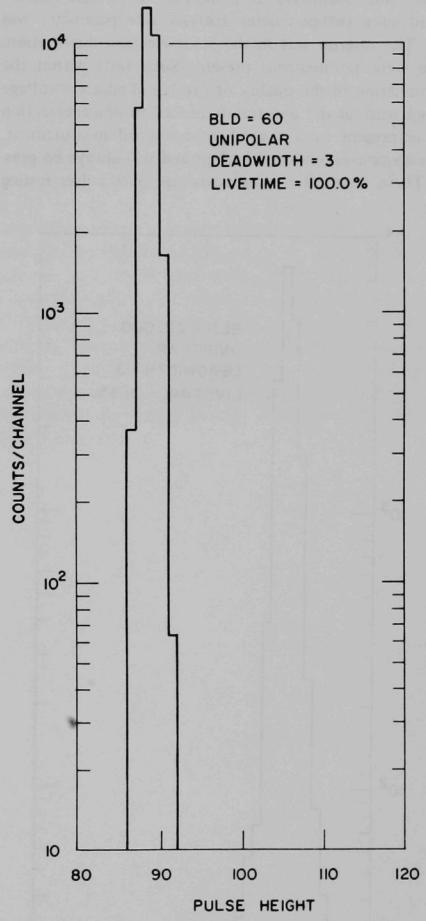

Fig. 7. Pulser Pulse-height Spectrum Using Unipolar Pulse Shaping and a Preset Dead Width of 3 with Zero Counter Voltage. ANL Neg. No. 116-310.

The system was also checked for differential linearity in the various modes by using a ramp generator as the voltage reference for the test pulser. The 2.54-cm-dia hydrogen counter at 4400 V was used.

C. GAMMA-SPECTRUM TESTING OF SYSTEM

Tests of the electronic system were also made by looking at the recoil electrons from the wall of the counter when a

cesium gamma source was placed near the counter. Various voltage and count-rate combinations were investigated. Instead of a two-parameter analysis, one parameter was used. The interest was in the recoil-electron distribution. There were no neutrons present. Such tests permit the determination of the quality of overlap of adjacent voltage settings without the uncertainty of background subtraction that is present in a typical proton-recoil measurement, where gamma-ray-induced background will always be present. These tests offer some advantage over pulser testing

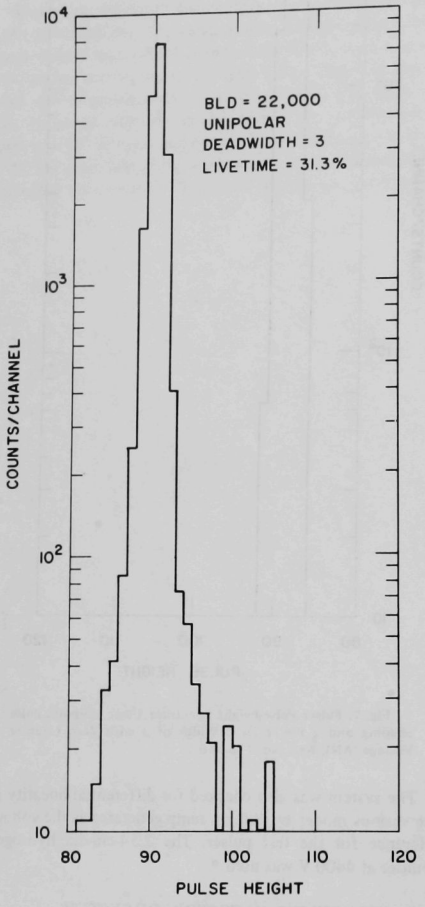

Fig. 8. Pulser Pulse-height Spectrum Using Unipolar Pulse Shaping and a Preset Dead Width of 3 in the Presence of 22,000 counts/sec from a Hydrogen-filled Counter. ANL Neg. No. 116-312.

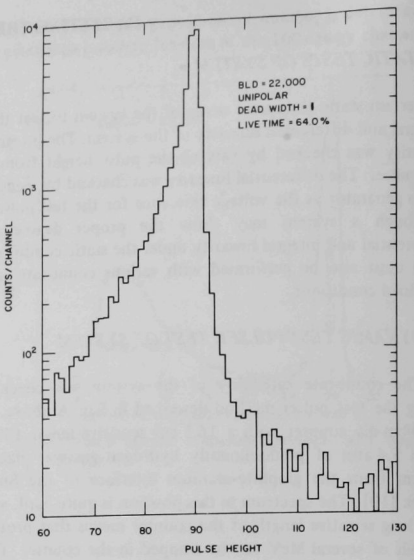

Fig. 9. Pulser Pulse-height Spectrum Using Unipolar Pulse Shaping and a Preset Dead Width of 1 in the Presence of 22,000 counts/sec from a Hydrogen-filled Counter. ANL Neg. No. 116-309.

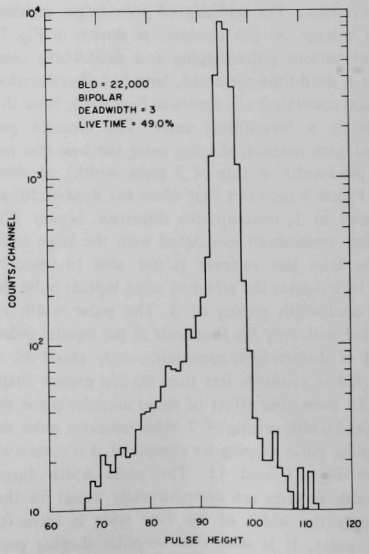

Fig. 10. Pulser Pulse-height Spectrum Using Bipolar Pulse Shaping and a Preset Dead Width of 3 in the Presence of 22,000 counts/sec from a Hydrogen-filled Counter. ANL Neg. No. 116-311.

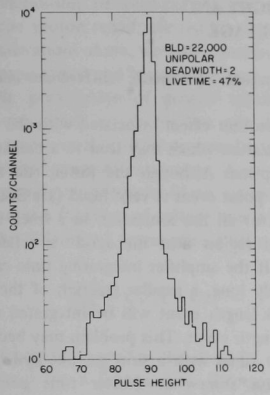

Fig. 11. Pulser Pulse-height Spectrum Using Unipolar Pulse Shaping and a Preset Dead Width of 2 in the Presence of 22,000 counts/sec from a Hydrogen-filled Counter. ANL Neg. No. 116-313.

because one is looking at legitimate counter pulses with their variety of profiles. However, these tests are dependent on relative calibration data for the various voltages. (The accuracy of calibration data are discussed in Sec. V below.) Good overlap was realized for the various voltages in the tests, indicating that probably no systematic errors were being overlooked.

An undue emphasis may appear to have been placed in detailing the types and quality of the tests performed. Nevertheless, the tests proved essential in determining the quality of the electronic system. About two years ago a solid-state, voltage-sensitive preamplifier passed all the static tests described above, as well as the dynamic tests with the test pulser. However, all data taken with this preamplifier showed differences of a few percent in overlap of data taken at different voltages. Only after careful tests with the gamma-spectrum method were made could the overlap difficulty be attributed to a small differential nonlinearity for proportional-counter pulse profiles. The preamplifier was subsequently replaced with the one described above.

V. RELATIONSHIP BETWEEN PULSE HEIGHT AND IONIZATION AS A FUNCTION OF VOLTAGE

In the next two sections the relationship between pulse height and proton-recoil energy is discussed. The measured distribution is one of a number of events per unit pulse height and must be transformed to one of a number of events per unit energy. If one has an accelerator that can provide monoenergetic neutrons over the full range of interest, it is possible, in principle, to determine the relationship between pulse height and energy. However, if measurements are to be made in the energy region of less than tens of keV, an accelerator cannot provide suitable low-energy neutrons for a determination of this relationship. It is also inconvenient to have to use an accelerator every time there is a change in detector parameters to recalibrate the detector.

The problem of relating pulse height to energy can be meaningfully divided into two parts: the first part of the problem is to determine the relationship between pulse height and ionization created by the proton recoil as a function of voltage; the second part is to determine the relationship between ionization created by the proton recoil and its energy. This division of the problem is attractive because the first part depends on the properties of the counter such as the anode size and pressure, whereas the second part depends only on the intrinsic properties of the gas. In solving the first part of the problem, gas gain as a function of voltage is obtained. Knowledge of this relationship is necessary for the determination of the electric field response functions (see Sec. VII). In this section we consider the first part of the problem.

A. PULSE HEIGHT AND GAS GAIN

It is usually assumed that the pulse height is proportional to the product of ionization created by the proton recoil times the gas gain. If the gas gain as a function of voltage is determined, the first part of the problem is solved. Before methods of determining the gas gain as a function of voltage are outlined, factors that can cause the above assumption to be violated are considered. One such factor is space-charge saturation. If space-charge saturation is occurring, the gas gain will not only be a function of voltage, but also of the amount and distribution of ionization before multiplication. Although gas gain as a function of voltage may be accurately known, the pulse height for a given ionization and voltage is then not predictable. The onset of space-charge effects is rather gradual. An attempt should be made to operate at as low multiplication as electronic noise considerations permit (see Sec. II.B). One can test for space-charge saturation by observing the pulse-height distributions following changes in gas gain and amplifier gain which should preserve the pulse-height distribution. Any significant space-charge effects will induce systematic differences between the distributions.

There is another effect associated with the distribution of initial ionization which may lead to a breakdown in the above assumption. Although the initial rise time of the pulse from a point event is very rapid (see Sec. III.A), the time needed for all the ionization in a track to reach the multiplication region near the anode is reflected in the pulse shape. If the amplifier integrating time constants are not adequately long, a smaller fraction of the pulse from the long-track-length event will be integrated than from a short-track-length event. This problem may become serious for a counter filled with a slow gas like hydrogen. One is forced to use somewhat shorter time constants than desirable if a reasonable count-rate capability is to be maintained. This effect has been seen in the pulse-height distributions from hydrogen counters for events above a few hundred keV—an energy region at which the track length begins to become significant. Data from the hydrogen-filled counter above a few hundred keV are not used in constructing the full proton-recoil distribution. If it is not necessary to count at high rates, or if a gated integrator is used, adequate time constants can be used to eliminate this source of difficulty. This effect became apparent from a systematic bias noted in the energy scale of short-track-length events when the long-track-length protons from the $^{14}N(n,p)^{14}C$ reaction (the use for calibration is described in Sec. B below) was used to determine the energy calibration.

Another effect which can also cause the violation of the above assumption is introduced by excessive amounts of contaminants in the gas. The average distance that an undistorted track—one that has not been truncated by a collision with the walls—has to travel to reach the anode becomes shorter as the track length becomes longer. Long tracks far from the anode are likely to become distorted. The average number of collisions that electrons in long tracks suffer on their way to the anode with electron-attaching contaminants decreases as the track length increases. High-energy recoils will have a higher fraction of their ionization reach the multiplication region than low-energy recoils. In Sec. IX (see Fig. 34), a representative fast-reactor spectrum measured with the methane- and hydrogen-filled counters described previously is compared with a calculated spectrum. The part of the neutron spectrum derived from the methane-filled counter seems to indicate this behavior. The evidence is that neutron spectra measured with better resolution counters, i.e., ones with fewer contaminants, seem to indicate less of a disagreement between the measured and calculated neutron-scattering resonance structure.

Bearing in mind that the above difficulties may destroy

the simple relationship between pulse height and ionization created by the proton recoil inferred from gas-gain-versus-voltage considerations alone, we now consider the relationship between gas gain A and counter voltage.

No simple prescription of general validity has been completely successful in relating gas gain A to counter voltage, although several of those proposed are adequate for use over a limited range of parameters. A prescription that appears to provide an adequate fit to measured values of multiplication as a function of voltage over a larger voltage range than the "Diethorn" prescription [20] is

$$\frac{\log A}{VQ} = C1*V + C2. \qquad (4)$$

The power factor Q, as well as the slope C1 and intercept C2, are derived by a least-squares fitting procedure. A simple program to derive values for Q, C1 and C2 is included in Appendix A. No physical significance whatsoever is attached to the prescription of Eq. 4; it is merely a way of parameterizing (with the use of only three numbers) a measured gain-voltage relationship.

B. PEAK-PULSE-AMPLITUDE CALIBRATION

This section and Sec. C below describes two methods for determining gas gain as a function of voltage. The first method is based on the observation of the shift in the peak pulse amplitude from monoionizating events in the counter gas as a function of voltage. A small amount of nitrogen gas is included in a normal counter-filling mixture. The pulse-height distribution of the $^{14}N(n,p)^{14}C$ reaction on exposure of the counter to thermal neutrons is observed as a function of voltage. The proton has an energy of 585 keV. However, the ionization from the carbon recoil is simultaneously collected with that of the proton. The equivalent energy of the combination, as determined by comparison with accelerator neutrons, is 615 keV with an uncertainty of about 1%. The peak amplitude may be followed up to gas gains at which space-charge effects begin to distort the distribution. The electron collection at this point will usually be in the neighborhood of 10^7 electrons, and one cannot proceed higher. By including a small amount of ^{37}Ar (2.8-keV β emitter), one may extend the calibration to higher voltages before space-charge limitations appear. A sufficient region of voltage overlap using these two sources exists to allow a normalization to be made.

A joint argon-nitrogen calibration over the voltage region from 2800 to 4600 V is listed in Table III. The chamber was filled with a mixture consisting of 0.03 atm of both nitrogen and methane to a total pressure of 5.4 atm of hydrogen. The counter anode and cathode diameters were 0.00254 and 2.54 cm, respectively. Also shown in the table are values for A derived by use of Eq. 4, where values for Q, C1, and C2 were determined by the least-squares fitting procedure described in Appendix A. The simple prescription of Eq. 4 is able to produce accurate gain values over the entire voltage region. Any change in detector design, filling pressure, gas type, etc., would require recalibration which would lead to different values for Q, C1, and C2. If data are available only from the $^{14}N(n,p)^{14}C$ reaction and if the power factor Q is known, the prescription of Eq. 4 will permit an accurate extrapolation to higher voltages. Some extrapolation from nitrogen-based data alone is usually required to provide multiplication values at the higher voltages required for a measurement. For a methane-filled counter, only nitrogen data are required, since the counter is operated at low multiplication.

TABLE III. Measured and Fitted Gain as a Function of Voltage

Voltage	Measured Multiplication[a]	Fitted Multiplication[b]
2800	17.80[c]	17.71
2900	23.15	23.17
3000	30.27	30.58
3100	40.60	40.72
3200	54.58	54.68
3300	74.12	74.05
3400	102.2	101.1
3500	140.5	139.2
3600	197.1	193.3
3700	271.4	270.5
3800	380.0	381.5
3850	457.3	454.5
3900	541.1	542.5
3950	644.1	648.7
3800	377.1[d]	381.5
3850	445.8	454.5
3900	537.1	542.5
3950	651.4	648.7
4000	777.1	777.4
4050	937.1	933.3
4100	1135	1123
4150	1371	1353
4200	1649	1634
4300	2418	2397
4400	3547	3542
4500	5300	5273
4600	7835	7910

[a]The argon measurement is normalized to the nitrogen results in the overlap region.
[b]Q = 0.70, slope = 7.442×10^{-6}, intercept = 9.733×10^{-3}.
[c]Start of nitrogen data.
[d]Start of argon data.

C. ELECTROMETER CALIBRATION

The proton-recoil chamber, though designed and optimized for fast-pulse counting, functions as a current chamber without modification. The cathode of the chamber whose calibration by argon and nitrogen pulse counting is listed in Table III was connected to negative high voltage. The anode was connected directly to an electrometer, whose output drove a voltage-to-frequency converter which could be scaled over known time intervals. A thick cadmium sheet was wrapped around the chamber, which

was then placed in a well-thermalized neutron flux. Capture gammas from the cadmium induced substantial current in the chamber. To determine the gas gain, the amplitude of this current was followed as a function of voltage. To make certain that space-charge effects were small, the electrometer output was also followed as a function of pile power at the maximum voltage used (4600 V) in the calibration. The point of onset of nonlinearity indicated the tolerable limit for pile power, and the measurement of chamber current versus voltage was made well below this limit. No absolute multiplication values can be obtained by this method, since the source intensity is unknown.

The ratio of calibration by electrometer current to that from argon and nitrogen counting is plotted against voltage in Fig. 12. The ratio is not independent of voltage, as one would expect, but decreases as voltage increases. The reason for this is found in the fact that the true detector-response function changes with increasing voltage due to the electric field effect (see Sec. VII). The mean value of the calculated response function decreased by about 5% from the bottom to the top of the voltage range. This caused a corresponding decrease in the output current. The effect is considerably less significant when the peak amplitude of a monoionizing particle distribution is used, since in determining the peak

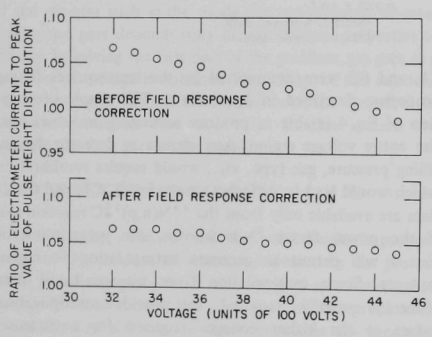

Fig. 12. Effect of Internal Fields upon Multiplication Calibration. ANL Neg. No. 116-169 Rev. 1.

value one automatically biases the distribution towards those events occurring in the midchamber region where the electric field is strongest. Also plotted in Fig. 12 is the ratio of calibration after the electrometer result was divided by the mean value of the response-function distribution at each voltage. The ratio changes very little after the correction has been made. The electrometer method serves as a cross-check of the peak-amplitude method. Systematic errors introduced by collection time effects or track orientation would be uncovered.

In summary, if care is taken to avoid factors that destroy the assumed proportionality between pulse height and the product of ionization created by the proton recoil times gas gain, the distribution per unit ionization, dN/dI, is readily constructed from the distribution per unit pulse height, dN/dP. The relationship between the distributions is

$$\frac{dN}{dI} = \frac{dN}{dP}\frac{dP}{dI}. \qquad (5)$$

The above assumption states that dP/dI is a constant for each voltage. The constant is determined from the relationship of gas gain to voltage. Space-charge effects, short time constants, or an excessive number of contaminants will cause dP/dI to be a function of I. This relationship would have to be determined before the ionization distribution could be constructed.

The calibration of gas-multiplication change with voltage may be done conveniently either by observing the change in the peak amplitude of a monoionizing source with voltage or by following the increase of the direct-current chamber output with voltage in response to any high-level (spatially uniform) ionizing source. Absolute multiplication values are difficult to measure and not necessary when an appropriate proton source such as is produced by the $^{14}N(n,p)^{14}C$ reaction is available. The relationship of pulse height to ionization to voltage is fixed at the calibration point. Direct-current calibration must be corrected for the change with voltage of the detector response function due to electric-field effects, and when this is done one may expect that the results of either method of calibration will agree.

VI. VARIATION OF W WITH ENERGY

The ionization-scale calibration of counters may be conveniently determined as indicated in the previous section. The number of events per unit ionization is determined as a function of ionization, and if W is known the density of events per unit energy is given by

$$dN/dE = (dN/dI)/W. \quad (6)$$

It is necessary to have the proton distributions per unit energy to determine the neutron spectrum.

The remarkable thing about W is that it varies so slightly with energy, especially for noble gases and hydrogen. The ionization mechanisms operating to produce free electrons at the expense of an energy loss by a fast proton are markedly different at different energies. Theories valid for proton velocities much greater than orbital electron velocities, such as the Bethe-Block formulation, are not correct for protons in the kilovolt energy region [21]. Phenomena such as charge exchange occur with high probability, and a kilovolt proton actually spends a considerable fraction of its time in an uncharged state. With due regard to the considerable theoretical and experimental effort that has gone into the problem of W determination, no results currently exist that are entirely adequate for proton-recoil neutron spectroscopy [22].

Many measurements are of the integral-energy-versus-ionization variety and are not sufficiently precise for differential dE/dI analysis [1,23]. Also, a filling gas most useful for high-gain proportional counters would normally require some additives, for instance, methane for quenching and nitrogen for calibration in predominantly hydrogen-filled counters. These additives may only occur at low partial pressure, but their effect could be significant nonetheless [22].

To be useful for neutron spectroscopy, W must be known precisely at all energies below the energy of interest in the measurement. Not only is it necessary to divide ionization density by W to produce proton-energy-density spectra (Eq. 6), but the energy assigned to any ionization value I is obtained by the integral

$$E = E_{th} + \int_0^I W(I)\, dI, \quad (7)$$

where E_{th} is a threshold energy below which ionization is energetically impossible. Knowledge of W at higher energies only is insufficient to allow the evaluation of Eq. 7. Measurements of W inevitably terminate at some finite energy and associated ionization values (here denoted by EL and BI), and if W is known only in excess of these values, Eq. 7 may be modified to read

$$E = EL + \int_{BI}^I W(I)\, dI. \quad (8)$$

A minimum understanding of the energy-ionization relationship for spectroscopy requires that W be known in excess of an energy and ionization (both also known) that form a lower bound to the range of experimental interest.

A. MEASUREMENTS

The most recent direct observation of W for protons in hydrogen at energies as low as 1 keV are from experiments using a lead slowing-down spectrometer [6]. These are difficult experiments to perform, and only limited accuracy can be obtained, but an interesting variation in W was observed in which W decreased in value as energy decreased in the region of a few keV. W must ultimately increase with further decreasing energy, and the initial decrease is an indication of competition between the several processes responsible for ionization at these energies.

Reference 6 also mentions the better agreement with calculation achieved using the observed W variation when applied to neutron-spectrum measurements. That proton-recoil distributions measured in certain neutron flux spectra may be quite sensitive to the W variation is clear from Eq. 6. If the neutron spectrum is hard to the extent that very little of the actual flux exists below a few kilovolts, the proton-recoil distribution per unit energy is flat. Any observed variation in this distribution will, in the absence of other effects, such as field-response distortion, directly reflect a variation in W. A selection of proton-recoil data from hard neutron spectra were analyzed to elucidate this trend in W more clearly. These were spectra measured in a predominantly uranium metal environment with no light material for moderation [19]. Theory predicts lack of any significant flux below about 5 keV, and the variation of W shown in Fig. 13 was arrived at by comparing the residual

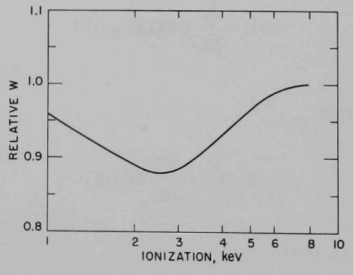

Fig. 13. Variation of W with Energy for Protons in Hydrogen Gas. ANL Neg. No. 116-26.

curvature of proton spectra after making a correction for electric-field-response effects. These results were found to be in reasonable agreement with those reported in Ref. 6 above about 2 keV and also clearly showed the downward trend in W as energy decreases. Unfortunately, neither the analysis reported here nor that in Ref. 6 contains any meaningful data below about 2 keV. The upturn in Fig. 13 is not significant relative to errors in the analysis, which are conservatively estimated as ±3% in relative W between 2 keV and about 8 keV above which the variation appears to cease.

The data relating to W variations in methane are also not sufficiently well known for spectroscopy—this in spite of the fact that most measurements with methane chambers are made above about 100 keV where monoenergetic accelerator neutrons are available for calibration. Again, it is the differential W measured everywhere below a few MeV that is needed. Existing data for methane show a definite curvature in ionization-versus-energy plots [1]. If one does a linear fit to the data from 100 keV to 1 MeV, an intercept at about 4 keV on the energy axis is found.

B. PARAMETERIZATION

To take advantage of the existing evidence relating W to energy, and to provide a framework for improvement as better data become available, it is convenient to introduce an expression relating W to I in parametric form. An expansion of W in powers of log I works well, since the resulting expression can be integrated exactly. In addition, it is reasonable to introduce an ionization TI about which W is constant. This constant may be taken as unity; the absolute value will not matter when calibration is done relative to a known proton energy. TI for hydrogen appears to occur at about 8 keV, and there is no clear experimental evidence for a change in W above this energy. Let the expansion coefficients be designated by CW(J), where J ranges from 1 to 6. W is then given by

$$W(I) = \sum_{J=1}^{6} CW(J)(\log I)^{J-1}. \qquad (9)$$

E is given by

$$E = EL + \int_{BI}^{I} W(I)\, dI \qquad (10)$$

for $I < TI$, and by

$$E = EL + \int_{BI}^{I} W(I)\, dI + I - TI \qquad (11)$$

for $I > TI$.

If Eq. 9 is introduced into Eqs. 10 and 11, the results may be written as

$$E = EL + I \sum_{J=1}^{6} CE(J)(\log I)^{J-1} - BI \sum_{J=1}^{6} CE(J)(\log BI)^{J-1} \qquad (12)$$

for $I < TI$, and

$$E = EL + I - TI + TI \sum_{J=1}^{6} CE(J) \log (TI)^{J-1} - BI \sum CE(J)(\log BI)^{J-1} \qquad (13)$$

for $I > TI$. The coefficients CE in the energy expansion of Eqs. 12 and 13 are obtained from the W expansion coefficients CW according to

$$\left.\begin{aligned} CE(1) &= CW(1) - CW(2) + 2CW(3) - 6CW(4) \\ &\quad + 24CW(5) - 120CW(6); \\ CE(2) &= CW(2) - 2CW(3) + 6CW(4) - 24CW(5) \\ &\quad + 120CW(6); \\ CE(3) &= CW(3) - 3CW(4) + 12CW(5) - 60CW(6); \\ CE(4) &= CW(4) - 4CW(5) + 20CW(6); \\ CE(5) &= CW(5) - 5CW(6); \\ CE(6) &= CW(6). \end{aligned}\right\} \qquad (14)$$

If one defines a parameter BS as

$$BS = BI \sum_{J=1}^{6} CE(J)(\log BI)^{J-1} \qquad (15)$$

and another parameter TS as

$$TS = TI \sum_{J=1}^{6} CE(J)(\log TI)^{J-1}, \qquad (16)$$

the expression relating energy to ionization may be put in the form

$$E = EL - BS + TS - TI + I \qquad (17)$$

for $I > TI$, and

$$E = EL - BS + I \sum_{J=1}^{6} CE(J)(\log I)^{J-1} \qquad (18)$$

for $I < TI$.

The W variation shown in Fig. 13 is consistent with the

following choice of expansion terms: EL = 0.6, BI = 0.5, TI = 8.0, CW(1) = 0.962014, CW(2) = -0.143042, CW(3) = 0.0200147, CW(4) = 0.0515192, CW(5) = 0.0146597, CW(6) = -0.0125811. These coefficients are based upon meager experimental evidence and are only to be considered valid for energies above 2 keV for protons in predominantly hydrogen gas.

An approximation appropriate to methane gas when used above 200 keV is to assume W constant (CW(1) = 1 and all other CW values 0) with an EL of 4.1 and a BI and TI of 0.1. This produces the 4-keV intercept observed in ionization-versus-energy plots over energy values greater than 100 keV.

The numbers provided here for W are to be considered as an improvement over the assumption that it is everywhere constant. They are by no means adequate to the accuracy desired. Neutron spectra with weak amplitude at low energies measured in the presence of a more intense high-energy component may reflect large percentage systematic errors in the absence of an accurately known W variation. Uncertainty in W is probably the factor most strongly limiting the low-energy measurements of spectra, and it is clear that useful spectroscopy will be possible below 1 keV only with some substantially improved data (see Sec. X.B).

VII. THE INTERNAL ELECTRIC FIELD IN CYLINDRICAL PROPORTIONAL COUNTERS

The response function and the sensitive volume of cylindrical proportional counters depends upon the manner in which an effective length is defined. It has been recognized that difficulties arise due to the method of end definition, and some measurements have been made. One of the earliest relevant studies is contained in the familiar text of Rossi and Staub [24], and results of more recent work can be found in Refs. 25 and 26.

Numerous arrangements of electrode structures have been used in the past to define an end over which ionization is not recorded. Reference 25 contains a detailed summary of some of the types of structures, including references to original sources, and no attempt will be made here to cover this material again.

The simplest method of defining an end is by inserting a section of tubing (several times the diameter of the anode) over the anode. The tube extends well inside the counter from the electrical insulation at the extreme end. Tubing and anode are in electrical contact, and the tube also serves as a support for the anode, which may be extremely fragile. This simple end design is the most widely used, and counters of small size are as readily assembled as are larger ones. A defect in counters built in this way is associated with the transition region near the tip, where field strengths at the anode surface are weakening (ultimately to a value too low to cause multiplication). If the transition were rapid, multiplication would be reduced over an axial distance too short to be of significance (assuming negligible axial broadening of the electron pulse). In practice, and even with a minimal increase of diameter in the end region, multiplication decreases gradually. This produces a low-energy tail on the distribution of monoionizing events, causes the active volume to differ from the mechanical one, and degrades the instrument for spectroscopy.

Counters with large length-to-diameter ratios are correspondingly less disturbed by tip-effect problems; the transition region is relatively less significant as the anode length increases for a fixed tube diameter. If the particular counting application permits a large diameter, the addition of an intermediate-potential field tube may be feasible, and this will also improve the electrical characteristics. Counters with the intermediate-potential structure are difficult to construct in diameters less than about 5 cm, and this is unacceptably large for some applications, including in-reactor neutron spectroscopy.

A detailed theoretical study of the effect of a particular end-electrode structure upon the response function of proportional counters was not feasible before the availability of computers. The problem is the familiar one of solving Laplace's equation for boundary configurations not reducible to an easily managed form. Straightforward numerical methods have been widely used for similar problems and are applicable here as well [27].

A. DESCRIPTION OF A NUMERICAL SOLUTION

Figure 14 is a schematic diagram of the "simple" end, consisting of a concentric field tube (of several anode radii) and maintained at anode potential. Some electric field lines have also been included. The drawing is not to scale; in practice, the cathode-to-anode ratio may easily be 1000 while the field-tube-to-anode ratio may be 10 or so. The field-tube radius must be sufficiently greater than the anode radius to reduce gas multiplication to a negligible value over its entire length.

The response function of a detector is altered from the ideal by the complex behavior of field lines near the tip discontinuity. The field in the immediate vicinity of the anode (where gas multiplication occurs) shifts continuously from values too low to cause multiplication to an asymptotic value achieved at a distance of about 1.5 cathode radii from the discontinuity. The asymptotic value of the electric field is that appropriate to infinite concentric cylinders, $V/[r \log (c/a)]$, where V is the potential difference. In addition to a gradual weakening of the anode field, field lines will not lie precisely along the radial; and since ionization collected will follow field lines, the electrical volume of the detector will be different from the mechanical volume.

All these effects are described qualitatively in Ref. 25. Even the simple end-electrode structure of Fig. 14 does not, apparently, permit a solution of the variation in anode field strength along the z direction expressed in tabulated functions.

To study in detail the variation of the electric field near

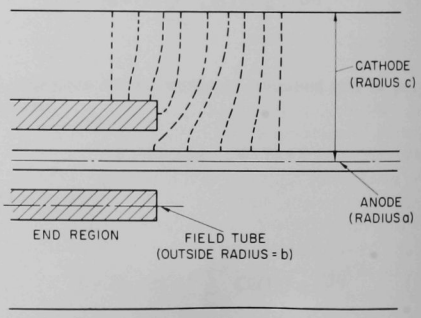

Fig. 14. Internal Construction Detail of Proportional Counter. ANL Neg. No. 113-2297.

tips and the resulting effect upon pulse-height spectra, Laplace's equation for the potential with appropriate boundary conditions was solved by iteration. A standard finite-difference approximation was used; and in the most elementary way the potential at any interior mesh point was expressed as a suitable "four-point" average over adjacent mesh points [27]. The radial dimension, r, was first mapped into a variable u = log (r/a), a being the anode radius. A fixed mesh interval was chosen in u space. The axial dimension was broken into mesh intervals that increased in geometric progression as distance from the discontinuity increased both along the anode region and along the end. This initial mapping of both radial and axial distance permitted a much more efficient (mesh-point number and iteration time) solution to the problem.

The boundary conditions maintained the anode (including the field-definition tube) and cathode at a fixed potential difference. At the midplane of the counter, potential gradients along the z axis were set to zero for all radial mesh points. At the extreme counter-end boundary, an arbitrary set of radial potentials could be input in order to ascertain any possible effect of end construction upon anode field. The true field pattern at the extreme end is generally complicated, since lead-in seals and anode supporting structures cause distortion. The calculation indicated an insensitivity of anode field to reasonable end potentials where field-tube insertion exceeded 1.5 cathode radii.

After a sufficient number of iterations of the finite-difference expression, potentials converged to values that were essentially independent of details of dimensioning and mesh spacing over a broad range of these variables. The electric field at the anode was taken to be the value of potential at the radial mesh point adjacent to the anode; absolute electric fields were not relevant to the problem. Appendix B includes additional detail describing the way in which the field calculation was done, together with a FORTRAN code.

In practice, the field-tube inside diameter will be several times the diameter of the anode; and, apart from misalignment in construction, the actual region near the tip will be as shown in Fig. 14. The calculation was set up to solve this case, but no significant effect upon anode field was observed when a solid field-tube structure was used, as would occur for example if solder filled the anode-field-tube space during construction of the counter. The anode is usually not precisely aligned within the field tube, and the fact that little effect can be seen by filling in the field tube (in the symmetrical case) indicates that misalignment does not lead to troublesome consequences.

The anode-field variation derived for a counter used in a spectroscopy application is shown in Fig. 15. The counter had an anode radius of 0.0127 mm. The ratio of field-tube radius to anode radius was 10.0, and the ratio of cathode to anode was 625. The total length of anode was 4000 anode

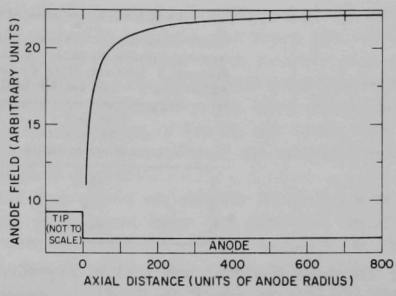

Fig. 15. Anode-field Dependence upon Distance from Field-tube Tip for Nominal Cylindrical Chamber. ANL Neg. No. 116-506.

radii, and at the half-anode distance (2000 radii), axial potential gradients were set to zero. At 912 radii from the discontinuity measured along the field-definition tube, the potentials were maintained at infinite cylinder values.

The initial rapid increase in anode field is seen in Fig. 15, followed by a rather slow approach to asymptotic. Gas multiplication is extremely sensitive to field strength, and the results of Fig. 15 clearly indicate that end effects will persist for some considerable distance along the anode region.

To estimate the influence upon "electrical volume" of field-line bowing, field lines originating at the anode were followed outward radially to their termination at the cathode. Several of these lines are shown in Fig. 16 for the test counter (the Case 1 "nominal counter" in Table IV). The mechanical volume is 4.92 (in units 10^9 cubic anode radii); the volume contained by field lines touching the tip-anode discontinuity is only 4.71. This very substantial discrepancy is of considerable importance, especially in absolute measurements. The electrical volume is well defined (and independent of voltage), but the actual amount of gas contained within it is considerably less than calculated from internal tube dimensions alone.

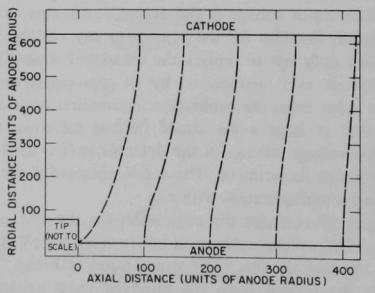

Fig. 16. Field Patterns for Nominal Chamber. ANL Neg. No. 116-509.

TABLE IV. Description of Chambers Used in Field-response Study

Anode diameter = 0.0254 mm. Field-tube diameter = 0.254 mm.
Nominal cathode diameter = 1.59 cm. Voltage = 4050 V.
Pressure = 5.03 atm H_2(0°C) with 1/2 volume percent CH_4.
Anode length = 5.08 cm. Mechanical volume = 0.491 × 10^{10} cubic anode radii.

Case	True End-cathode Diameter, units of anode radius	Mesh Equivalent-cathode Diameter, units of anode radius	Electrical Volume, units of 10^{10} cubic anode radii
1	625	625	0.471
2	468	500	0.483
3	312	321	0.487

The calculation described here (and in Appendix B) includes an option to permit the cathode to assume a diameter over the end region that is less than its value over the cathode. A reduction in cathode diameter over the region occupied by field tubes has two obvious advantages. The end region from which particle tracks may enter the effective anode volume is reduced, and the field at the anode varies more uniformly as distance increases from the tip. The operation of detectors constructed with a reduced cathode radius over the field-tube region is explored more fully in Sec. E below.

B. COUNTER RESPONSE FUNCTIONS

The numerical solution to the internal radial and axial potential variation can be used to produce a response function for the counter which will be appropriate for ionizing events of negligible spatial extent arising uniformly in the gas volume (see Appendix C). The electric-field variation along the anode surface is that of the potential gradient at the surface and is calculated together with the volume enclosed by any field line originating at the anode. The electrical volume is needed as a weighting factor, since the number of events enclosed by adjacent field lines is relatively fewer near the tips.

In proportional counters, gas multiplication occurs only in the immediate vicinity of the anode. If the electric-field variation and differential electrical volume along the anode are known, and if a calibration expressing gas multiplication as a function of voltage is also available, it is easy to derive a response function for the counter at any voltage. To do this, one only has to replace the calculated anode field (a function of axial distance z) by an appropriate multiplication value from the calibration. Normalization is chosen such that at large z the anode field is set equal to the nominal voltage setting for the detector as it is used in the spectroscopy experiment. The result obtained is the variation in gas multiplication with z.

Figure 17 contains the calibration for the test counter using ^{37}Ar as the calibration source (see Sec. V.B). The peak channel of the ^{37}Ar distribution is broad, but is readily determined from the observed pulse height spectrum (see Fig. 19 later). The data are fit with the parameterization discussed in Sec. V. All of the response-function derivations presented here use the parameterization given in Fig. 17.

To derive an amplitude distribution of events, it is necessary to transform from the (constant) density of events per unit anode to the corresponding density per unit multiplication. The actual prescription for expressing A versus V is irrelevant to the transformation from events per unit anode length to events per unit amplitude. Any relationship superior to Eq. 4 will improve, correspondingly, the end result. Equation 4 fails for very low values of multiplication (in the transition region between ion collection and proportional modes of counter behavior), as do other prescriptions that have been

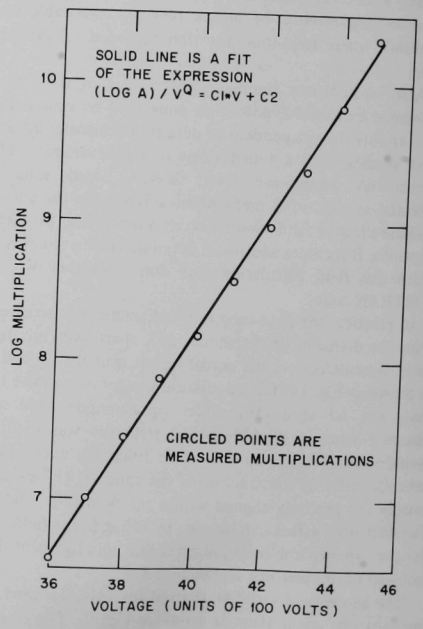

Fig. 17. Gas Multiplication Variation with Counter Voltage. Solid-line is a fit with Q = 0.2, C1 = 0.00070247, and C2 = -1.2503. ANL Neg. No. 116-507 Rev. 1.

proposed [20]. A FORTRAN code deriving the transformation from field strength to pulse height is given in Appendix C.

The computed amplitude distribution will be voltage-sensitive. Figure 18 shows the calculated distribution at 3500 and 4500 V using the test counter and its calibration. The distributions are normalized such that the amplitude at maximum gain is placed at full scale. The maximum amplitude is achieved for events in excess of about 1000 anode radii from the tip, and the distributions increase sharply for amplitudes greater than 70% of maximum. As may be seen, the response distribution depends upon counter voltage. Operating at lower voltages produces a response behavior closer to ideal, since relatively fewer events are strongly degraded by the field.

C. TEST OF THE CALCULATED RESPONSE

A comparison of predicted response with a pulse-height distribution of ^{37}Ar is given in Fig. 19. Two distinct deexcitation modes occur; one, involving betas at about 2.8 keV, is the dominant peak in the figure. Another mode, with energy about 200 eV, also occurs; and this line causes the sharp increase in the spectrum below channel 20. A discriminator blocks all events below about channel 13. Statistical effects introduce substantial broadening into the measured result.

The calculated pulse-height distribution was smoothed using a Gaussian shape with width chosen to match the observed distribution over the peak. Calculated and measured distributions were normalized in the region of the main peak. The extent of agreement over the limited region between soft beta decay at low channels and the onset of the statistically broadened dominant peak at high channels can be seen. The calculated distribution falls somewhat below the data at low pulse heights, even after allowing for the fact that the soft (200 eV) beta emission increasingly dominates the distribution at low values of pulse height. From the comparison of Fig. 19, one cannot draw any conclusion as to the validity of the calculated response below about channel 25.

Any disagreement can probably be attributed to two effects of unrelated origin not accounted for in the response-function calculation. As can be seen in Fig. 16, the total path ionization must follow before collection is substantially longer for events collected near the tip than for events collected near the counter midplane. One consequence of the lengthened field line is that the average field over the line is weaker. This combination of circumstances will ensure that ionization collected near tips remains in transit for a much longer time than the average, and probability for electron attachment by contaminants is correspondingly greater. The effect upon the response is to raise the low-amplitude distribution in accord with observations in Fig. 19.

Another effect not involved in the response calculation is related to axial diffusion of the assumed initial point-ionization distribution [14]. By the time this ionization is collected, a substantial axial broadening has occurred, especially near the tip where time to collection is greatest. Because of the nature of the change in multiplication with distance along the anode, this broadening will also serve to enhance the low-amplitude response.

It is feasible to use the calculated response to correct measured distributions. Counters of practical interest will usually possess sufficiently long anode regions to maintain field-distortion effects at a low level. Expected systematic errors in the response determination will be of limited

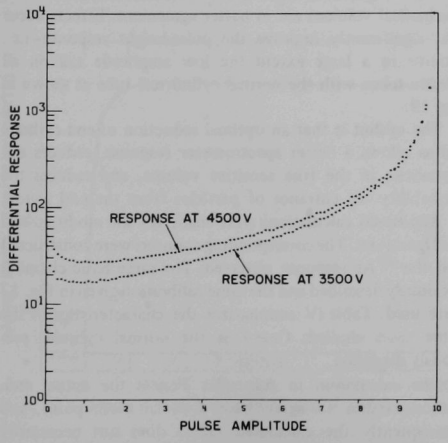

Fig. 18. Effect of Voltage upon Response. ANL Neg. No. 116-508.

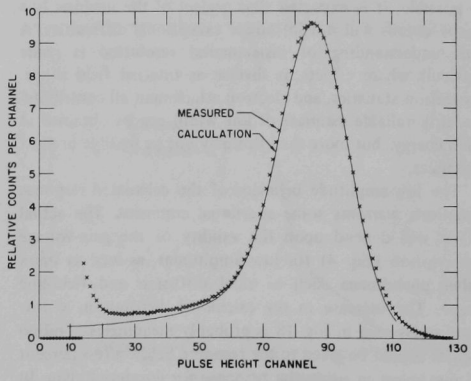

Fig. 19. Comparison of Measured and Calculated Spectra of ^{37}Ar for Nominal Chamber. ANL Neg. No. 116-513 Rev. 1.

extent in applying this correction to data in most practical situations.

D. PARAMETERIZATION OF COUNTER RESPONSE FUNCTION

The calculated pulse-height distributions, as determined from the electric-field anode variation increase rapidly as pulse height approaches its maximum value. To utilize, in the simplest manner, the calculated response to unfold response effects from measured data, it was found convenient to break the distribution into two parts. The dividing amplitude was chosen to be 70% of the maximum of the distribution. All events in excess of 70% of maximum were lumped together into a "contained" response fraction and assigned an amplitude equal to the maximum value. The tail of the distribution below 70% of maximum varied smoothly and was least-squares fit to a polynomial of fifth order for use in response-correction codes (see Sec. XI.B.2).

Splitting the response into a "contained" fraction and a "tail" is convenient for unfolding purposes, but is not a justifiable procedure. The neglect of the actual shape near maximum can be expected to introduce some systematic error; it is difficult to treat this region in any precise manner. The intrinsic line shape for the counter will not generally be Gaussian and will depend upon energy. A "complete" response function at each energy could be derived by smoothing the field effect with the line shape (if known). Use of the resulting distribution would require more elaborate numerical methods and would certainly limit the problem to the larger, faster computers for solution. We have tried to manage most of the response correction using the same (8k, 18 bit) computer available for on-line accumulation of pulse-height information.

The use of detectors with relatively little distortion due to field effects is obviously to be desired, and insofar as this is possible, it is expected that neglect of the intrinsic line shape details will not introduce exceptional difficulties. A full understanding of instrumental resolution is made difficult where effects as diverse as internal field shape, ionization statistics, and electron attachment all contribute. A fairly reliable estimate of line width can be obtained at each energy, but more than this may not be feasible in most instances.

The low-amplitude behavior of the calculated response functions warrants some additional comment. The actual shape will depend upon the validity of the gain-voltage prescription (Eq. 4) for low amplitudes, as well as upon other phenomena such as axial diffusion and field-line shape. The increase in the calculated distribution at low amplitudes seen in Fig. 18 is probably meaningless, and no weight should be given to the response below a few percent of maximum in using the response for correcting data. In most applications, this low-amplitude detail will have little effect upon spectra.

Another point regarding the field-effect-associated response functions is that they are calculated from the electric-field pattern assuming a point source of initial ionization distributed uniformly over the anode. This may not necessarily apply in a measurement, however, and if track lengths extend significantly, or if a nonuniform spatial distribution is encountered, the effect upon response functions will have to be taken into consideration. The complete response, where track truncation (wall-and-end effect) occurs coincidentally with field distortion, cannot be treated in any simple way. For extended tracks a spatial averaging automatically occurs, and these events tend to be less affected by the field-distortion problem, which remains localized near counter ends. Additional discussion of this point appears in Sec. VIII.

E. EFFECT OF A REDUCTION IN CATHODE DIAMETER OVER THE END REGION

The code described in Appendix B is equipped to compute the counter potential map, assuming that the cathode radius over the end region is reduced from that over the anode. Actually, the code will round off to force the true radius over the end to conform to the radial mesh structure. This will cause some discrepancy between the end radius actually solved for in the problem and the radius as input.

The advantages of a reduction in end radius are twofold. First, there is less end area from which particles with substantial range can enter the effective anode region. Events of this type are more difficult to include in a finite-range wall-and-end effect analysis than events originating within the effective anode region. Second, a pattern of field lines is established in which the electrical and mechanical volumes are in better agreement. Effects occur that significantly improve the pulse-height response–i.e., remove to a large extent the low amplitude tail on all spectra taken with the normal cylindrical tube as shown in Fig. 19.

The upshot is that an optimal reduction of end-cathode radius allows a better spectrometer response, reduces uncertainties in the true sensitive volume, and reduces the probability for entrance of particles from the end region.

Additional calculations were made for the modified end configurations. The corresponding counters were constructed and the ^{37}Ar response observed. The same basic chamber previously described and the same calibration given in Fig. 17 were used. Table IV summarizes the characteristics of the three cases studied; Case 1 is the normal cylinder previously discussed.

The calculation in Appendix B sets the actual end-cathode radius to agree with a radial mesh point, and consequently the calculated radius does not necessarily agree with the radius of the physical chamber. Table IV lists both the true chamber end radius and the radius for which

the calculation was done. The electrical volumes are also shown for the three cases. These are the volumes contained by the field line touching the tip-anode discontinuity.

Case 3 is a rather extreme reduction, by a factor of 2, in the radius of the cathode over the end region. The dependence of anode field upon distance from the tip is shown in Fig. 20 (this to be compared with the normal cathode configuration in Fig. 15). As expected, the effect of a reduction in end-cathode diameter causes a more rapid initial increase in field with distance from the tip. This, in effect, reduces the relative number of highly degraded events and strongly depresses the low-energy tail on the response function. The slight overshoot of anode field before relaxing to an asymptotic value for Case 3 has the effect of producing a high-amplitude tail on the response function. Figure 21 is a field-line pattern for Case 3 comparable to that for Case 1 shown in Fig. 16. Field lines are very markedly warped near the ends, but the electrical volume (that volume enclosed by the field line touching the tip) is close to the mechanical one, as shown in Table IV. One other consequence of the warping of lines is that the differential volume contained by adjacent field lines touching on the anode near the tip is less than its value at a distance from the tip, and this also reduces the amplitude of degraded events in the response.

Figure 22 compares the calculated response to the measured ^{37}Ar pulse-height spectrum for the Case 3 detector. In all the response-function computations, a Gaussian-smoothing full width at half maximum of 27% was used. Abscissa and ordinate were scaled in each case to produce a best eye fit to the measured distribution. The agreement between calculated response and spectrum measurement is quite good, and the high-amplitude overshoot is correctly predicted. Some residual excess of measured amplitude over

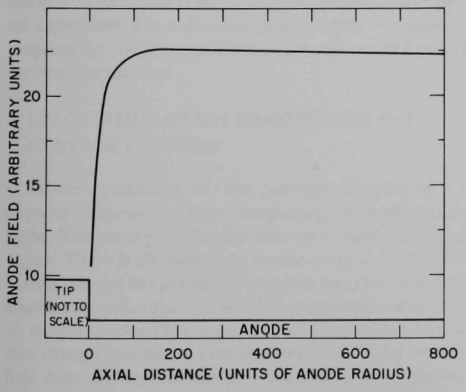

Fig. 20. Anode-field Dependence upon Distance from Tip for Case 3 Chamber. ANL Neg. No. 116-505.

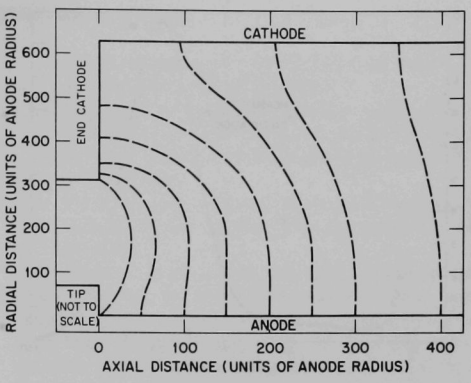

Fig. 21. Internal Field Pattern for Case 3 Chamber. ANL Neg. No. 116-510.

that calculated still remains in the minimum between about channels 20 and 40; the explanation is probably that given previously in the discussion of the normal counter. The discrepancy is small, however, and it is apparent that a chamber designed as in Case 3 is markedly superior for absolute rate determinations than the normal chamber of Case 1.

Case 2 with end-cathode radius reduced by $\sqrt{2}$ is intermediate between Cases 1 and 3. The anode field does not overshoot its asymptotic value, and the field pattern is not as violently distorted near the ends. Figure 23 shows the result of a response calculation compared to the measured ^{37}Ar result. Again, the agreement with experiment is good, and the low-energy tail is strongly depressed. Case 2 represents a near-optimum design for good resolution, as is required in a spectroscopy problem. Case 3 is a better

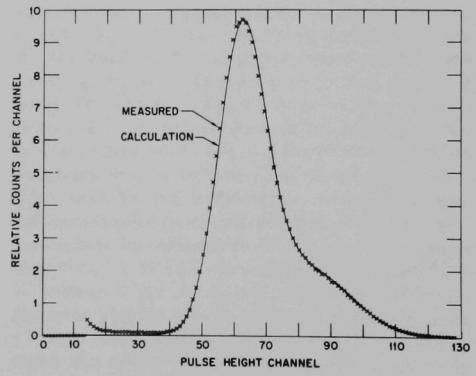

Fig. 22. Comparison of Measured and Calculated Spectra of ^{37}Ar for Case 3 Chamber. ANL Neg. No. 116-511 Rev. 1.

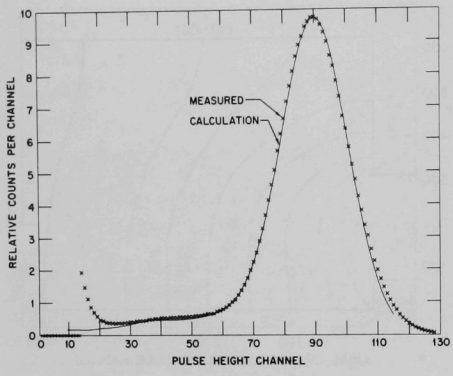

Fig. 23. Comparison of Measured and Calculated Spectra of ^{37}Ar for Case 2 Chamber. ANL Neg. No. 116-512 Rev. 1.

design for absolute counting, where spectroscopic quality can be sacrificed to some extent to improve the plateau.

The generally satisfactory agreement between the calculated response function and that observed by counting ^{37}Ar beta emission indicates that a fairly detailed study of the spectroscopic quality of a cylindrical detector desensitized at the ends by a field tube can be made using simple numerical techniques. The several parameters affecting counter behavior can be adjusted to optimize the objective, i.e., a good plateau as for Case 3, or a clean line response as for Case 2. There is unlikely to exist any simple rule of thumb by which this optimization can be arrived at, and the computer studies, with the method used here, are time-consuming. Nevertheless, substantial improvements in cylindrical chamber spectrometers can be achieved by optimizing the design of the cathode in the region near the ends.

We intend to use the modified-end cathode structures in future applications to proton-recoil neutron spectroscopy. Since a good line response is essential here, the reduction in end-cathode radius will correspond to the Case 2 study, although the chambers will be of different size.

The Case 3 study was sufficiently encouraging that an enriched BF_3 chamber identical to Case 3 was acquired and, if practical, will be used for absolute ^{10}B capture-rate determinations in fast-reactor spectra. The improvement in plateau for the Case 3 chamber over that for Case 1 (as compared in a fast-neutron spectrum) has been observed. Results will be published if in-core feasibility can be shown.

VIII. WALL-AND-END RESPONSE FUNCTION

If neutron spectra are to be accurately determined with proton-recoil proportional counters, it is necessary to correct for wall-and-end distortion. Some proton-recoil tracks are truncated by collisions with the walls, or they pass into an end region, where there is no multiplication. For these events there is an incomplete collection of ionization in the sensitive region, and the relationship of proton energy to collected ionization is distorted.

It is assumed that to first approximation wall-and-end distortion and electric-field distortion may be treated independently; i.e., the complete response function is separable. The wall-and-end part of the response function for a 4π-geometry counter is the energy distribution from monoenergetic protons of a given energy generated uniformly and isotropically throughout a particular counter. The determination of response functions for 4π-geometry proton-recoil counters has been considered in a number of papers. Various methods have been employed. Monte Carlo techniques have been used for spherical counters [3,28] as well as for cylindrical counters used with neutron beams parallel to the counter axis [29]. A method has been developed to empirically determine response functions for 4π-geometry counters [26]. Meantime, analytical solutions to the wall-and-end problem have been found for both spherical and cylindrical counters [30]. The analytical solutions have been applied to correction schemes for measurements with spherical counters [31].

This section indicates the method of calculation of the wall-and-end part of the response function, compares calculated response functions with measured distributions, and outlines application to proportional-counter spectrometry. In Section X the extent of wall-and-end response corrections on a representative fast-reactor spectrum is assessed. Appendixes D and E contain detailed mathematical expressions and a description and listing of computer programs for the determination of the wall-and-end part of the response function.

A. CALCULATION OF WALL-AND-END PART OF RESPONSE FUNCTION

In the calculation of the wall-and-end part of the response function, certain simplifying assumptions are made. The counter is divided into three right cylindrical region. There is the central or sensitive region, in which it is assumed that the gas multiplication is constant, and there are the two end regions, in which it is assumed that there is no multiplication. Thus the volume changes and multiplication changes associated with the distortion of the internal field lines discussed in the previous section are neglected. Tracks of detectable events—ones that create ionization in the sensitive region—can be divided into four mutually exclusive categories.

1. The track starts in the sensitive region and ends in the sensitive region without distortion.
2. The track starts in the sensitive region and is truncated by the walls or extends into an end region.
3. The track starts in an end region and stops in the sensitive region.
4. The track starts in the end region and is truncated by the walls in the sensitive region or extends into the other end.

Probability functions with the path lengths in the various regions as independent variables have been derived [30] for each of these categories under the assumptions that (1) it is equally likely that a track starts anywhere in the volume—uniform distribution; and (2) it is equally likely that a track starts in any direction—isotropic distribution. For protons of range R_0 and energy E_0, the response function $R(E,E_0)$ in terms of track-length functions for each category is

$$
\begin{aligned}
R(E,E_0) = {} & V_s F(R_0)\delta(E - E_0) + V_s \left.\frac{dR}{dE}\right|_{E_0-E} N[R_0 - R(E_0 - E)] \\
& + 2V_d \left.\frac{dR}{dE}\right|_{E} G[R_0 - R(E), R_0] \\
& + 2V_d \int_{E'=0}^{E_0-E} \left.\frac{dR}{dE}\right|_{E_0-E'-E} \left.\frac{dR}{dE}\right|_{E_0-E'} \\
& M[R_0 - R(E_0 - E'), R_0 - R(E_0 - E' - E)]\, dE'. \qquad (19)
\end{aligned}
$$

The first two terms on the right-hand side of Eq. 19 are associated with events starting in the sensitive region whose volume is V_s. In the first term, $F(\ell)$ is the probability that the path length to a surface is greater than ℓ and thus, with ℓ equal to R_0, is the probability for the first category of tracks. The term $\delta(E - E_0)$ is a delta function. Figure 24 shows $F(\ell)$ for a counter with a 1.27-cm radius for various cylinder lengths. In all cases, once the track length becomes comparable with the diameter of the counter, $F(\ell)$ becomes rather small. For path lengths up to a radius, $F(\ell)$ is rather well approximated by a straight line—the result that arises if one neglects the curvature of the surfaces. In the second term of Eq. 19, $N(\ell)\, d\ell$ is the probability that a path length is between ℓ and $\ell + d\ell$ and thus is the probability associated with the second category of tracks. The length $\ell = R_0 - R(E_0 - E)$ is the length of track in the sensitive region of a proton that starts in the sensitive region and deposits an amount of energy E in the sensitive region. Figure 25 shows $N(\ell)$ for a counter with a 1.27-cm radius

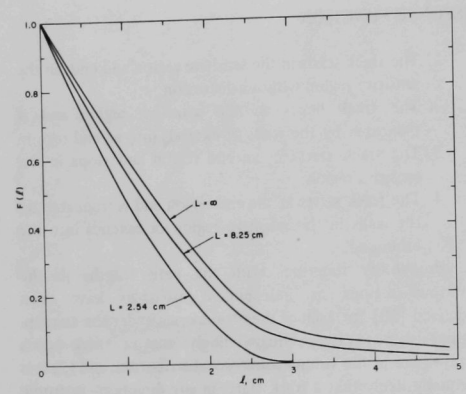

Fig. 24. The Probability F(ℓ) That a Track of Length ℓ Will Not Be Truncated or Pass through the End of a Cylinder of Radius a Equal to 1.27 cm and Various Lengths L. ANL Neg. No. 113-2303 Rev. 1.

for various cylinder lengths. For small values of ℓ, N(ℓ) is constant—the result which arises if one neglects the curvature of the surfaces. The term dR/dE is the inverse of the stopping cross section $\epsilon(E)$ of the counter gas adjusted for the density N of the gas

$$\left.\frac{dR}{dE}\right|_{E_0\text{-}E} = \frac{1}{N\epsilon(E_0 - E)} . \qquad (20)$$

Figure 26 shows ϵ versus energy and range versus energy for methane gas—the dominant filling gas for the counters for which the response functions are determined.

The last two terms on the right-hand side of Eq. 19 are associated with events that emanate from the end regions, each with a volume V_d. In the third term, $G(\ell', \ell)\, d\ell'$ is the probability that the path length is between ℓ' and $\ell' + d\ell'$ in

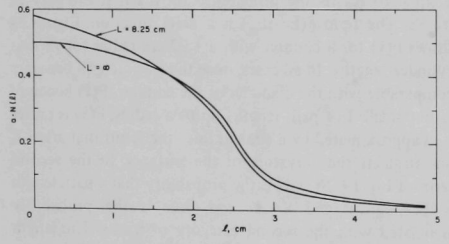

Fig. 25. The Probability N(ℓ) dℓ That a Track Is between ℓ and ℓ + dℓ for a Cylinder of Radius a Equal to 1.27 cm for Various Lengths L. Normalization is that one track starts per unit volume. ANL Neg. No. 113-2313 Rev. 1.

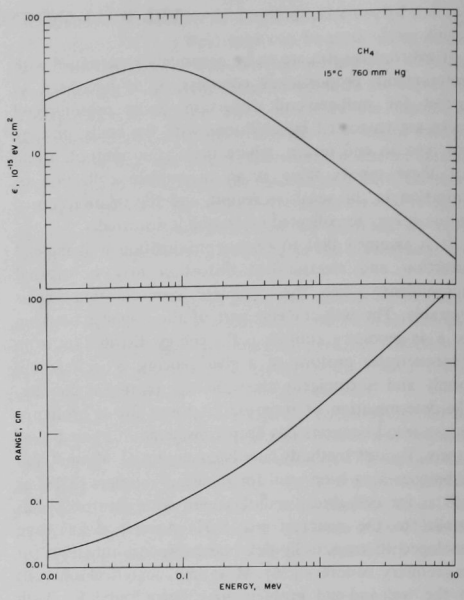

Fig. 26. Stopping Cross Section ϵ vs Energy, and Range vs Energy, of Protons in Methane Gas. ANL Neg. No. 113-2314.

an end region, and that the total length to the surface is greater than ℓ. The length $\ell' = R_0 - R(E)$ is the length of track in an end region of a proton that deposits energy E in the sensitive region. In the fourth term, $M(\ell', \ell)\, d\ell' d\ell$ is the probability that a track starting in an end region with a length between ℓ' and $\ell' + d\ell'$ has a total length to the surface between ℓ and $\ell + d\ell$.

The third term of Eq. 19 is rather easily evaluated. However, the fourth term is calculationally cumbersome, requiring a numerical integration for its evaluation. In this report the events from the end regions are neglected. The influence of these end events is presently being investigated. Wherever possible, the correction schemes have been constructed to allow suitable changes when the end regions are taken into account. For a counter with reduced-diameter cathodes over the end regions, the influence of end events is proportionally less.

When the ends are neglected, only the first two terms on the right-hand side of Eq. 19 are required. The first term is the number of events not distorted and is referred to as the undistorted part of the response function; the second term constitutes the distorted part of the response function. The detailed expressions for the probability functions F(ℓ) and N(ℓ), as well as the program that calculates the response function are contained in Appendix D.

For a given geometry the response function is a

two-dimensional function depending on both the energy E_0 and the range R_0 of the protons. If E_0 is held constant, the pressure is inversely proportional to R_0, and the pressure or R_0 can be used to parameterize $R(E,E_0)$. The significance of this case is made clear in Sec. B below. If the pressure is held constant, the relationship between E_0 and R_0 is fixed and either variable can be used to parameterize the response function. This is the response function that applies to a counter used as a spectrometer. In general, if R_0 is less than the radius of the counter, $N(\ell)$ is almost constant and the energy dependence of $R(E,E_0)$ results from the energy dependence of ϵ. Once the range of the protons becomes comparable with the diameter of the counter, the energy dependence of ϵ dominates $R(E,E_0)$ for E much less than E_0 and the form of $N(\ell)$ dominates $R(E,E_0)$ for E close to E_0. Calculated distributions of the distorted part of the response function for which E_0 is held constant and the pressure is varied are shown in Fig. 29. Distributions for which the pressure is held constant and E_0 is varied are shown in Fig. 32. The distributions are discussed in more detail in Sec. C below.

B. COMPARISON OF MEASURED DISTRIBUTIONS WITH CALCULATED DISTRIBUTIONS

One would ideally like to compare calculated and measured proton-recoil distributions for a fixed counter pressure as a function of E_0 over the full range of proton-recoil energies. However, it is not experimentally feasible to generate such distributions. Since the response function is a two-dimensional function, an alternative is to consider distributions from a fixed-energy proton source and vary the counter pressure. This sequence is easy to realize experimentally. If the counter contains some nitrogen and is placed in a uniform and isotropic thermal flux, a uniform and isotropic distribution of 585-keV protons will result from the $^{14}N(n,p)^{14}C$ reaction. This is the same reaction used for calibration (see Sec. V). The response function for a given energy E_0 and density N is related to that for a different E_0' and N' by

$$R(E,E_0) = \frac{N\,\epsilon\,(E_0 - E)}{N'\,\epsilon\,(E_0' - E')}\,R(E,E_0). \qquad (21)$$

Thus the ability to determine response functions for a fixed E_0 as a function of pressure is meaningful in ascertaining how well one can determine response functions for a fixed counter pressure.

The experimental method is described in detail elsewhere [26]. A schematic drawing of the counter used for these tests is shown in Fig. 27. For each pressure, the counter was filled from a mixture of 49% CH_4 and 51% N_2. The large amount of nitrogen was desirable to keep background contributions negligible. For all pressures, the

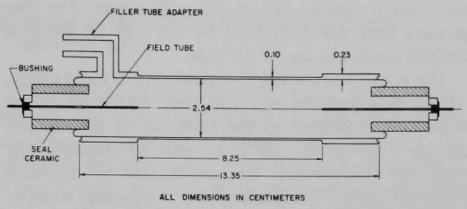

Fig. 27. Schematic Drawing of Proton-recoil Counter. Field tubes are 0.25-mm-dia hypodermic needles; anode is a 0.025-mm-dia stainless steel wire. ANL Neg. No. 113-2305.

overall gain of the system was kept fixed by varying only the counter voltage. A fission counter was used to monitor the relative number of thermal neutrons during each measurement.

Figure 28 shows a measured distribution for which the range of the 585-keV protons is 1.53 cm. The rapid increase in the number of counts per channel at lower energies results from the detection of Compton electrons from the interaction of gamma rays with the material in the walls of the counter. As the pressure is increased, the electrons are able to lose more energy in the counter, and the tail of these events moves out to higher energies. Carbon recoils from the $^{14}N(n,p)^{14}C$ reaction are also detected. The carbon recoils deposit an equivalent ionization of 30 keV, and thus bias the whole distribution by this amount, since their ionization is collected simultaneously with that from the protons.

Measurements were made from a pressure of 5.3 atm (which corresponds to a range of 0.20 cm) to 0.27 atm (which corresponds to 3.87 cm). The high-pressure limit was determined by the movement of the gamma-ray-induced

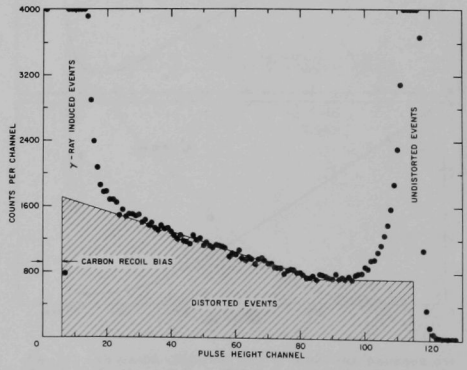

Fig. 28. Measured Pulse-height Spectrum from $^{14}N(n,p)^{14}C$ Reaction with Thermal Neutrons. Range R_0 of the 585-keV protons was 1.53 cm. ANL Neg. No. 113-2309 Rev. 1.

event tail to almost 50% of the peak energy. The low-pressure limit was determined by the point at which it was still possible to discern the peak.

The presence of the tail from gamma-ray-induced events, distortions introduced by electric field effects, as well as distortions introduced by the resolution of the detector prevent a straightforward comparison of measured and calculated distributions. An examination of calculated distorted distributions indicates how comparisons might be made. Figure 29 shows two calculated distributions for which E_0 is 585 keV. R_0 is small for one and large for the other. In both cases, the calculations indicate that from zero energy to almost the peak energy a straight-line fit to the curve is possible. The extrapolation in the measured distributions to zero energy is obvious. For small values of R_0, there is a rapid change in the calculated distributions near the peak energy introduced by the energy dependence of the stopping cross section (see Fig. 26). The rapid variation occurs so near the peak energy that if the resolution of the detector is taken into account, these events cannot be distinguished from undistorted events. Fortunately, this region of the distribution does not introduce a serious problem in comparing measured and calculated distributions, because the number of events contained in the region is small compared to the total number of distorted events.

It was decided to compare two parameters of the measured and calculated distributions: the fraction of events that are not distorted and the slope of the straight-line fits to the distributions over the energy region for which a straight line is a good approximation. Figure 28 indicates how the two parameters are obtained from a measured distribution. A bias is set to take into account the energy deposited by the carbon recoils. Assuming a straight-line fit to the data in the region just beyond the tail of the gamma-ray-induced events, the line is extrapolated back to zero energy. Near a peak, a horizontal line is drawn from the energy at which the slope is zero to the peak energy. The shaded area indicates the events that are considered distorted. The remaining events in the peak are considered to be undistorted. The consistency of the extrapolation method to zero energy was checked by totaling the number of events thought to be protons and comparing it with the number consistent with the thermal flux and amount of nitrogen in the counter. In all cases the agreement was good.

Figure 30 shows the measured fractions of undistorted events versus R_0, and Fig. 31 the measured slopes versus R_0. The figures also contain calculated curves of these quantities. The solid lines result from using Eq. 19 to calculate the distributions. Only wall-and-end distortions, or, as they are referred to on the figures, geometry effects, are taken into account. The solid curves do not provide a good fit to the data. This is not surprising, since the discussion in Sec. VII indicated the importance of accounting for electric-field distortions. The same type of approach as outlined in that section could be used to determine the electric-field part of the response function, which could be combined with the wall-and-end part to yield the full response function. However, for purposes of this comparison, it was found suitable to use an approximation to the true electric-field response function. It was assumed that the fraction of events distorted by the electric field would

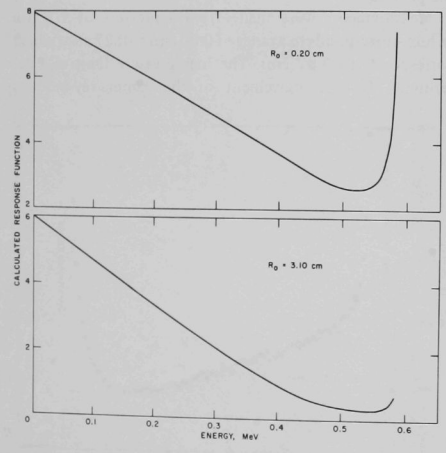

Fig. 29. Calculated Distorted Part of Response Function for Counter with 1.27-cm Radius and an 8.25-cm Length Filled with Methane. Range R_0 for protons of energy E_0 equal to 585-keV is indicated. ANL Neg. No. 113-2304 Rev. 1.

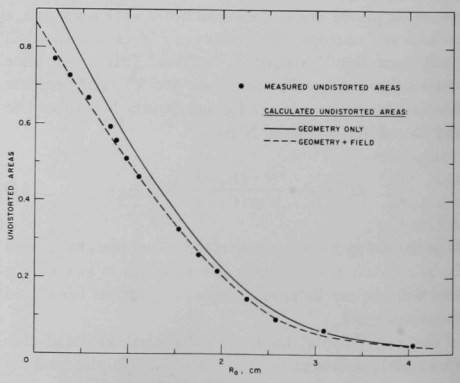

Fig. 30. Measured Fraction of Distribution That Is Undistorted vs Range R_0 of 585 keV Protons. The solid (dashed) curve is the calculated fraction and takes into account geometrical (geometrical and field) effects. ANL Neg. No. 113-2307.

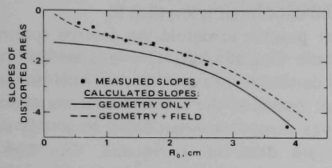

Fig. 31. Measured Slope of Straight-line Fits to Distorted Distributions vs Range R_0 of 585-keV Protons. The solid (dashed) curve is the calculated slope and takes into account geometrical (geometrical and field) effects. ANL Neg. No. 113-2308.

correspond to any event starting in a right cylindrical transition region with volume V_t, and that the energy distribution of events that start in this region can be represented by a straight line with slope S_t. V_t and S_t are parameters estimated from the field calculation. Since the gas multiplication was kept the same for all measurements, the assumption of a single electric-field response function independent of R_0 is probably rather good. The expression for the fraction of events not distorted when both geometry and electric-field effects are taken into account assumes the form

$$UN(R_0) = \frac{V_s F(R_0)}{V_s + 2V_t}. \qquad (22)$$

The expression for the slope $S(R_0)$ of the composite distribution is

$$S(R_0) = \frac{2V_t S_t}{V_s + 2V_t - V_s F(R_0)} + \frac{[V_s - V_s F(R_0)]\, S_g(R_0)}{V_s + 2V_t - V_s F(R_0)}, \qquad (23)$$

where $S_g(R_0)$ is the slope associated with the geometrical response function. The areas of the energy distributions of events from each type of distortion, as well as the area for the combined distorted distribution are normalized to unity. The dashed lines, which result from Eqs. 22 and 23, produce significantly better agreement. The exception is for the slopes associated with large values of R_0. This is not surprising, since protons with long track lengths lose only a small fraction of their energy in the transition region and thus are not influenced by this region.

These comparisons between the calculated and measured distributions indicate the importance of taking into account electric-field distortions. Once this is done, one can reproduce the measured distributions. It is also reassuring to see that it is possible to a good approximation to separate the two sources of distortion. The electric-field part of the response function dominates the total response function for short track lengths, and the wall-and-end part dominates it for long track lengths. Neglecting events from the end regions has not led to serious differences between the calculated and measured distributions.

C. APPLICATION TO PROPORTIONAL-COUNTER SPECTROMETRY

The appropriate response function for application to proportional-counter spectrometry is that for a fixed counter-gas pressure. Since a neutron can create a proton recoil with an energy equal to the incident neutron energy, it is necessary in principle to determine the response function for energies equal to the maximum neutron energy. Figures 32 and 33 show the response function at various energies for the counter described in Sec. B above filled with about 6.5 atm methane. This pressure is close to that at which the resolution begins to appreciably worsen because of contaminants in the gas. In Fig. 32 two examples of calculated distorted distributions are represented by the solid curves. For this illustration, the same values of R_0 were chosen as appear in Fig. 29. For a fixed value of R_0, the transformation of a distribution for one value of E_0 to another is independent of energy, except in the neighborhood of the peak. Figure 33 shows three examples of calculated response functions which are representative of the behavior of the response function in various energy regions. The uppermost response function represents the region in which the distorted part of the response function can be represented by a straight-line fit for energies almost up to the peak energy. The dashed line represents the undistorted events. The middle response function represents the region in which the distorted part of the response function assumes a more complicated shape, but a region in which R_0 can still be contained in the sensitive region. In this case, the number of undistorted

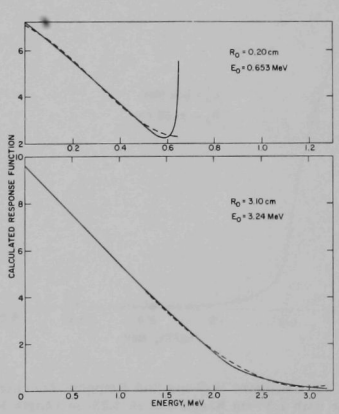

Fig. 32. Calculated Distorted Part of Response Function for Counter with 1.27-cm Radius and an 8.25-cm Length Filled with Methane. The range R_0 and corresponding energy E_0 are indicated. The solid curve is the calculation, and the dashed curve is a fit with four Legendre polynomials. ANL Neg. No. 113-2316 Rev. 1.

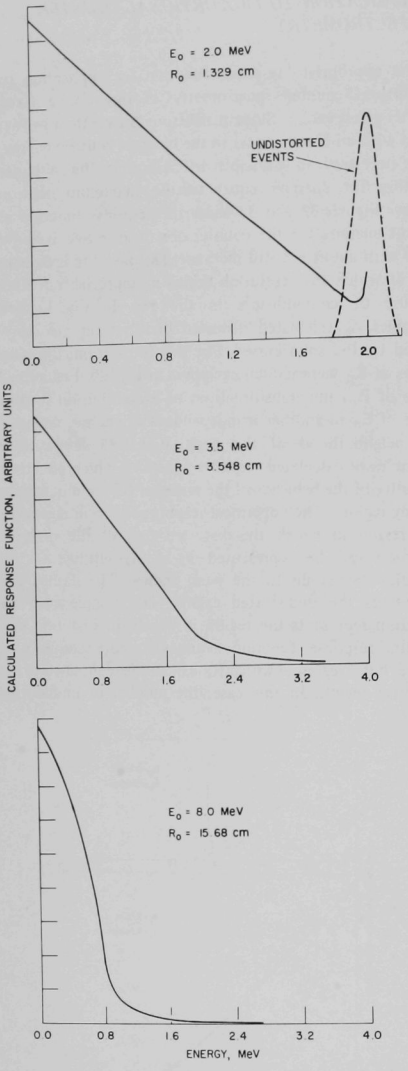

Fig. 33. Calculated Wall-and-End Response Function for Counter with 1.27-cm Radius and an 8.25-cm Length Filled with 6.5 atm Methane. The range R_0 and corresponding energy E_0 are indicated. ANL Neg. No. 116-475.

events is so small that they are not even shown on the figure. The bottom response function represents the region in which all tracks are distorted. The maximum energy a proton recoil can deposit is less than E_0.

It is not possible to unfold the neutron spectrum for energies above that at which all events are distorted. To accurately determine neutron spectra with proton-recoil proportional counters, the neutron spectrum above some energy E_c—an energy somewhat below the energy at which all events are distorted—is required. This high-energy spectrum may be obtained from measurements with emulsions, foils, or other techniques or under certain conditions from calculations. In any case, the neutron spectrum above E_c is used to generate the corresponding proton-recoil distribution. The wall-and-end response function is then applied to this distribution to obtain the distorted proton-recoil distribution. This distribution, which may be referred to as the downscatter distribution, is then subtracted from the measured proton-recoil distribution. The resulting distribution then has no contribution from neutrons above E_c. This proton-recoil distribution is then unfolded with the response function from E_c on down in energy to yield the proton-recoil distribution corrected for wall-and-end distortion.

The way one applies the response function to correcting measured proton-recoil distributions depends on the computing facilities available and the efficiency required. The response function for E_0 above E_c has a rather complicated shape and is not amenable to parameterization. However, $F(\ell)$ and $N(\ell)$ may be parameterized over various ranges of ℓ. Using a range-energy table and stopping power parameterization, the response function may be rather rapidly calculated. One then can generate the response function during the calculation of the downscatter distribution. A computer code for generating the downscatter matrix is presented in Appendix E. If end events are taken into account, one must evaluate the third and fourth terms on the right-hand side of Eq. 19. In that case, it would be better to develop a response matrix for E_0 greater than E_c, which could be permanently stored. This matrix would be called out during the calculation of the downscatter matrix.

For energies less than E_c, the distorted part of the response function at a given energy may be fit with the first four Legendre polynomials. In Fig. 32 the dashed lines are fits to the distorted part of the response function. The use of this parameterization for unfolding the data is outlined in Sec. XI.

The undistorted part of the response function is represented by a delta function. One could take into account the resolution of the counter by smoothing the calculated response function. However, as pointed out in the discussion of the electric-field response function (see Sec. VII.D), there are many factors that contribute to broaden the distribution, and furthermore, the intrinsic line shape is not known. A smoothing of the proton-recoil distribution is introduced by the numerical differentiation used to obtain the neutron spectrum. Smoothing the response function has little effect on the derived neutron spectrum [26].

IX. CORRECTION FOR CARBON RECOILS

When methane is used as the filling gas, the ionization spectrum contains not only proton recoils and electrons from gamma-ray interactions, but also carbon recoils from elastic scattering of neutrons on carbon. A simple correction scheme for this effect has been described elsewhere [26]. The topic is introduced here simply for completeness. In Sec. X the influence of various corrections on a representative reactor spectrum is assessed; the influence of carbon-recoil correction is included there.

In the correction scheme presently employed, a number of simplifying assumptions are made. It is assumed that the center-of-mass scattering cross section is isotropic and that it may be represented by

$$\sigma_C(E) = \frac{5520}{E + 1150}, \qquad (24)$$

with E in keV and σ_C in barns. The cross section is known to have several resonances above 2 MeV and to be anisotropic above 100 keV. A cross section that is isotropic in the center-of-mass produces a simple recoil distribution in the laboratory; for a given neutron energy, the number of recoils per unit energy is constant up to the maximum energy the recoil can obtain. For scattering on carbon, this energy is 28% of the incident neutron energy. One also has to know W for the correction. Limited measurements have indicated that, relative to protons, the carbon recoil creates about 75% as much ionization. It is assumed that this value holds for all energies, even though it is known that there are substantial changes in W for heavy fragments, especially at lower energies.

The importance of the carbon-recoil correction will depend on the hardness of the spectrum. The harder the spectrum, the more important the correction becomes. Because of the assumptions used in correcting for carbon recoils, one does not like to see the correction become large. If the correction is greater than several percent, one might consider using a heavier gas to get a good stopping cross section, but a gas whose recoils are not important until lower energies. Krypton combined with hydrogen has been successfully used in proton-recoil proportional counters, and becomes increasingly attractive as an alternative to methane when the carbon-recoil component induces a very significant effect [32].

X. INFLUENCE OF THE VARIOUS CORRECTIONS ON A REPRESENTATIVE SPECTRUM

In the previous sections, correction schemes were outlined for various sources of systematic errors encountered in the determination of neutron spectra with proton-recoil proportional counters. In this section, the extent of these corrections is assessed for a representative fast-reactor spectrum. The central spectrum in a mockup of the Fast Flux Test Facility core was chosen as the representative spectrum [33]. This facility is to be a plutonium oxide-fueled, sodium-cooled fast reactor.

Figure 34 shows the measured central spectrum corrected for the various systematic errors together with a fundamental-mode calculated spectrum. The error bars on the measured points indicate only statistical uncertainties and do not include uncertainties associated with the various corrections. In order that a meaningful comparison may be made between the calculated and measured spectrum, the calculated spectrum, which was produced as a histogram in 1/120 lethargy width, was smoothed with a Gaussian window whose width corresponded to the experimental resolution. Various scattering resonances are clearly seen: the oxygen resonances at 400 keV and 1 MeV, a chromium resonance at 50 keV, an iron resonance at 30 keV, and a sodium resonance at 3 keV. In general, the agreement is good, except in the neighborhood of the resonances.

A. INFLUENCE OF ELECTRIC-FIELD CORRECTIONS

Figure 35 contains the neutron spectrum derived from the uncorrected proton-recoil distribution and the spectrum from the electric-field-response-corrected distribution. The part of the spectrum derived from the methane-filled

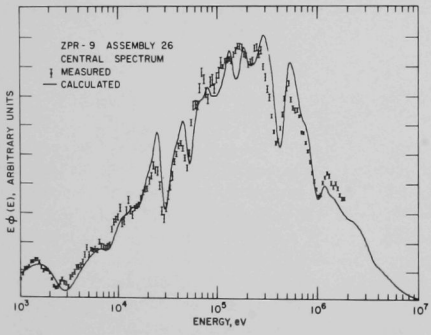

Fig. 34. Central Neutron Spectrum in Mockup of Fast Flux Test Facility Core, Together with Smoothed Fundamental-mode Calculation. ANL Neg. No. 900-308 Rev. 1.

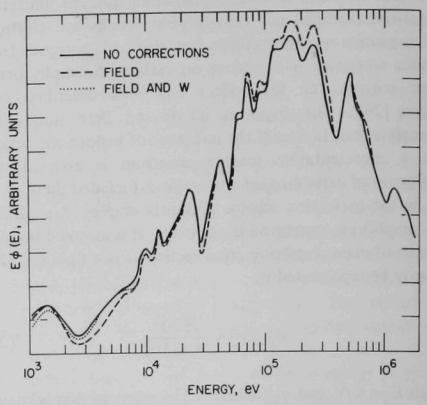

Fig. 35. Measured Neutron Spectra from Uncorrected Proton-recoil Distribution, One Corrected with Electric-field Response Function and One Corrected with Electric-field Response Function and for W Variation. ANL Neg. No. 116-372.

counter data extends above 100 keV, and that from the hydrogen-filled counter below 100 keV. For both the methane and the hydrogen counter data, the correction is only applied at energies at which the track lengths are short (see Sec. VII.D). The assumptions under which the electric-field response functions were derived break down for long track lengths. For the methane counter data, this energy is assumed to be somewhat lower than 1 MeV. Changing this cutoff energy within reasonable limits has little effect on the neutron spectrum. For the methane counter data, the correction becomes significant at the lower end of its range, i.e., below a few hundred keV. Both the shape of the spectrum and the shape of the response function as a function of voltage contribute to magnify the effect in this range. When the spectrum is rapidly falling off with increasing energy, the influence of the tail of response function from higher-energy events will be minimized. At the lower energies, the higher gas multiplications are used. The electric-field response function becomes more distorted as the voltage increases (see Fig. 18). Note also that the magnitude of the oscillation associated with the oxygen resonance is increased.

For the data taken with the hydrogen counter, the influence of the electric-field correction is seen over the whole range. Since the hydrogen counter is only used in the short-track-length region (see Sec. V.A), the cutoff energy is above the top of the data. The larger effects are seen at the lower energies. Percentagewise, the correction is large. If the spectrum were not decreasing as rapidly with decreasing energy as in this example, the magnitude of the

effect would be about the same and the percentage importance of the effect would decrease.

B. INFLUENCE OF W *CORRECTION*

Figure 35 also contains the neutron spectrum derived from the electric-field-response-corrected and W-corrected proton-recoil distribution. W is assumed to be constant for the methane-counter data and for the hydrogen-counter data above 8 keV. The data above this energy are unchanged. Below 8 keV the correction is significant and for this example is the same order of magnitude as the electric-field response correction. As for the electric-field correction, the percentage importance of the W correction depends on the spectrum shape. The large uncertainty in the value of W is seen to be the limiting factor in determining the spectra in the keV range.

If Fig. 34 is reexamined, one notices that the positions of the resonances obtained from the methane-counter data are in systematic disagreement with the calculated resonance energies. Accelerator measurements of pulse height versus energy rule out attributing all of the disagreement to W variation. As indicated in Sec. V.A, this disagreement is probably introduced by an excessive number of contaminants in the gas.

C. INFLUENCE OF WALL-AND-END CORRECTION

For the example under consideration, the neutron spectrum above E_c—the energy above which one must have an independent determination of the neutron spectrum—was assumed to be that predicted by a fundamental-mode calculation. E_c was chosen to be 2.5 MeV, and it was found that the energy dependence of the spectrum could be represented by

$$N(E) \propto \sqrt{E}e^{-E/T}, \qquad (25)$$

where T is a coefficient adjusted to fit the calculated spectra. It may be noted that the functional form is the same as that used to describe the fission spectrum, but with a different value for T. In making the downscatter correction, the calculated distorted proton-recoil distribution from neutrons above 2.5 MeV was normalized to the measured distribution between 2.5 MeV and the end of the measured data at about 3 MeV. Thus, only the shape of the neutron spectrum above 2.5 MeV was required.

Figure 36 shows the neutron spectrum derived from the uncorrected proton-recoil distribution, the spectrum derived from a downscatter-corrected distribution, and the spectrum derived from the downscatter- and upscatter-corrected distribution. Only the data taken with the methane-filled counter are presented in the figure. The upscatter correction is for wall-and-end distortion suffered by recoil protons produced by neutrons with energies less

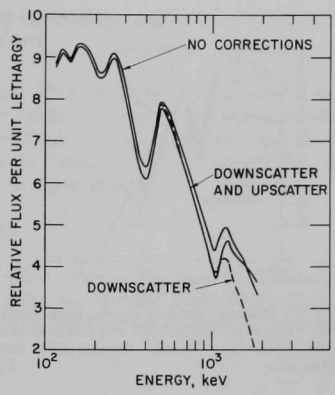

Fig. 36. Measured Neutron Spectra from Uncorrected Proton-recoil Distribution, One Corrected for Upscatter Events, and One Corrected for Upscatter and Downscatter Events. ANL Neg. No. 900-301.

than E_c. The downscatter correction significantly reduces the spectrum for energies greater than 1 MeV. The combined downscatter and upscatter correction raises the high energy end of the neutron spectrum, but has little effect at lower energies. It is interesting that the complete wall-and-end effect corrected neutron spectrum is not much different than that derived from an uncorrected proton-recoil distribution. This situation will usually not apply for neutron spectra with shapes significantly different than that of a degraded fission source. It is difficult to ascertain the uncertainty associated with the wall-and-end correction for energies above 1.5 MeV. Part of the problem is associated with uncertainty in the energy calibration and part with uncertainty in the response function introduced by neglecting events entering the sensitive volume from the end region.

D. INFLUENCE OF CARBON-RECOIL CORRECTION

Figure 37 presents the neutron spectrum derived from the uncorrected proton-recoil distribution and the spectrum derived from a proton-recoil distribution corrected for carbon recoils. The correction becomes significant at lower energies. As long as the neutron spectrum is falling off rapidly with energy, carbon recoils from higher-energy neutrons will only slightly distort the rapidly increasing proton-recoil distribution. Because of the approximations contained in the carbon-recoil correction scheme, one would like to see the extent of this correction remain small. For the neutron spectrum under consideration, the size of the correction is rather large at the lower energies.

In summary, the corrections for the most part can be considered as small perturbations on the spectrum. This is

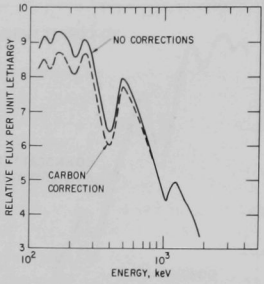

Fig. 37. Measured Neutron Spectra from Uncorrected Proton-recoil Distribution and One Corrected for Ionization from Carbon Recoils. ANL Neg. No. 900-302.

rather reassuring since the various correction schemes contain simplifying assumptions which limit their accuracy. Furthermore, the order in which the various corrections were applied introduced almost no change in the resulting neutron spectrum. This encourages the conclusion that the corrections are to first order separable. Of course, some care must be taken in extending these conclusions to a spectrum with a substantially different shape than that of a degraded fission source.

Accuracy at lower energies is presently limited by uncertainties in the variation of W. At higher energies the accuracy is limited by uncertainties as to the extent to which inclusion of events from the ends might alter the wall-and-end response function. An uncertain relationship of pulse height to energy for proton recoils stopping in methane also limits the accuracy.

XI. CODES FOR DATA REDUCTION FOR PROTON-RECOIL NEUTRON SPECTROSCOPY

The small computer used as part of the pulse-analysis system for collecting proton-recoil spectra is also used extensively for reduction of data at the termination of an experiment. This reduction is done with standard FORTRAN programming. The number of codes and the way in which they are written reflect the very limited capability of the machine and its software. A larger computer would be able to manage several of these reduction codes simultaneously. A breakdown of the analysis into several steps is, in some respects, not undesirable. Admittedly, some time is lost in the paper-tape communication of data from succeeding stages of the reduction, but results from each step are preserved and the progress of the reduction is readily followed. A considerable amount of computational detail to provide electric-field and wall-and-end response functions must necessarily be done with larger, faster computers. Those codes are described in Appendixes B-E. Once the parameters have been generated for a given detector and its operating conditions, they may be used in the reduction of data from any spectrum measurement. Only the small computer is necessary. The composition and use of the data-reduction codes are discussed in this section.

A. INITIAL FORMAT OF UNCORRECTED PROTON-RECOIL DATA

Ionization spectra are accumulated at various voltages with a methane-filled and a hydrogen-filled counter. Due to memory capacity during the data reduction, the maximum number of voltage runs is limited to eight, and the maximum number of these that may be taken with the methane-filled counter is limited to three. Ordinarily, eight runs will suffice to provide data over the energy range from 1 keV to about 3 MeV, which is near the practical measurement limit for the counters described in Sec. II.B. It is desirable to have as much overlap as possible for adjacent voltage runs, since the quality of results will be reflected in the closeness of agreement of spectra in overlap regions.

For each ionization spectrum at a given voltage, the keV-per-channel ionization scale factor A(J) and a normalization factor C(J) are known. A(J) are determined through calibration with sources of known energy as described in Sec. V. C(J) are the product of live times and hydrogen atom number in the effective detector volume (in units of 10^{24} atoms). This information becomes part of a header tape.

The ionization spectra are each of 100 channels extent—the upper 100 channels of a 128-channel (linear to full scale) spectrum. The lower 28 channels are ignored during the analysis because electronics noise compromises the data. Each point of the spectrum consists of two single-precision numbers (six digits), the second of which is the overflow count. The maximum single-precision number stored in the computer is $2^{17} - 1 = 131071$. (The 18th bit is the sign bit and is not used.)

B. CODES

The various Proton Spectrum to Neutron Spectrum (PSNS) codes are described below. The codes and tables describing the input formats are listed in Appendix F.

1. PSNS-1

This code is intended as a survey of an experiment immediately after termination. Any measurement problems will probably show up in this survey. The heading material is read in, and then each of the hundred-channel spectra. The spectra are normalized and denoted by RAPS.

According to the sense-switch options, the data may be written onto the storage scope either over an interval (input) of voltage sets or over an arbitrary ionization range. Before plotting, the distributions are scaled to the range of maximum scope deflection.

The spectrum RAPS may be punched on tape; this tape is in format to serve as input to the remaining PSNS codes. A sense-switch option permits rereading an output tape. This feature is sometimes useful for a scope inspection of data from a completed run.

2. PSNS-2

This code corrects the spectrum with the electric-field response function (see Sec. VII) and for W variation (see Sec. VI).

If $R(I,I')$ denotes the response function by which an event initially of amplitude I' leads to a measured effect of amplitude I ($I' > I$), the measured distribution $M(I)$ in response to a source distribution $S(I)$ is

$$M(I) = \int_I^\infty R(I,I')S(I')\,dI'. \tag{26}$$

It is assumed that the response function can be written as

$$R(I,I') = [A\delta(I - I') + BR_0(I,I')]/I', \tag{27}$$

where

$$\int_0^{I'} R_0(I,I')\,dI/I' = 1, \tag{28}$$

and also that A + B = 1. A and B are the integral amplitudes for "on-diagonal" and "off-diagonal" terms, respectively.

We recognize that this procedure is overly simple. As was discussed in Sec. VII.D, it is not possible to parameterize the response in this simple way, since the response is a smoothly varying function of amplitude and the delta function contribution is actually nonexistent.

If Eq. 27 is placed into the integral of Eq. 26, the result

$$S(I) = \frac{M(I) - B\int_I^\infty R_0(I,I')S(I')\,dI'/I'}{A} \qquad (29)$$

is obtained. By proceeding with the correction from high to low I values, we remove the effect of "off-diagonal" effects from higher ionization events from the distribution.

In PSNS-2, the response function describing the effects of nonideal electric fields is expressed as an expansion in a polynomial (fifth order) of the form

$$R(I,I') = \sum_{J=1}^{6} PC(J)\left(\frac{I}{I'}\right)^{J-1} \qquad (30)$$

The six coefficients and a normalization (AREA) for each voltage are sufficient to describe, in an approximate way, the response function. The coefficients PC are input such that the integral over R (with the argument I/I' ranging from 0 to RHI) is unity. AREA is the fractional weight of the "contained" part of the response defined to include amplitudes in excess of RHI of maximum.

Input to PSNS-2 consists in addition to the A and C values, i.e., the header tape (common to all codes) of cutoff values COME and COHY for both methane and hydrogen chambers. Following these are AREA values expressing the fraction of events in excess of some fraction RHI of maximum for each chamber and voltage. Next are the six coefficients from which the response (normalized) can be derived at any amplitude below RHI. Last is the fraction RHI (usually set to 0.7) separating the response into diagonal and off-diagonal parts. These data are contained on the electric-field response function tape.

The cutoff values COME and COHY require comment (see Sec. VII.D). The integral in Eq. 29 cannot be extended infinitely, since the data are never that extensive and, in addition, the response function produced for the field distortion was generated on the assumption of a point-like proton track extension. As track lengths increase, an automatic spatial averaging over the axial counter direction occurs (together with wall-and-end truncation effects). This averaging will rather quickly cause the field-response distribution to lose its low-amplitude tail. To account for this effect, the field-response correction integration in Eq. 30 terminates when ionization exceeds the cutoff value. The contained fraction AREA is increased by the fraction of response function that is in excess of cutoff to preserve the correct normalization for the correction and to allow for the change in response shape for long tracks.

The effect upon the correction of changing this cutoff value over a reasonable range is very slight. The two-parameter mode of pulse analysis used to accumulate spectra and described in Sec. I also provides a method of estimating the cutoff energy. The width of the fast-rising (proton-recoil) component broadens quickly at energies for which track extent starts to increase.

The response-function integration in PSNS-2 is a correction to the ionization spectrum; as a consequence, no effects involving W (energy per ion pair) enter. After the correction is made, however, the ionization spectrum RAPS is divided by W. All subsequent use of RAPS will assume it to be spectra per unit energy. The data for W correction is contained on the W-to-ionization and energy-to-ionization tape.

The scope display is organized to allow the spectrum to be plotted before and after the electric-field response connection.

3. PSNS-3

PSNS-3 treats response corrections to the data taken only with methane counters. It corrects with the wall-and-end response function and for the effects of carbon recoils.

The code has an option to allow subtracting from the proton spectrum RAPS, a spectrum calculated to be the downscatter from track truncation effects occurring above an energy RLME which is input (see Sec. VII.C and Appendix E). A normalization of the calculated downscatter spectrum to the data over energies above RLME is made prior to subtraction. RLME must be chosen somewhat less than the maximum energy point and not above a point where the Legendre parameterization of the response loses significance. In practice, RLME will usually be 2 MeV or above for the counters described in Sec. II.A.

The carbon-recoil correction described in Sec. IX is made next. It requires the neutron spectrum at energies higher than the point at which the correction is made. An adequate neutron spectrum is produced by first neglecting the carbon-recoil problem and the wall-and-end problem and analyzing the uncorrected methane data. Fortunately, this correction is usually small.

After the downscatter and carbon-recoil corrections are made, a correction for upscatter is made (see Sec. VIII.C and Appendix D). The approach, by correcting the distribution from high energies downward, is basically the same as was discussed under PSNS-2. Since the "off-diagonal" response is energy-dependent, the expressions are correspondingly more elaborate.

The response function has the form

$$R(E,E_0) = CLEG(1)\delta(E - E_0) + CLEG(2) + CLEG(2)\sum_{i=3}^{5} CLEG(i)P_{i-1}(E/E_0), \qquad (31)$$

where P_i are Legendre functions. The five amplitudes CLEG are generated from a polynomial expansion (fifth order) in energy. The coefficients of the expansion are designated by CPFT. The first coefficient CLEG(1) is the "diagonal" amplitude, the number of events (relative to unit-sensitive volume) that originate in the sensitive region and stop without truncation. The next four coefficients, CLEG(2) through CLEG(5), are coefficients of the analysis of the off-diagonal distribution using the first four Legendre amplitudes.

CLEG(2), the first term in the Legendre analysis of the off-diagonal distribution is also the integral of the off-diagonal distribution, and the sum CLEG(1) + CLEG(2) would be unity if no contribution to the distribution from events originating in the dead region at counter ends occured. As was discussed in Sec. VIII.A, the contribution from events entering at ends is small relative to the totality of events and may be neglected without serious error, except for the high-energy, long-track events, which are relatively few in number. These events were not included in the calculated response function, but the codes described here will accommodate them if desired.

The first four Legendre functions of argument $0 < x < 1$ are:

$$\begin{aligned} P_1 &= 1 \\ P_2 &= 1.722(2x - 1) \\ P_3 &= 2.236[6x(x - 1) + 1] \\ P_4 &= 2.646\left\{x[12 - x(30 - 20x)] - 1\right\}. \end{aligned} \tag{32}$$

The amplitude of each P_i is determined by analysis of the off-diagonal finite-range problem. The Legendre polynomials in Eq. 32 are orthogonal and unit-normalized from 0 to 1.

The expansion coefficients CPFT as used in the code are not directly those determined by analysis with the functions of Eq. 32. Some rearranging was done for convenience and in order to avoid repetitious computation time. The last four CPFT coefficients, as input, are related to those derived in the following way:

$$\left.\begin{aligned} &\text{CPFT(2) for } P_1 = \text{derived coefficient}, \\ &\text{CPFT(3) for } P_2 = \frac{(\text{derived coefficient})\ 1.732}{\text{CLEG(2)}}, \\ &\text{CPFT(4) for } P_3 = \frac{(\text{derived coefficient})\ 2.236}{\text{CLEG(2)}}, \end{aligned}\right\} \tag{33}$$

and

$$\text{CPFT(5) for } P_4 = \frac{(\text{derived coefficient})\ 2.646}{\text{CLEG(2)}}.$$

The response-function expansion is valid only in the energy region below RLME.

The scope plotting routines in PSNS-3 display two distributions (RAPS, COPS) simultaneously. In this way the effect of each correction can be seen directly. Arrays may be transferred between RAPS and COPS; this must be done, for example, after the carbon-recoil correction and before the finite proton-range correction, since the RAPS are considered "uncorrected" and the COPS "corrected" distributions.

4. PSNS-4

This calculation continues the finite proton-range correction to data for the hydrogen counters at lower energies. If corrected methane spectra are available, these may be read in. The coefficients that parameterize the response function, CPFT, are of the same type used in PSNS-3 (they are relevant, of course, to the hydrogen gas filling which has less stopping power than methane). The limit energy for use of these response functions is input as RLHY.

The response-function tape format is the same as for PSNS-3. Both methane and hydrogen data are placed on a single tape; the methane numbers are deleted prior to reading those for hydrogen.

Due to the numerical tedium involved in generating appropriate response functions at each energy used in the integral, PSNS-4 requires a relatively long running time (approximately three hours) for a full data set. For fast-reactor spectra the effect of this correction is small and in most cases can be ignored altogether.

5. PSNS-5

The series of codes described up to this point has dealt with the proton distribution exclusively. Corrections for various nonideal response effects are made within the framework of PSNS codes 2, 3, and 4, and the end product should be the ideal density (per unit energy) of recoil events.

The extraction of a neutron spectra is a very simple procedure (see also Ref. 2). The slope of the proton distribution is derived at a series of equally spaced (in lethargy) energies. Factors involving energy and the known n-p scattering cross sections are applied to produce the neutron spectrum (see Eq. 1), and a calculation of the resolution (at each energy) is made.

In addition to the header tape and the tape relating energy to ionization, information is entered on the teletype keyboard.

RA and RB specify the slope-taking half interval STHW, which is derived from the equation

$$\text{STHW} = \sqrt{\text{RA}^2 + \text{RB}^2/\text{E}}. \tag{34}$$

At each energy in a sequence (with lethargy spacing DINC)

of energies, EDEN, data within the range ±STHW are searched out and the slope and error computed. This is done for each set of data that include changes in counter type as well as changes in voltage for a given counter. Data are read in set by set, and neutron spectra derived from data for the set of EDEN values spanned by the set. Where data from different sets overlap, a (statistically) weighted mean is produced at the value of EDEN.

Equation 34 generates an energy-dependent slope-taking interval which increases (if RB is nonzero) with decreasing energy. If RB is taken to be ~0.8, the purely statistical effects that broaden resolution will be of about the right magnitude. Since the ultimate resolution attainable will be limited by statistics and since no additional accuracy is achieved by using slope-taking intervals less than statistics, the prescription in Eq. 34 will permit a gradual increase in slope-taking with no loss in overall accuracy.

The intrinsic resolution FWHM for a detector with a mechanical resolution (full width half maximum) of FW is derived from the expression

$$\text{FWHM} = \sqrt{\text{FW}^2 + 0.17/\text{E}}. \qquad (35)$$

As energy increases, the statistical contribution, 0.17/E, becomes insignificant and only the "mechanical" part remains. The effective resolution achieved here is dependent upon both the slope-taking interval and the intrinsic width; a discussion in detail has been provided in Ref. 2. Values for mechanical widths for methane and hydrogen are required as input, and the code produces an effective resolution FWHM at each EDEN value and outputs this number together with flux and error at the termination of the problem.

An input option will cause neutron spectra to be computed only for the methane detector. This option may be used for the carbon-recoil correction described in PSNS-3.

The punched output of PSNS-5 consists of an energy, flux, statistical error, and effective resolution for each nonempty value in the energy sequence generated by DINC. A scope plot of the neutron spectrum may be done prior to punching.

APPENDIX A

ANALYSIS OF GAIN-VOLTAGE DATA

The short FORTRAN program that follows is used to fit the measured multiplications as a function of voltage with the prescription

$$\frac{\log A}{VQ} = C1*V + C2, \qquad (A1)$$

where V is the voltage and Q, C1, and C2 are constants. Input data consist, initially, of voltages and corresponding gas multiplications (a total of N points).

A request for the voltage power factor Q is made, and a number (usually near unity) is entered on the teletype keyboard. The coefficients C1 and C2 are determined from a least-squares fit and the root-mean-square deviation of fitted A from measured A is printed. The process may be repeated for different Q until a minimum rms deviation is found.

Raising sense switch 2 will cause the quantities C1 and C2 (slope and intercept) to be printed together with a table of input-voltage values, input multiplications, fitted multiplications, and the percentage deviation.

If, after the table is completed, sense switch 1 is observed to be up, six additional numbers are read from paper tape. The first three are voltage limits and a voltage increment used in forming a calibration table of energy full scale and energy per channel. The following pair of numbers, VREF and TEST, are a particular voltage and corresponding peak channel value for the $^{14}N(n,p)^{14}C$ (615 keV) reaction used in the calibration (see Sec. V.B). The last number, EXCS, is the ratio of the 615-keV proton pulse height that would occur with an arbitrarily long amplifier integrating time constant to the actual pulse height. EXCS for methane will be close to unity, but for the slower hydrogen-filled chambers, especially those of large diameter, it may be as high as 1.10.

```
C
C  620 PROGRAM TO ANALYSE AND LIST A COUNTER VOLTAGE CALIBRATION.
C  LOG(A)/V**X VARIES LINEARLY WITH V.
C  IF AMPLIFIER CLIPPING MODIFIES CALIBRATION, THE QUANTITY EXCS
C  WHICH IS THE RATIO OF POINT-SOURCE PULSE HEIGHT TO CALIBRATION
C  SOURCE PULSE HEIGHT IS INPUT IN EXCESS OF UNITY.
C
      DIMENSION A(99),V(99),Y(99)
      COMMON A,V,Y
   17 FORMAT(/37HANALYSE GAIN VERSUS VOLTAGE ASSUMING  /
     X38HTHAT LOG(A/V**X VARIES LINEARLY WITH V.  ///)
   18 FORMAT(6E12.4)
   19 FORMAT(/35H  RESIDUAL ROOT MEAN SQUARE ERROR =  / E10.4 )
   20 FORMAT(I2)
   21 FORMAT(//48H      VOLTAGE     INPUT A     EVAL. A     % ERROR  /)
   24 FORMAT(/48H  THE SLOPE AND INTERCEPT FOR THE LINEAR FIT ARE/
     X 2E14.5)
   26 FORMAT(/46H  BELOW ARE LISTED REF. VOLTAGE, NITROGEN TEST  /
     X61H  CHANNEL, ENERGY EXCESS , AND MAXIMUM COLLECTED IONIZATION. )
   27 FORMAT(///51H INTERPOLATED IONIZATION (KEV) VERSUS VOLTAGE TABLE
     X//38H   COUNTER     ENERGY(KEV)   IONIZATION /
     X39H   VOLTAGE     FULL SCALE     PER CHANNEL  / )
   28 FORMAT( ///28H  VOLTAGE POWER FACTOR IS -  )
   29 FORMAT(F6.3)
C
      WRITE(0,17)
      READ(2,20) N
      DO 1 I=1,N
    1 READ(2,18) V(I),A(I)
   34 WRITE(0,28)
C
C  COMPUTE THE RMS ERROR BETWEEN THE VALUE OF A FROM THE LINEAR FIT
C  FOR EACH X INPUT AND THE MEASURED VALUE OF A.
C
      READ(0,29) X
      SY=0.0
      SV=0.0
      SVSQ=0.0
      SYV=0.0
      DO 2 I=1,N
      Y(I)=ALOG(A(I))/V(I)**X
      SY=SY+Y(I)
      SV=SV+V(I)
      SVSQ=SVSQ+V(I)*V(I)
    2 SYV=SYV+Y(I)*V(I)
      DEN=FLOAT(N)*(SVSQ)-SV*SV
      C1=(FLOAT(N)*SYV-SY*SV)/DEN
      C2=(SVSQ*SY-SV*SYV)/DEN
      RESQ=0.0
      DO 3 I=1,N
      DIF=(Y(I)-C1*V(I)-C2)/Y(I)
    3 RESQ=RESQ+DIF*DIF
      RESQ=SQRT(RESQ/FLOAT(N))
      WRITE(0,19) RESQ
      PAUSE
C
C  SHOW QUALITY OF FITTED A VALUES IF SS2 IS LIT.
C
      IF(ISSNS(2))31,31,32
   32 WRITE(0,24) C1,C2
      WRITE(0,21)
      DO 35 I=1,N
      AEV=EXP((V(I)**X)*(C1*V(I)+C2))
      PCD=100.*(AEV-A(I))/A(I)
   35 WRITE(0,18) V(I),A(I),AEV,PCD
C
C  TERMINATE BY LISTING IONIZATION VERSUS VOLTAGE IF SS1 IS LIT.
C  IF SS1 IS NOT LIT, CONTINUE FITTING TO INPUT X VALUES.
C
   31 IF(ISSNS(1))30,30,33
   33 READ(2,18) VFRST,VLAST,VINCR,VREF,TEST,EXCS
      A0=EXP((VREF**X)*(C1*VREF+C2))
      EMAX= A0*128.0*615.0/(TEST*EXCS)
      WRITE(0,26)
      WRITE(0,18)VREF,TEST,EXCS,EMAX
      WRITE(0,27)
      U=0.0
   10 U=U+VINCR
      IF(U-VFRST)10,11,11
   11 IF(VLAST-U)12,13,13
   13 GAIN=EXP((U**X)*(C1*U+C2))
      EFULL=EMAX/GAIN
      EPCHA=EFULL/128.0
      WRITE(0,18) U,EFULL,EPCHA
      GO TO 10
   12 STOP
      END
```

APPENDIX B

ELECTRIC-FIELD CALCULATION

A finite-difference solution to Laplace's equation for the electrode structure of Fig. 14 was sought. The peculiar feature of the problem is the relatively small ratio of anode to cathode. Typically the cathode radius is 1000 times the anode radius, while the field-tube radius is about 10 times the anode radius.

One would expect that any finite-difference approximation would have to possess a relatively fine radial and axial mesh spacing near the tip where potentials undergo a rapid variation. However, if a uniform spacing comparable to anode size is chosen in both radial and axial dimensions, an unreasonably large array results, and convergence is very time-consuming.

The problem has cylindrical symmetry, and it is convenient to map radial distance, r, into a dimensionless variable, u, according to

$$u = \log (r/a), \tag{B1}$$

where a is the anode radius. For infinite coaxial cylinders, u is the potential at any point in the region $a < r < c$, with c the cathode radius. The mapping $u = \log (r/a)$ permits a coarse u-mesh to contain a relatively large number of points in the radial region between the anode and the outer-field-tube radius. If, in addition, the axial dimension z (whose origin is the field-tube-anode discontinuity) is measured in units of a, Laplace's equation becomes

$$e^{-2u}\frac{\partial^2 V}{\partial u^2} + \frac{\partial^2 V}{\partial z^2} = 0. \tag{B2}$$

Boundary conditions were chosen as follows: At the midplane, due to symmetry, the axial electric field vanishes for all values of u. At the absolute end, distant from the field tube tip and measured along the end region, potentials appropriate to infinite cylinders,

$$V = \frac{\log (r/b) \log (c/a)}{\log (c/b)} \tag{B3}$$

with b the field tube radius, were usually assumed. If desired, other than infinite cylinder values for the radial potential values along the absolute end may be input. In practice, a complication in the form of electrical insulation exists at the absolute end. The actual end boundary will not influence the anode field significantly if the field tube extends more than about 1.5 cathode radii into the counter. Also, it was observed that axial potential gradients were quite small as distance along the anode exceeded about 1.5 cathode radii.

In the radial direction, the potential was maintained at zero over the anode and end electrodes and was set to the value log (c/a) at the cathode.

A choice of mesh spacing along the u and z dimensions was made in a way consistent with the mapping of r into u and with the requirement of a dense mesh near the tip. A fixed interval, H, sufficed along u. A z-mesh was chosen in which successive mesh intervals increased by a fixed ratio, γ, as distance increased both along the anode and end regions. The progression, γ, will differ over anode and end regions if the number of mesh points in these regions differs. If the zeroth mesh point is taken at the anode-end interface, the kth mesh spacing is given by

$$\Delta z_k = \text{BASE}\ \gamma^{k-1}, \tag{B4}$$

where BASE is the initial mesh interval, for both the anode and end regions. After a total of N intervals, the axial distance to the Nth point is

$$z = \text{BASE}\ (\gamma^N - 1)/(\gamma - 1). \tag{B5}$$

A first-order approximation to the second derivative of V at the z-mesh point k is given by

$$\frac{d^2V}{dz^2} = \left[\frac{V(z_{k+1}) - V(z_k)}{\Delta z_{k+1}} - \frac{V(z_k) - V(z_{k-1})}{\Delta z_k}\right] \Bigg/ \frac{\Delta z_{k+1} + \Delta z_k}{2}. \tag{B6}$$

Equation B2 and the approximation of Eq. B6 lead, with a little manipulation, to the following finite-difference relation at the radial mesh point j and axial point k:

$$V(k,j) = \frac{T1\,[V(k+1,j) + \gamma V(k-1,j)] + V(k,j-1) + V(k,j+1)}{T_2 + 2}, \tag{B7}$$

where

$$T1 = T2/(1 + \gamma),$$

and

$$T2 = 2H^2 \exp[2(j-1)H]/\gamma(\Delta z_k)^2. \tag{B8}$$

H is the mesh interval along u. The initial u-mesh point (j = 1) is taken at the anode surface. The factor γ weighting the term V(k - 1,j) in Eq. B7 is due to the second finite-difference approximation applied along the z axis where successive intervals are of slightly different extent (their ratio is γ).

Equation B7 is the elementary result solved by repeated iteration. The starting potentials over both the anode and end regions are those appropriate to infinite coaxial cylinders. The radii of the field tube (inside and outside)

are adjusted by the code to agree with the choice of mesh interval, H. Consequently, the problem solved will not, in general, be exactly the desired one; parameters for the problem solved are listed by the code.

The iteration proceeds initially along the anode for all k_j values with k in excess of the tip mesh point. Iteration over the end region follows, first for j values in excess of the outer-field-tube radii, and finally, inside the field tube if the field tube is chosen to be "hollow." The prescription (Eq. B7) is slightly different for j (radial) points at the tip-end discontinuity, since the adjacent k (axial) mesh points both have the same spacing.

The input data and its format are listed in Table B.I. The total number of iterations performed is determined by the convergence requirement that the greatest change in anode field V(k,2) not exceed 10^{-4} times the asymptotic value of field between 1000 iterations. The problem, as presented, is well converged after about 10,000 passes, this number depending upon mesh size. For a problem with adequate dimensioning (NANO = 110, NEND = 30, NUMP = 30), an iteration time of about 3 hr on an SEL-840 with hardware arithmetic was required for convergence. The code listing is for a version run on an SEL-840 computer with 16k of core memory. It appears that 16k is adequate; use of radial arrays larger than those in the DIMENSION statement will improve the accuracy of the electrical-volume calculation somewhat at the expense of additional time required for convergence.

The sensitivity of the computed field to parameter changes was studied. It was noticed that some deviation of the computed field occured if the initial mesh spacing (BASE) exceeded four anode radii. Most runs were made with BASE set equal to two radii. At least 75 anode mesh points (NANO) were required to produce a field sufficiently smoothly varying for use with the calculation in which the counter response function was derived and parameterized. Only a small change in anode field was observed on increasing the radial mesh (NUMP) from 10 to 30 points. However, a fine radial mesh structure is desired to improve the calculation of electrical volume, and most runs were made with the full 30 radial mesh points.

A series of boundary potentials at the absolute end (NBND > 0) was input, and the effect upon anode field observed. On the assumption that the field tube extends 1.5 radii into the counter, no significant perturbation upon anode field could be seen from reasonable assumptions concerning potentials at the absolute end.

No significant effect upon anode field was observed when a "hollow" tip condition (TIRA > 1) was employed.

After convergence has been obtained, a map of potential along the radial for each axial mesh point is printed. It is possible to estimate the direction of the electric field at each point; the tangent of the field angle is the ratio of the axial field component to the radial component. The axial potential gradient over the kth mesh interval at the radial mesh point j is just

$$[V(j,k+1) - V(j,k)]/\Delta z_k, \tag{B9}$$

the difference between successive potentials along the axial divided by the corresponding interval. The radial potential gradient at the axial mesh point k is

$$\frac{dV}{dr} = \frac{dV}{du} \cdot \frac{du}{dr} = \frac{dV}{du} \frac{1}{r} \simeq \frac{V(j+1,k) - V(j,k)}{H} \cdot \frac{1}{r}, \tag{B10}$$

where H is the fixed radial mesh interval.

During calculation of the path of field lines, the subroutine ANGLE (R,Z) is used to determine the sine and

TABLE B.I. Input for Program That Determines the Electric Field and Sensitive Volume

Card	Variable	Format	Description
1	NANO	I10	Number of mesh points in the anode.
	NEND	I10	Number of mesh points in the end.
	NUMP	I10	Number of mesh points along the radius.
	NPRN	I10	Block iteration count; after NPRN iterations, the block iteration and maximum change in anode field may be printed depending on sense switch options.
	NBND	I10	Greater than zero if absolute-end boundary potentials are to be input.
2	DANO	E12.5	Length of anode in units of anode radii.
	DEND	E12.5	Length of end in units of anode radii.
	BASE	E12.5	Initial z-mesh spacing in units of anode radii.
	CATH	E12.5	Cathode radius over anode in units of anode radii.
3	TORA	E12.5	Outer-field-tube radius in units of anode radii.
	TIRA	E12.5	Inner-field-tube radius in units of anode radii. If set to 1.0, problem solved for solid-field-tube configuration.
	EIRA	E12.5	Cathode radius over ends in units of anode radii.
4	BNDR	6E12.5	Radial potential boundary values for the absolute end if infinite cylinder values are not used. NBND must be positive. First potential is zero and last equal to log (CATH).

After convergence is obtained, the direction of field lines may be determined by a sense-switch option. The anode terminus of a field line START, in units of anode radii, and the fixed path increment DEL, in units of anode radii, are input in F8.2 format on the teletype.

cosine of the field at any radial and axial distance r,z. A fixed path increment, DEL, is propagated from anode to cathode; its orientation to the radial direction is computed by ANGLE as its proceeds along. According to a sense-switch option, one may select a particular anode terminus of a field line and follow the detailed path taken by the field line to the cathode. In addition to the anode starting point, a path length DEL is needed as input. The accumulative radial and axial termini are calculated as the total path, in increments of DEL, until finally the cathode is reached. The number of increments and the field angle and position are provided as output. From these calculations, pattern diagrams such as shown in Figs. 16 and 21 may be drawn.

The electrical volume enclosed by each axial mesh point is essential for a response function derivation, since the difference in volume enclosed by successive points provides the weighting appropriate to events in corresponding gas-multiplication intervals. By a sense-switch option, a terminal calculation is done in which DEL is set to 3.0 and the electrical volume calculated point by point. Decreasing DEL below 3.0 did not improve the accuracy of the volume calculation. As the calculation proceeds, both the near-anode potential (proportional to electric field at the anode surface) and the electrical volume are punched for use as input in the response-function determination described in Appendix C.

The FORTRAN code listing follows.

```
C
C  ELECTRIC FIELD DETERMINATION FOR CYLINDRICAL PROPORTIONAL COUNTERS
C  WITH SIMPLE END-DEFINITION STRUCTURES.   VERSION FOR THE SEL-840.
C  ALL DIMENSIONS ARE IN UNITS OF ANODE WIRE RADIUS.
C  DIMENSION Z AXIS ARRAY NOT GREATER THAN 1 BELOW MAXIMUM.
C
      DIMENSION V(141,30),TERM(30),TMNT(141),BNDR(30)
      COMMON V,TERM,TMNT,BNDR,NUMP,ML,L,H,SINA,COSA
C
      ZDIS(I,L)=BASE*(RAND**(I-L)-1.0)/(RAND-1.0)
      EDIS(I,L)=BASE*(REND**(L-I)-1.0)/(REND-1.0)
    1 FORMAT(5I10)
    2 FORMAT(6E12.5)
    3 FORMAT(    50H MESH POINTS IN ANODE, END, AND RADIAL DIRECTION - /
     X/X,3I10)
    4 FORMAT(///47H ANODE LENGTH, PROGRESSION FACTOR, INITIAL AND /
     X33H FINAL MESH SPACINGS ALONG WIRE -/2X,4E14.5)
    5 FORMAT(///51H FIELD TUBE LENGTH, PROGRESSION FACTOR, INITIAL AND /
     X32H FINAL MESH SPACINGS ALONG END - /2X,4E14.5)
    6 FORMAT(///47H ACTUAL OUTER TIP RADIUS AND RADIAL MESH POINT-  /
     X 2X,F10.2,I10///47H ACTUAL INNER TIP RADIUS AND RADIAL MESH POINT-
     X/2X,F10.2,I10///42H ACTUAL END CATHODE RADIUS AND RADIAL MESH
     X 7H POINT- /2X,F10.2,I10)
    7 FORMAT(///30H ITERATIONS DONE IN BLOCKS OF-  / 2X,I10)
    8 FORMAT(1H133H ITERATION CYCLES TO THIS POINT -  I10//  )
    9 FORMAT(8X,14,F8.2,10F10.5)
   10 FORMAT(1H1,26H INCORRECT INPUT MESH DATA )
   11 FORMAT(///14H POINT   DIST.30X,32H RADIAL    POTENTIAL   VARIATION)
   12 FORMAT(I6,3(6X,E12.5))
   13 FORMAT(1H1,45H ELECTRIC FIELD DETERMINATION FOR CYLINDRICAL
     X61H PROPORTIONAL COUNTERS WITH SIMPLE END-DEFINITION STRUCTURES.
     X/////)
   14 FORMAT( //38H THE CATHODE RADIUS OVER THE ANODE IS- /6X,F10.2 //
     X 36H THE CATHODE RADIUS OVER THE END IS- /6X,F10.2)
   15 FORMAT(1H1///50H FIELD LINES TERMINATE AT ANODE AND CATHODE AT THE
     X18H Z DISTANCE SHOWN. ///6H ZMESH8X,6H ANODE12X,8H CATHODE  /)
   16 FORMAT(16,2F12.6)
   17 FORMAT(/47H INPUT ANODE TERMINUS AND INCREMENT (F8.2/F8.2) /)
   18 FORMAT(F8.2/F8.2)
   19 FORMAT(1H1,30X,23H FIELD ANGLE VARIATION. ///
     X4X,2H N7X,11H SINE ANGLE 6X,12H AXIAL DIST. 6X,13H RADIAL DIST.)
  201 FORMAT(/10X,20H VOLUME ENCLOSED IS-  E12.5)
C
      READ(3,1)NANO,NEND,NUMP,NPRN,NBND
      READ(3,2)DANO,DEND,BASE,CATH
      READ(3,2)TORA,TIRA,EIRA
C
C  FIX THE MESH SPACING ALONG THE RADIAL AND FIND THE MESH POINTS WHICH
C  ACTUALLY CORRESPONDS TO THE OUTSIDE SURFACE OF THE FIELD TUBE (JTIP)
C  AND TO THE INSIDE SURFACE OF THE FIELD TUBE (JINS).
C  ALSO FIX THE INSIDE END-REGION MESH POINT NEMP.
C
      UMAX=ALOG(CATH)
      NUM1=NUMP-1
      H=UMAX/FLOAT(NUM1)
      JTIP=1+IFIX(ALOG(TORA)/H+0.5)
      AKO=EXP(H*FLOAT(JTIP-1))
      JINS=1+IFIX(ALOG(TIRA)/H+0.5)
      ARI=EXP(H*FLOAT(JINS-1))
      JIM1=IFIX(ALOG(EIRA)/H+0.5)
      AIND=EXP(H*FLOAT(JIM1))
      NEMP=JIM1+1
      JT1=JTIP+1
      IF(JIM1-JT1)63,63,30
   30 DO 36  J=2,NUMP
   36 TERM(J)=H*H*EXP(2.0*H*FLOAT(J-1))
C
C  INPUT END BOUNDARY IF NBND POSITIVE. FIRST POTENTIAL MUST BE 0.0,
C  LAST POTENTIAL MUST BE UMAX.
C
      IF(NBND)25,25,26
   26 READ(3,2)(BNDR(J),J=1,NEMP)
   25 M=NANO
      L=NEND+1
      ML=M+L
C
C  FIX THE RATIO FACTORS (RANO,REND) FOR BOTH ANODE AND END REGIONS.
C
      NR=1
      N=NANO
      X=DANO/BASE
   59 AN=FLOAT(N)
      IF(X-AN)63,63,62
   63 WRITE(5,10)
C
   62 NC=4
      DEL=0.01
      R=1.01
   53 Y=(R**AN-1.0)/(R-1.0)
      IF(X-Y)51,51,52
   52 R=R+DEL
      GO TO 53
   51 R=R-DEL
      DEL=DEL/10.0
      NC=NC-1
      IF(NC)54,53,53
   54 IF(NR)60,60,61
   61 RANO=R
      NR=NR-1
      X=DEND/BASE
      N=NEND
      GO TO 59
   60 REND=R
C
C  FIND THE MAXIMUM MESH SPACING AND THE TRUE ANODE AND END LENGTHS.
C
      SANO=BASE*RANO**(FLOAT(NANO-1))
      SEND=BASE*REND**(FLOAT(NEND-1))
      EANO=(RANO*SANO-BASE)/(RANO-1.0)
      EEND=(REND*SEND-BASE)/(REND-1.0)
C
C  LIMIT THE LEFT ITERATION WITHIN FIELD TUBE TO 20 POINTS OR LESS.
C
      KLFT=1
      IF(NEND-20)64,64,65
   65 KLFT=NEND-19
C
C  FIX SOME VARIABLES USED IN THE ITERATION.
C
   64 W1A=1.0/(RANO*RANO)
      W1E=1.0/(REND*REND)
      W2A=1.0/(1.0+RANO)
      W2E=1.0/(1.0+REND)
      T2AO=2.0/(BASE*BASE*RANO)
      T2EO=2.0/(BASE*BASE*REND)
C
C FORM BOUNDARIES AND STARTING POTENTIAL.
C
      DO21 K=1,ML
      DO21 J=1,NUMP
   21 V(K,J)=FLOAT(J-1)*H
      DO22 K=1,L
      DO22 J=JTIP,NEMP
   22 V(K,J)=FLOAT(J-JTIP)*UMAX/FLOAT(NEMP-JTIP)
      DO24 K=1,L
      DO24 J=NEMP,NUMP
   24 V(K,J)=UMAX
      DO23 K=1,L
      DO23 J=1,JTIP
   23 V(K,J)=0.0
      DO20 K=L,ML
   20 TMNT(K)=V(K,2)
      AITR=0.0001*V(ML,2)*FLOAT(NPRN)/1000.
C
C  IF EXTERNAL END BOUNDARY CONDITION, I NTRODUCE HERE.
C
      IF(NBND)28,28,29
   29 DO27 J=JTIP,NEMP
   27 V(1,J)=BNDR(J)
C
C  INITIAL DATA PRINT, ONLY ONCE PER PROBLEM.
C  PAUSE AFTER FINISH TO TURN OFF PRINTER. DISC ETC.
C
   28 WRITE(5,13)
      WRITE(5,3)NANO,NEND,NUMP
      WRITE(5,14)CATH,EIRA
      WRITE(5,4)EANO,RANO,BASE,SANO
      WRITE(5,5)EEND,REND,BASE,SEND
      WRITE(5,6)ARO,JTIP,ARI,JINS,AIND,NEMP
      WRITE(5,7)NPRN
      PAUSE
C
C  ITERATE THROUGH AND RETURN HERE UNLESS CONVERGED OR TERMINATED.
C  FIRST ITERATION GOES RIGHT (ANODE REGION) FOR ALL RADIAL POINTS.
C
      ITNO=1
   47 IT=1
   46 DO39  J=2,NUM1
      K=1+J
      U=TERM(J)
      JM1=J-1
      JP1=J+1
      T2A=T2AO*U
      T1A=W2A*T2A
   33 KM1=K-1
```

```
      KP1=K+1
      V(K,J)=(T1A*(V(KP1,J)+RAND*V(KM1,J))+V(K,JP1)+V(K,JM1))/(T2A+2.0)
      K=K+1
      IF(K-ML)31,35,35
   31 T2A=T2A*W1A
      T1A=T2A*W2A
      GO TO 33
   35 KM1=K-1
      V(K,J)=V(KM1,J)
   39 CONTINUE
C
C  ITERATE LEFT (END REGION) FOR ALL RADIAL MESH POINTS IN EXCESS
C  OF THE OUTER TUBE RADIUS.
C
      DO41 J=JT1,JIM1
      K=L
      U=TERM(J)
      JM1=J-1
      JP1=J+1
      Z1=U+2.0/(BASE+BASE)
      Z2=Z1/2.0
      KM1=K-1
      KP1=K+1
      V(K,J)=(Z2*(V(KP1,J)+V(KM1,J))+V(K,JP1)+V(K,JM1))/(Z1+2.0)
      K=K-1
      T2E=T2EO*U
      T1E=W2E*T2E
   38 KM1=K-1
      KP1=K+1
      V(K,J)=(T1E*(V(KM1,J)+REND*V(KP1,J))+V(K,JP1)+V(K,JM1))/(T2E+2.0)
      K=K-1
      IF(K-1)41,41,37
   37 T2E=T2E*W1E
      T1E=T2E*W2E
      GO TO 38
   41 CONTINUE
C
C  ITERATE TO LEFT INSIDE FIELD TUBE IF PROBLEM SO REQUIRES.
C
      IF(JINS-1)77,77,71
   71 IF(JINS-JT1P)72,63,63
   72 JFIN=JINS-1
      IF(JFIN-1)63,63,76
   76 DO75 J=2,JFIN
      K=L
      U=TERM(J)
      JM1=J-1
      JP1=J+1
      Z1=U+2.0/(BASE+BASE)
      Z2=Z1/2.0
      KM1=K-1
      KP1=K+1
      V(K,J)=(Z2*(V(KP1,J)+V(KM1,J))+V(K,JP1)+V(K,JM1))/(Z1+2.0)
      K=K-1
      T2E=T2EO*U
      T1E=W2E*T2E
   73 KM1=K-1
      KP1=K+1
      V(K,J)=(T1E*(V(KM1,J)+REND*V(KP1,J))+V(K,JP1)+V(K,JM1))/(T2E+2.0)
      K=K-1
      IF(K-KLFT)75,75,74
   74 T2E=T2E*W1E
      T1E=T2E*W2E
      GO TO 73
   75 CONTINUE
   77 IT=IT+1
      IF(IT-NPRN)46,46,49
C
C  TEST IF CONVERGED. REQUIRES THAT GREATEST CHANGE IN ANODE VOLTAGE
C  NOT EXCEED .0001 OF NOMINAL BETWEEN 1000 ITERATIONS.
C
   49 DEF=0.0
      DO120 K=L,ML
      VARA=V(K,2)-TMNT(K)
      IF(VARA)124,125,125
  124 VARA=-VARA
  125 TMNT(K)=V(K,2)
      IF(VARA-DEF)120,120,121
  121 DEF=VARA
  120 CONTINUE
      IF(DEF-AITR)48,48,122
C
C  IF SENSE 2 UP, MARK THE END OF EACH NPRN ITERATION BLOCK BY
C  LISTING THE ITERATION NUMBER, THE FIRST ANODE VOLTAGE AND THE
C  GREATEST CHANGE IN VOLTAGE. CAN FORCE TERMINATION WITH SENSE SWITCH 6
C  IF SENSE 3 UP, PRINT THE VOLTAGE MAP BEFORE CONTINUING.
C
  122 CALL SSWTCH(2,N)
      GO TO(141,142),N
  141 WRITE(1,16)ITNO,V(L+1,2),DEF
  142 CALL SSWTCH(6,N)
      GO TO (48,123),N
  123 CALL SSWTCH(3,N)
      GO TO(143,145),N
  146 DO147 K=L,ML
  147 TMNT(K)=V(K,2)
  145 ITNO=ITNO+1
      GO TO 47
C
C  AFTER LAST ITERATION COMPLETED,
C  PRINT VOLTAGES AT EACH Z-AXIS MESH POINT. SENSE 3 MUST BE DOWN.
C
   48 PAUSE
  143 DO103 K=1,ML
      IF(K-L)101,101,102
  101 TMNT(K)=ED1
      GO TO 103
  102 TMNT(K)=ZDIS(K,L)
  103 CONTINUE
      WRITE(5,8) ITNO
      I=1
      IF(NUMP-10)83,83,82
   82 WRITE(5,11)
      K=1
      JLF=I+9
   80 VARA=TMNT(K)
      WRITE(5,9)K,VARA,(V(K,J),J=I,JLF)
      K=K+1
      IF(K-ML)80,80,81
   81 I=I+10
      IN=NUMP-I-9
      IF(IN)83,83,82
   83 WRITE(5,11)
      K=1
   85 VARA=TMNT(K)
      WRITE(5,9)K,VARA,(V(K,J),J=I,NUMP)
      K=K+1
      IF(K-ML)85,85,144
  144 CALL SSWTCH(3,N)
      GO TO(146,111),N
C
C  IF SENSE 1 DOWN, CALCULATE THE FIELD CONTOUR AND ENCLOSED VOLUME FOR
C  AN INPUT STARTING POINT. SENSE 1 UP CALCULATES THE VOLUME ENCLOSED
C  BY EACH FIELD CONTOUR AND EXITS BY PUNCHING THE ANODE FIELD AND
C  THE VOLUME ENCLOSED BY THAT FIELD LINE.
C
  111 PAUSE
      CALL SSWTCH(1,N)
      GO TO(110,116),N
  110 WRITE(3,16)M,BASE,RAND
      DEL=3.0
      K=L+1
  117 START=ZDIS(K,L)
      GO TO 119
  116 WRITE(5,19)
  118 WRITE(1,17)
      READ(1,18)START,DEL
      IF(START-DAND)119,118,118
  119 J=1
      SINA=0.0
      COSA=1.0
      Z=START
      R=1.0
      VOL=0.0
  112 CALL SSWTCH(1,N)
      GO TO (109,114),N
  114 WRITE(5,12)J,SINA,Z,R
  109 J=J+1
      DELZ=DEL*SINA
      DELR=DEL*COSA
      Z=Z+DELZ
      R=R+DELR
      IF(Z)130,130,115
  115 IF(R-CATH)113,131,131
  113 VOL=VOL+(DAND-Z+DELZ/2.)*6.2832*DELR*(R-DELR/2.0)
      CALL ANGLE(R,Z)
      GO TO 112
  130 VOL=VOL+3.1416*DAND*(CATH*CATH-R*R)
      GO TO 132
  131 X=DELR-R+CATH
      VOL=VOL+6.2832*(DAND-Z)*X*(CATH-X/2.0)
  132 CALL SSWTCH(1,N)
      GO TO (133,134),N
  134 WRITE(5,201)VOL
      GO TO 111
  133 WRITE(3,2)V(K,2),VOL
      K=K+1
      IF(K-ML)117,50,50
   50 VOL=0.0
      WRITE(3,2)V(K,2),VOL
      STOP
      END
C
C  SUBROUTINE ANGLE COMPUTES THE ANGLE OF TILT OF THE ELECTRIC FIELD
C  TO THE RADIAL AT ANY AXIAL-RADIAL COORDINATE.
C
      SUBROUTINE ANGLE(R,Z)
      DIMENSION V(141,30),TERM(30),TMNT(141),BNDR(30)
      COMMON V,TERM,TMNT,BNDR,NUMP,ML,L,N,SINA,COSA
C
      DO1 K=L,ML
      ZWT=Z-TMNT(K)
      IF(ZWT)2,1,1
    1 CONTINUE
    2  DELZ=TMNT(K)-TMNT(K-1)
      U=ALOG(R)
      DO3 J=2,NUMP
      UWT=U-H*FLOAT(J-1)
      IF(UWT)4,4,3
    3 CONTINUE
    4 ESUBZ=((V(K,J)-V(K-1,J))*(H+UWT)+(V(K,J-1)-V(K-1,J-1))*(-UWT))/
     X(H*DELZ)
      ESUBR=((V(K,J)-V(K,J-1))*(DELZ+ZWT)+(V(K-1,J)-V(K-1,J-1))*(-ZWT))/
     X(H*R*DELZ)
      D=SQRT(ESUBZ*ESUBZ+ESUBR*ESUBR)
      SINA=ESUBZ/D
      COSA=ESUBR/D
      RETURN
      END
SO
```

APPENDIX C

FIELD-TO-PULSE-HEIGHT TRANSFORMATION

A knowledge of the axial dependence of anode field and the volume contained by successive anode mesh points, together with a relationship between gas multiplication and voltage, is sufficient to permit construction of the actual pulse-height response function (see Sec. VII.B). A uniform distribution of ionization from individual particle tracks of negligible spatial extent is assumed. Particles initiating ionization do not necessarily possess negligible track extent, however, and a more elaborate approach than that provided here would be necessary (see Sec. VII.D).

The input data and its format are listed in Table C.I. The code initially requires three numbers used to parameterize gas multiplication versus voltage (see Sec. V.B). The parameterization prescription is contained only in the function statement S(k) and consequently may be readily altered. Data required are the anode field strength and corresponding electrical volume derived from the calculation described in Appendix B.

For each voltage a calculation of the response distribution is made by first transforming from the initial (constant) density of events per unit anode length to the integral distribution at each amplitude. The integral distribution may be printed. The differential distribution is then derived, and the mean value of the distribution is output.

The quantity GMAX, which is the ratio of maximum gain to gain at the chamber center plane, is also output. For the normal case of a cathode uniform across both the end and anode regions (CATH and EIRA identical), the maximum multiplication will occur at the axial center plane. This is the situation in the example given in Fig. 15. If EIRA is reduced, the maximum gain may actually occur other than at the chamber center.

The differential distribution over four decades may be plotted next. Typical results are shown in Fig. 18.

After derivation of the "ideal" differential distribution, smoothing with a Gaussian may be done to approximate detector resolution. The percent full-width-at-half-maximum is required as input together with horizontal and vertical scaling. Typical results are shown in Figs. 19, 22, and 23.

Another code (not given here) uses the differential distribution in a polynomial fitting routine. The coefficients of a fifth-order fit are derived from the distribution below 0.70 of maximum, together with the fraction of the distribution in excess of 0.70 of maximum. These parameters are in a form suitable for subsequent use in simple integral unfolding routines used to correct measured spectra for response effects (see Sec. XI.B).

The FORTRAN code listing follows.

TABLE C.I. Input for Program That Transforms Field-to-Pulse-height Distribution

Card	Variable	Format	Description
1	Q	E12.5	Coefficient in the expansion of log A (see Sec. V.B).
	C1	E12.5	Coefficient in the expansion of log A.
	C2	E12.5	Coefficient in the expansion of log A.

The anode field strength and corresponding electrical volume, which were punched on paper tape in the program described in Appendix B, are read in.

The reference voltage VREF is input in F12.4 format on the teletype.

If smoothing of the distribution with a Gaussian is to be done, the percent full-width-at-half-maximum WIDTH and the amount the abscissa is to be scaled XNRM and the amount the ordinate is to be scaled YNRM are input in F12.4 format on the teletype.

```
C
C  FIELD TO PULSE HEIGHT TRANSFORMATION FOR COUNTERS WITH FIELD TUBES
C  AT ANODE POTENTIAL DEFINING THE ENDS.
C  RESULTS MAY BE FOLDED WITH A GAUSSIAN APPROXIMATION FOR RESOLUTION.
C
      DIMENSION V(125),Z(125),PAMP(100),XYZ(125),VOL(125)
      COMMON PAMP,Z,V,VOL
      EQUIVALENCE(Z(1),XYZ(1))
      G(I)=0.01*FLOAT(I)*GMAX
C  H IS THE VOLUME WEIGHT AT MESH POINT K AND S- THE MULTIPLICATION.
      H(K)=VOL(K-1)-VOL(K)
      S(K)=EXP((V(K)**Q)*(V(K)*C1+C2))
C
    6 FORMAT( I4,2E14.5)
    8 FORMAT(//32H INPUT REFERENCE VOLTAGE (F10.2)  //)
   10 FORMAT(//37H RATIO OF MAXIMUM GAIN TO NOMINAL IS-  F10.3)
   11 FORMAT( 16,2F12.6)
   12 FORMAT( 1H1,6H LISTED BELOW ARE TOTAL POINTS, ANODE LENGTH,  /
     X  44H MINIMUM MESH SPACING AND PROGRESSION RATIO, /
     X,60H AND FINALLY, THREE COEFFICIENTS WHICH PARAMETRIZE GAIN VS V/
     X/2X,I9,/(1PE15.5) )
   13 FORMAT(6E12.5)
   14 FORMAT(/51H INPUT THE AVERAGING FULL WIDTH (F12.4) IN PERCENT-  )
   15 FORMAT(//39H THE MEAN VALUE OF THE DISTRIBUTION IS  F8.4  //)
   16 FORMAT(//34H SCALE ABSCISSA BY AMOUNT (F12.4)-  )
   17 FORMAT(//34H SCALE ORDINATE BY AMOUNT (F12.4)-  )
   18 FORMAT( 54H SS2 LISTS INTEGRAL DIST. SS3 PLOTS DIFFERENTIAL DIST.
     X/ 51H SS4 PLOTS THE GAUSSIAN SMOOTHED DIFFERENTIAL DIST. //
     X        32H INPUT REFERENCE VOLTAGE (F12.4)  )
   19 FORMAT(F12.4)
   22 FORMAT( 1H1,45H                INTEGRAL AMPLITUDE DISTRIBUTION  //)
   23 FORMAT(  6X,I6,6X,E12.5,6X,I12,6X,E12.5)
C
      READ(3,13)Q,C1,C2
      CALL ASCII
      READ(2,11)MZ,BAND,RAND
      DO93 K=1,MZ
   93 READ(2,13)V(K),VOL(K)
C
C  CHECK THAT VOLUME WEIGHTS ARE CONSISTENT NEAR TIPS.
C
      K=MZ
   96 IF(VOL(K-1)-VOL(K))94,95,95
   94 VOL(K-1)=VOL(K)
   95 K=K-1
      IF(K-1)97,97,96
   97 BAND=BAND*(RAND**(FLOAT(MZ))-1.0)/(RAND-1.0)
      WRITE(1,12)MZ,BAND,BAND,RAND,Q,C1,C2
C
   92 WRITE(1,18)
      READ(1,19)VREF
      DO56 I=1,100
   56 PAMP(I)=0.0
      DO71 K=1,MZ
   71 V(K)=V(K)*VREF/V(MZ)
      AREF=S(MZ)
C
      Z(1)=0.0
      DO52 K=2,MZ
      DUM=S(K)
      IF(DUM-1.0)53,52,52
   53 DUM=1.0
   52 Z(K)=DUM/AREF
      GMAX=0.0
      DO91 K=1,MZ
   91 GMAX=AMAX1(GMAX,Z(K))
C
C  DETERMINE THE INTEGRAL AMPLITUDE DISTRIBUTION.
C
      I=1
   60 K=1
   68 IF(Z(K)-G(I))61,61,62
   61 K=K+1
      GO TO 68
   62 DZ=H(K)*(Z(K)-G(I))/(Z(K)-Z(K-1))
   31 K=K+1
      IF(K-MZ)32,32,65
```

```
   32 IF(G(I)-Z(K-1))33,33,34
   33 IF(G(I)-Z(K))35,35,36
   35 DZ=DZ+H(K)
      GO TO 31
   36 DZ=DZ+H(K)*(Z(K-1)-G(I))/(Z(K-1)-Z(K))
      GO TO 31
   34 IF(G(I)-Z(K))37,37,31
   37 DZ=DZ+H(K)*(Z(K)-G(I))/(Z(K)-Z(K-1))
      GO TO 31
   65 PAMP(I)=DZ
      I=I+1
      IF(I-100)60,88,88
C
C  LIST THE INTEGRAL DISTRIBUTION IF SSWTCH 2 IS UP.
C
   88 CALL SSWTCH(2,N)
      GO TO(76,77),N
   76 WRITE(4,22)
      DO78I=1,50
      NLL=I
      NLR=I+50
   78 WRITE(4,23) NLL,PAMP(NLL),NLR,PAMP(NLR)
C
C  CHANGE INTEGRAL TO DIFFERENTIAL DISTRIBUTION.
C
   77 DO54 I=1,99
   54 PAMP(I)=PAMP(I)-PAMP(I+1)
C
C  CALCULATE THE MEAN VALUE OF THE AMPLITUDE DISTRIBUTION.
C
      SUD=0.0
      AVG=0.0
      DO55 I=1,99
      AVG=FLOAT(I)*PAMP(I) + AVG
   55 SUD=SUD+PAMP(I)
      AVG=0.01*AVG/SUD
C
C  PRINT DETAILS OF THE DIFFERENTIAL DISTRIBUTION.
C
      WRITE(1,15)AVG
      WRITE(1,10) GMAX
C
C  IF SENSE 3 IS UP, PLOT THE TRANSFORMED DISTRIBUTION.
C  IF SENSE DOWN, DO NOT PLOT.
C  IF SENSE 4 IS UP, PLOT THE GAUSSIAN-SMOOTHED DISTRIBUTION.
C  IF SENSE 4 IS DOWN, DO NOT PLOT.
C
      PAUSE
      CALL SSWTCH(3,N)
      GO TO(58,47),N
C
C  PLOT DISTRIBUTIONS.  4 DECADES FOR AMPLITUDE, LINEAR FOR HEIGHT.
C
   58 YY1=0.0
      DO40 I=1,99
   40 YY1=AMAX1(YY1,PAMP(I))
      DO41 I=1,99
   41 PAMP(I)=10000.*PAMP(I)/YY1
      CALL PLOT(0.,0.,-3)
      CALL PLOT (10.,0.,3)
      CALL PLOT (10.,10.,2)
      CALL PLOT (0.,10.,2)
      CALL PLOT (0.,0.,3)
      CALL AXIS (0.,0.,10.,0.,0.,1.0,-17)
      CALL PLOT (0.,0.,3)
      CALL LOGAX (0.,0.,+23,10.0,90.0,4,4,0.20)
      CALL PLOT (0.,0.,3)
      DO 42 I=1,99
      X=10.0*G(I)/GMAX
      IF(PAMP(I)-1.0)43,43,44
   43 Y=0.0
      GO TO 45
   44 Y=10.0*ALOG(PAMP(I))/ALOG(10000.)
   45 CALL SYMBOL (X,Y,.45,.03,26,1)
   42 CONTINUE
      CALL PLOT (12.0,0.,3)
      PAUSE
   47 CALL SSWTCH(4,N)
      GO TO(48,92),N
C
C  FORM AVERAGE OVER A GAUSSIAN SHAPE FUNCTION.
C
   48 WRITE(1,14)
      READ(1,19)WIDTH
      DO149 I=1,125
  149 XYZ(I)=0.0
      DELTA = 4.*ALOG(2.)
      DO151 J=1,99
      EJ=FLOAT(J)
      DENGY=WIDTH*EJ/100.
      CON1=PAMP(J)*SQRT(DELTA/3.14159)/DENGY
      CON2=DELTA/(DENGY*DENGY)
      MOR=IFIX(SQRT(21./CON2))
      DO 152 K=1,125
      IF(J-K-MOR)150,150,152
  150 IF(K-J-MOR)153,153,152
  153 EK=FLOAT(K)
      ARG = (EJ-EK)*(EJ-EK)*CON2
      XYZ(K)=XYZ(K)+CON1* EXP(-ARG)
  152 CONTINUE
  151 CONTINUE
C
C  PLOT DATA.
C
      YY1=0.0
      DO75 I=1,125
   75 YY1 = AMAX1(YY1,XYZ(I))
      WRITE(1,16)
      READ(1,19)YNRM
      WRITE(1,17)
      READ(1,19)YNRM
C
      CALL PLOT(0.,0.,-3)
      CALL PLOT(13.,0.,2)
      CALL PLOT(13.,10.,1)
      CALL PLOT(0.,10.,1)
      CALL PLOT(0.,0.,1)
      XP=130.*XNRM/125.
      YP=XYZ(10)*10.0*YNRM/YY1
      CALL PLOT(XP,YP,3)
      DO73J=11,125
      XP=FLOAT(J)*(13./125.)*XNRM
      IF(XP-13.)72,73,73
   72 YP = (XYZ(J)/YY1)*10.0*YNRM
      CALL PLOT(XP,YP,2)
   73 CONTINUE
      CALL PLOT(15.,0.,3)
      PAUSE
      GO TO 92
      END
50
```

APPENDIX D

WALL-AND-END-EFFECT RESPONSE FUNCTION

Knowledge of the track-length probability functions and of the range-energy and stopping-power relations for a particular counter-gas filling permits the determination of the wall-and-end-effect response function (see Sec. VIII.A). At present the influence on the response function of events originating in the end regions is neglected—the response function is approximated by the first two terms on the right-hand side of Eq. 19. One has only to evaluate the track-length probability functions for: 1) a track starting in the sensitive region and ending in the sensitive region without distortion, $F(\ell)$, and 2) a track starting in the sensitive region and being truncated by the walls or extending into an end region, $N(\ell)$. This appendix describes the two codes that evaluate and parameterize the response function. The first code evaluates $F(\ell)$ and $N(\ell)$, as well as the first coefficient CLEG(1) in the expansion of the response function (see Sec. XI.B.3). The second code evaluates the distorted part of the response function over the energy region in which not all events are distorted—the region in which the upscatter correction is applied (see Sec. VIII.C). A Legendre fit is made to the distribution, and the coefficients CLEG(2) through CLEG(5) are determined. Appendix E considers the code for generating the proton-recoil distribution for the downscatter correction.

Under the assumption that the distribution of tracks is uniform and isotropic, the track-length probability function $F(\ell)$ for ℓ less than the diameter is [30]

$$
\begin{aligned}
F(\ell) = {} & [4(1-k^2)/(3\pi k)] \times [K(k) - F(\cos^{-1} m,k)] \\
& - [4(1+k^2)/(3\pi)] \times [E(k) - E(\cos^{-1} m,k)] \\
& + [(4k^2-1)/(4\pi\alpha k)] \times \sin^{-1} k - \left\{(2m/\pi)\right. \\
& \left. + [4k^2(1-m^2)-1]/(4\pi\alpha k)\right\} \times \sin^{-1} k(1-m^2)^{1/2} \\
& + m - km^2/(2\alpha) - \left\{[2km/(3\pi)] + [2k^2(1-m^2)+1]/(4\pi\alpha)\right\} \\
& \times \left\{(1-m^2)[1-k^2(1-m)]\right\}^{1/2} \\
& + [(1+2k^2)/(4\pi\alpha)] \times (1-k^2)^{1/2}, \qquad \text{(D1)}
\end{aligned}
$$

and for ℓ greater than the diameter

$$
\begin{aligned}
F(\ell) = {} & [4(k^2-1)/(3\pi)] \times \left\{K(1/k)\right. \\
& \left. - F[\sin^{-1} k(1-m^2)^{1/2},1/k]\right\} - [4(k^2+1)/(3\pi)] \\
& \times \left\{E(1/k) - E[\sin^{-1} k(1-m^2)^{1/2},1/k]\right\} \\
& - \left\{2m/\pi + [4k^2(1-m^2)-1]/(4\pi\alpha k)\right\} \\
& \times \sin^{-1} k(1-m^2)^{1/2} + m - 1/(8\alpha k) \\
& + k/(2\alpha)(1-m^2) \\
& - \left\{2km/(3\pi) + [2k^2(1-m^2)+1]/(4\pi\alpha)\right\} \\
& \times \left\{(1-m^2)[1-k^2(1-m^2)]\right\}^{1/2}. \qquad \text{(D2)}
\end{aligned}
$$

$F(\phi,k)$ and $E(\phi,k)$ are incomplete elliptic integrals of the first and second kind,

$$
\left.
\begin{aligned}
F(\phi,k) &= \int_0^{\phi} (1 - k^2 \sin^2\theta)^{-1/2}\, d\theta, \\
E(\phi,k) &= \int_0^{\phi} (1 - k^2 \sin^2\theta)^{-1/2}\, d\theta,
\end{aligned}
\right\} \qquad \text{(D3)}
$$

and $K(k) = F(\pi/2,k)$ and $E(k) = E(\pi/2,k)$. The parameters k and α are in units of radii and are

$$
\left.
\begin{aligned}
k &= \ell/(2a) \\
\text{and} \qquad & \\
\alpha &= L/(2a),
\end{aligned}
\right\} \qquad \text{(D4)}
$$

where a is the radius of the cylinder and L is the length of the sensitive region. The parameter m is the smaller of L/ℓ and 1.

The track-length probability function $N(\ell)$, where $N(\ell)\, d\ell$ is the probability that a path length is between ℓ and $\ell + d\ell$, is, for ℓ less than the diameter,

$$
\begin{aligned}
N(\ell) = {} & [2(1-k^2)/(3\pi\alpha k^2)] \times [K(k) - F(\cos^{-1} m,k)] \\
& - [2(1-2k^2)/(3\pi\alpha k^2)] \times [E(k) - E(\cos^{-1} m,k)] \\
& - [(1+4k^2)/(8\pi\alpha\alpha k^2)] \times \sin^{-1} k \\
& + \left\{[1+4k^2(1-m^2)]/(8\pi\alpha\alpha k)\right\} \times \sin^{-1} k(1-m^2)^{1/2} \\
& + m^2/(4\alpha a) + \left\{2m/(3\pi a) + [6k^2(1-m^2)-1]/(8\pi\alpha\alpha k)\right\} \\
& \times \left\{(1-m^2)[1-k^2(1-m^2)]\right\} \\
& + [(1-6k^2)/(8\pi\alpha\alpha k)] \times (1-k^2)^{1/2}, \qquad \text{(D5)}
\end{aligned}
$$

and, for ℓ greater than the diameter,

$$
\begin{aligned}
N(\ell) = {} & [2(2k^2-1)/(3\pi\alpha k)] \times \left\{E(1/k) - E[\sin^{-1} k(1-m^2)^{1/2},1/k]\right\} \\
& - [4(k^2-1)/(3\pi\alpha k)] \qquad \text{(D6)}
\end{aligned}
$$

(Contd.)

(Contd.) (D6)

$$\times \left\{K(1/k) - F[\sin^{-1}k(1-m^2)^{1/2}, 1/k]\right\}$$
$$+ \left\{[2m/(3\pi a)] + [6k^2(1-m^2)-1]/(8\pi a a k)\right\}$$
$$\times \left\{(1-m^2)[1-k^2(1-m^2)]\right\}^{1/2}$$
$$+ \left\{[4k^2(1-m^2)+1]/(8\pi a a k^2)\right\} \times \sin^{-1}k(1-m^2)^{1/2}$$
$$- [1+4k^2(1-m^2)]/(16 a a k^2).$$

$F(\ell)$ is related to $N(\ell)$ by

$$F(\ell) = \int_{\ell}^{\ell_{max}} N(\ell)\, d\ell, \qquad (D7)$$

where $\ell_{max} = (L^2 + 4a^2)^{1/2}$. Calculated $F(\ell)$ and $N(\ell)$ are shown in Figs. 24 and 25, respectively.

Besides the track-length probability functions, one must have the range-energy and stopping power $\epsilon(E)$ relationships. We will consider only the relationships for methane gas; similar ones may be worked out for hydrogen. A parameterization of $\epsilon(E)$ for methane at 76 cm Hg and 15°C was determined from a fit to the data contained in Ref. 34. For E greater than 300 keV, $\epsilon(E)$ was fit with the Bethe-Block formula

$$\epsilon(E) = \frac{0.235}{E}(10.0 \ln E + 40.0). \qquad (D8)$$

in the energy range of 30 to 300 keV, a fifth-order least-squares approximation to the data was used. For E less than 30 keV the data was approximated by

$$\epsilon(E) = 155.1\, E^{0.4}. \qquad (D9)$$

The ranges were taken from the table of Ref. 34. For E less than 30 keV, the ranges were determined to be consistent with the energy dependence assumed for ϵ in this range; i.e., the ranges were determined from

$$R(E) = \int_0^E \frac{dE}{\epsilon(E)}. \qquad (D10)$$

The uncertainties associated with the data below 30 keV are rather large. Fortunately, these uncertainties have little effect in the calculation of the response function.

The first program calculates the track-length probability function $F(\ell)$ and $a^*N(\ell)$ for values of $k = \ell/(2a)$ at which the elliptic integrals are evaluated. The values of the elliptic integrals may be obtained from interpolation of the tables in Ref. 35. The input variables and their formats are indicated in Table D.I. The track-length probability functions depend only on the counter geometry and are independent of the counter gas. However, since CLEG(1) is simply equal to $F(R_0)$ at E_0 corresponding to R_0, it is convenient to evaluate CLEG(1) in this program. The range-energy table must be input so that E_0 may be determined. The factor P times the density associated with the range-energy table gives the density of the counter gas for which CLEG(1) is evaluated. The output includes the input track length, E_0, CLEG(1), and the track-length probability functions $F(\ell)$ and $a^*N(\ell)$. The program is written for the SEL-840, and a listing appears at the end of this appendix.

The second program calculates the distorted part of the response function for a particular track length and fits it with a Legendre polynomial expansion. The function $a^*N(\ell)$ is only evaluated at certain values of ℓ in the first

TABLE D.1. Input for Program that Determines Track-length Probability Functions and CLEG(1)

Card	Variable	Format	Description
1	NPROB	17A 4	Title card—up to 68 characters.
2	A	E12.5	Radius in cm.
	SL	E12.5	Length of sensitive region in cm. Enter as 0, if L is infinite.
	P	E12.5	Pressure in atm at 15°C.
3-7	E	12F6.4	Energies in MeV in increasing magnitude at which the ranges are specified.
8-12	RGE	12F6.4	Corresponding proton ranges in cm.
	For each value of ℓ at which the track-length probability functions are to be calculated, one or two cards are required.		
13a	C	E12.5	Track length divided by the diameter k; $k = \ell/(2a)$.
	ASIN	E12.5	$\sin^{-1}$; deleted for k greater than one.
	F90	E12.5	Complete elliptic integral of first kind K(k); $K(k) = F(\pi/2,k)$.
	E90	E12.5	Complete elliptic integral of second kind E(k); $E(k) = E(\pi/2,k)$.
	If ℓ is greater than the length of the sensitive region, SL, card 13b is required.		
13b	BSIN	E12.5	$\sin^{-1}k(1-m^2)^{1/2}$ with m equal to the sensitive length divided by the track length.
	FIN	E12.5	Incomplete elliptic integral of first kind $F(\phi,k)$. For k less than one, $F(\cos^{-1} m,k)$; for k greater than one, $F[\sin^{-1} k(1-m^2)^{1/2}, 1/k]$.
	EIN	E12.5	Incomplete elliptic integral of second kind $E(\phi,k)$. For k less than one, $E(\cos^{-1} m,k)$; for k greater than one, $E[\sin^{-1} k(1-m^2)^{1/2}, 1/k]$.
Last	Cards 13a and 13b are repeated for each value of ℓ.		
	The program is terminated by a negative value of C on card 13a.		

program; it is necessary to have a continuous representation of it for the calculation of the response function. From Fig. 25 it is seen that $N(\ell)$ undergoes rapid change in shape near values of ℓ equal to the counter diameter. It was found that two sets of coefficients from least-squares polynomial fits of fifth order, one set for values of ℓ less than a diameter and the other for values greater than the diameter, adequately represent $a*N(\ell)$.

The two sets of coefficients and boundary value of ℓ between the two sets are input to the second program, as well as a range-energy table, the density factor, and EA and EB, which refer to the stopping cross-section data. The stopping cross-section data, or dE/dx data, are input as the statement functions EP1, EP2, and EP3. The variable EA defines the boundary between EP1 and EP2, and EB defines the boundary between EP2 and EP3. The input variables and their formats are shown in Table D.II.

For an input value of the range R_0, the program first calculates the corresponding value of E_0 from the range-energy table. A hundred equal-energy intervals are formed between zero and E_0. Using the stopping cross-section data, the range-energy table, and the approximation to $a*N(\ell)$, the values of the distorted part of the response function are calculated at values of E in the middle of each interval.

The hundred calculated points are plotted on a Calcomp plotter. Sense switch 1 is set up if scales are desired. Because of the rapid variation of the distorted distribution for small values of E_0 near the energy E_0 (see Fig. 29), it is desirable to modify the end part of the distribution before fitting is attempted. After the distribution is plotted, an integer, NFIT, is input on the teletype, and the program sets all points greater than the NFIT point equal to the value of the distribution at the NFIT point.

The program then performs a Legendre-polynomial analysis of the distorted distribution with four polynomials. The Legendre-polynomial coefficients are represented by C(1) through C(4). In terms of the coefficients listed in Sec. XI.B.3, the correspondence is that CLEG(2) through CLEG(5) are equal to C(1) through C(4), respectively. CLEG(2) is simply 1 - CLEG(1), when events from the ends are neglected. However, both CLEG(1) and CLEG(2) are kept as independent coefficients, so that when end events are included, no further modifications will be necessary to the data-reduction codes. The coefficients C(2) through C(4) [CLEG(3) through CLEG(5)] are normalized as if C(1) [CLEG(2)] were one. This permits a better fit to the coefficients at low energies. In the expansion of the response function (see Eq. 31), it is thus necessary to multiply the last three coefficients by CLEG(2). A FORTRAN listing for the SEL-840 appears at the end of this appendix.

From the first program, one has CLEG(1) for various values of E_0, and from the second program, CLEG(2) through CLEG(5) for various values of E_0. It was found that a satisfactory continuous representation of each coefficient could be obtained by a fifth-order least-squares polynomial approximation. The program for the fitting is not included here. Figures 38–41 show this fit. The coefficients of the least-squares fit parameterize the response function for energies at which there are still undistorted tracks. For higher energies no such simple parameterization is possible (see Appendix E).

TABLE D.II. Input for Program that Determines the Legendre Polynomial Coefficients for the Distorted Part of the Response Function

Card	Variable	Format	Description
1	NPROB	17A 4	Title card—up to 68 characters.
2	P	E12.5	Pressure in atm at 15°C.
	CUT	E12.5	For ℓ less than CUT, one set of coefficients for $a*N(\ell)$ is used; for ℓ greater than CUT, the other ℓ is input in cm.
	EA	E12.5	For energies less than EA, the function EP1 is used to determine dE/dx.
	EB	E12.5	For energies between EA and EB, the function EP2 is used to determine dE/dx. Both EA and EB are entered in MeV.
3-4	CAN	6E12.5	The coefficients of the polynomial expansion that approximates $a*N(\ell)$. The first six coefficients are for ℓ less than CUT, and the second six for ℓ greater than CUT.
5-9	E	12F6.4	Energies in MeV in increasing magnitude at which the ranges are specified.
10-14	RGE	12F6.4	Corresponding proton ranges in cm.
	For each value of R_0 at which the Legendre coefficients are to be calculated, one card is required.		
15	RO	E12.5	Range in cm of proton at which the coefficients are to be determined.
	After the distribution is plotted on the Calcomp, the integer NFIT is read in on the typewriter in I3 format. Use of NFIT in program is explained in text.		
Last	The program is terminated by a negative value of RO on Card 15.		

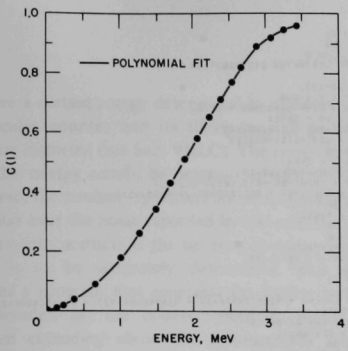

Fig. 38. Energy Dependence of Coefficient C(1) of First Legendre Polynominal for Counter with 1.27-cm Radius and 8.25-cm length Filled with 6.5 atm Methane. The curve is a fifth-order least-squares polynominal approximation. ANL Neg. No. 113-2315 Rev. 1.

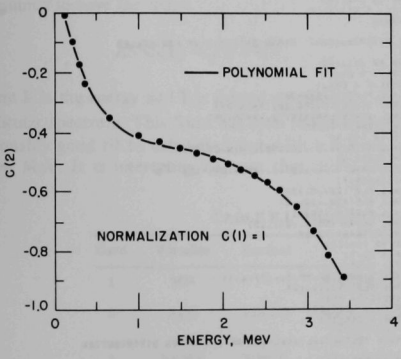

Fig. 39. Energy Dependence of Coefficient C(2) of Second Legendre Polynomial from Fits to Calculated Distorted Part of Response Function. The curve is a fifth-order least-squares polynomial approximation. The normalization is for C(1) equal to unity. ANL Neg. No. 113-2306 Rev. 1.

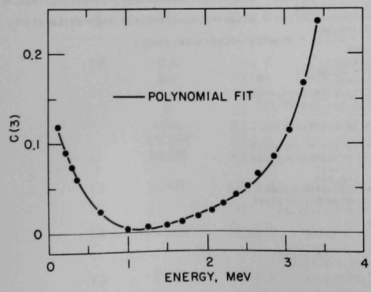

Fig. 40. Energy Dependence of Coefficient C(3) of Third Legendre Polynomial from Fits to Calculated Distorted Part of Response Function. The curve is a fifth-order least-squares polynomial approximation. The normalization is for C(1) equal to unity. ANL Neg. No. 113-2310 Rev. 1.

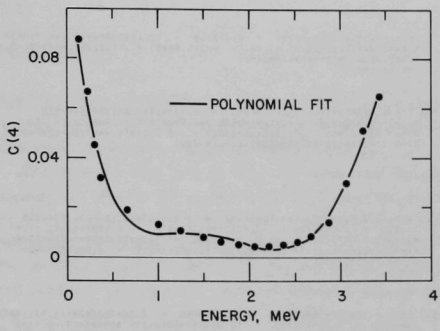

Fig. 41. Energy Dependence of Coefficient C(4) of Fourth Legendre Polynomial from Fits to Calculated Distorted Part of Response Function. The curve is a fifth-order least-squares polynomial approximation. The normalization is for C(1) equal to unity. ANL Neg. No. 113-2311 Rev. 1.

The FORTRAN code listing follows.

```
C  DETERMINATION OF THE TRACK LENGTH PROBABILITY
C  FUNCTIONS F(L) AND AN(L) AND OF CLEG(1)
10
      DIMENSION E(60),RGE(60)
      COMMON E, RGE
15
    1 FORMAT(6E12.5)
    2 FORMAT(    6X,8HRADIUS = E12.5,3H CM,8X,18HSENSITIVE LENGTH = E12.
     X5,3H CM,/,6X,1/PRESSURE FACTOR =  E12.5 / /)
    3 FORMAT(12F6.4)
    4 FORMAT(1HO,3X,4HL  CM,9X,2HE0,7X,7HCLEG(1),7X,4HF(L),8X,5HAN(L) )
  199 FORMAT(17A4)
  299 FORMAT(1H1/ X 1/A4)
C
      READ(4,199) NPROB
      WRITE(5,299) NPROB
      READ(4,1) A,SL,P
      WRITE(5,2) A,SL,P
      READ(4,3) E
      READ(4,3) RGE
      WRITE(5,4)
      DO 64 J = 1,60
   64 RGE(J) = RGE(J)/P
      DO 70 J = 1,60
      N = 61-J
      IF(RGE(N)) 70,70,9
   70 CONTINUE
    9 IF(SL) 10,10,11
   10 AB = 0.0
      GO TO 12
   11 AB = 2.*A/SL
   12 READ(4,1) C,ASIN,F90,E90
      AL = 2.*A*C
      IF(C) 99,13,14
   13 F = 1.0
      C1 = 0.0
      E0 = 0.0
      AN = 0.5 + 0.25*AB
      GO TO 69
   14 C2 = C*C
      C21 = 1.-C2
      IF(C-1.0) 114,114,115
  114 SC21 = SQRT(C21)
  115 IF(SL) 17,17,15
   15 AM = SL/(2.*A*C)
      IF(AM-1.) 16,17,17
   16 READ(4,1) BSIN, FIN, EIN
      GO TO 18
   17 AM = 1.0
      FIN = 0.0
      EIN = 0.0
      BSIN = 0.0
   18 AM2 = AM*AM
      AM21 = 1.-AM2
      SAM21 = SQRT(AM21)
   29 IF(C-1.0) 25, 90, 95
C
C  EVALUATION OF F(L)
C
C
C     K LESS THAN 1
C
   25 F1= 0.424414*C21/C*(F90-FIN)  -  0.424414*(1.+C2)/C*(E90-EIN)
     X  +  (4.*C2-1.)/(12.566636*C)*AB*ASIN  -  (0.636620*AM*(4.*C2*AM21
     X-1.)*AB+0.0/95/25/C)*BSIN
      F2 = AM - C*AM2*0.5*AB  -  (0.212207*C*AM*(2.*C2*AM21+1.)*0.079577
     X5*AB)*SAM21+SQRT(1.-C2*AM21)  +  (1.+2.*C2)*0.0795775*AB*SC21
      F = F1 + F2
      GO TO 125
C
C     K EQUALS 1
```

```
C
   30 F = -0.848828*(1.-EIN)  +  0.375*AB  -  (0.636620*AM*(3.-4.*AM2)*
     X AB*0.0795775)*BSIN  +  AM  -  AM2*0.5*AB  -  (0.212207*AM*(3.-2.*
     X AM2)*0.07957775*AB)*AM*SAM21
      GØ TØ 130
C
C
C     K GREATER THAN 1
C
   35 F = 0.424414*(-C21)*(F90-FIN)  -  0.424414*(C2+1.)*(E90-EIN)
     X  -  (0.636620*AM*(4.*C2*AM21-1.)*AB*0.0795775/C)*BSIN  +  AM
     X  -  AB/(8.*C)  +  0.5*C*AB*AM21  -  (0.212207*C*AM*(2.*C2*AM21+1.
     X)*0.07957775*AB)*SAM21*SQRT(1.-C2*AM21)
      GØ TØ 135
C
C  EVALUATION ØF AN(L)
C
C     K LESS THAN 1
C
  120 AN = 0.212207*C21/C2*(F90-FIN)  -  0.212207*(1.-2.*C2)/C2*(E90
     X-EIN)  -  0.0397888*(1.+4.*C2)*AB/C2*ASIN  +  0.0397888*(5.+4.*
     XC2*AM21)*AB/C2*BSIN  +  0.25*AM2*AB  +  (0.212207*AM+0.0397888*
     XAB*(6.*C2*AM21-1.)/C)*SAM21*SQRT(1.-C2*AM21)  +  0.0397888*AB*(
     X1.-6.*C2)/C*SC21
      GØ TØ 40
C
C     K EQUALS 1
C
  130 AN = 0.212207*(E90-EIN)  -  0.3125*AB  +  0.0397888*AB*(1.+4.*AM21
     X)*BSIN  +  0.25*AM2*AB  +  (0.212207*AM*0.0397888*AB*(5.-6.*AM2)
     X)*AM*SAM21
      GØ TØ 40
C
C     K GREATER THAN 1
C
  135 AN = 0.212207*(2.*C2-1.)/C*(E90-EIN)  -  0.424414*(-C21)/C*(F90-
     XFIN)  +  (0.212207*AM+0.0397888*AB*(6.*C2*AM2-1.))*SAM21*SQRT(1.-
     XC2*AM21)  +  0.0397888*AB*(4.*C2*AM21+1.)/C2*BSIN  -  (1.+4.*C2*
     XAM21)*AB/(16.*C2)
  40 EVALUATION ØF C1(E0) AND E0
C
   40 C1 = F
   60 IF(AL-HGE(N)) 66,65,65
   65 E0 = -1.0
      GØ TØ 69
   66 DØ 68 J = 2,N
      IF(AL - HGE(J)) 67,67,68
   67 RATIØ = (AL - HGE(J-1))/(RGE(J) - RGE(J - 1))
      E0 = E(J - 1) + RATIØ*(E(J) - E(J - 1))
      GØ TØ 69
   68 CØNTINUE
C
C  PRINT RESULTS
C
   69 WRITE (5,1) AL,E0,C1,F,AN
      GØ TØ 12
   99 STØP
      END
$D
C
C
C  DETERMINATIØN ØF THE LEGENDRE CØEFFICIENTS
C  C2(E0), C3(E0) AND C4(E0)
C
      DIMENSIØN CAN(12),E(60),RGE(60),EN(100),C(100),CS(100),ENS(100),
     XNPRØB(17),ASUBF(4)
C
      CØMMØN CAN,E,RGE,EN,C,CS,ENS
C
C  DE/DX DATA FØR PRØTØNS IN METHANE
C
      LESS THAN 30 KEV
      EP1(ZZ) = 152.1*(ZZ**0.40)
C  30 TØ 300 KEV
      EP2(ZY) = ZY*(555.9812 + ZY*(-6.468577E+3 + ZY*(2.67778
     X1E**4 + ZY*(-4.3/3933E+4 + ZY*1.756109E+4))))
      GREATER THAN 300 KEV
      EP3(ZX) = 0.235/ZX*(10.*ALØG(ZX) + 40.0)
C
    1 FØRMAT(17A4)
    2 FØRMAT(6E12.5)
    3 FØRMAT(12F6.4)
    4 FØRMAT(1H1/ X 17A4//10X, 17HPRESSURE FACTØR =  E12.5// )
    5 FØRMAT(/26H ENERGY TØ HIGH FØR TABLE    )
    6 FØRMAT ( 45H LEGENDRE PØLY FIT ØF DISTØRTED DISTRIBUTIØN     )
    7 FØRMAT( 7H ENERGY )
    8 FØRMAT(5H H0 =  F7.4, 2X 4HE0 = F7.4  )
    9 FØRMAT(I3)
   10 FØRMAT(// 16HOLEGENDRE CØEFF   )
   11 FØRMAT(10X  2HCI  11,3H) = E12.5 )
C
      READ(4,1) NPRØB
      READ(4,2) P,CUT,EA,EB
      READ(4,2) CAN
      READ(4,3) E
      READ(4,3) RGE
      WRITE(5,4) NPRØB,P
C
C  FØRM RANGE TABLE FØR CØUNTER CØNDITIØNS
C
      DØ 20 I = 1,60
   20 HGE(I) = RGE(I)/P
      DØ 21 J = 1,60
      NN = 61-J
      IF(RGE(NN)) 21,21,22
   21 CØNTINUE
C
C  READ RØ AND DETERMINE E0
   22 READ(4,2) RØ
      IF(RØ) 99,122,122
  122 IF(RØ-RGE(NN)) 23,23,123
  123 WRITE(1,5)
      GØ TØ 22
   23 DØ 25 J = 2,NN
      IF(RØ-RGE(J)) 24,24,25
   24 RATIØ = (RØ-RGE(J-1))/(RGE(J)-RGE(J-1))
      E0 = E(J-1) + RATIØ*(E(J)-E(J-1))
      GØ TØ 26
   25 CØNTINUE
C
C  CALCULATE DISTØRTED DISTRIBUTIØN
C
   26 DE = E0/100.
      DØ 39 I = 1,100
      EN(I) = FLØAT(I-1)*DE + DE/2.
      EØUT = E0 - EN(I)
      IF(EØUT-E(1)) 126,28,127
  126 RØUT = EØUT/E(1)*RGE(1)
      GØ TØ 30
  127 DØ 29 J = 2,NN
      IF(EØUT-E(J))27,28,29
   27 RATIØ = (EØUT-E(J-1))/(E(J)-E(J-1))
      RØUT = RGE(J-1) + RATIØ*(RGE(J)-RGE(J-1))
      GØ TØ 30
   28 RØUT = RGE(J)
      GØ TØ 30
   29 CØNTINUE
   30 RIN = RØ-RØUT
      IF(RIN-CUT) 31,31,32
   31 K = 1
      GØ TØ 33
   32 K = 7
   33 ANN = CAN(K) + RIN*(CAN(K+1) + RIN*(CAN(K+2) + RIN*(CAN(K+3) +
     XRIN*(CAN(K+4) + RIN*CAN(K+5)))))
      IF(EØUT-EA) 34,34,35
   34 DEDL = EP1(EØUT)
      GØ TØ 38
   35 IF(EØUT-EB) 36,36,37
   36 DEDL = EP2(EØUT)
      GØ TØ 38
   37 DEDL = EP3(EØUT)
   38 C(I) = ANN/DEDL
   39 CØNTINUE
      SUM = 0.
      DØ 40 I=1,100
   40 SUM = SUM + C(I)
      DØ 41 I=1,100
   41 C(I) = C(I)/SUM
      PAUSE
C
C  PLØT DISTRIBUTIØN.  SENSE SWITCH 1 UP FØR SCALES
C
      DØ 42 J=1,100
      CS(J) = C(J)
   42 ENS(J) = EN(J)
      CALL PLØT(0.,0.,-3)
      CALL SCALE(CS,100,10.,YMIN,DY)
      CALL SCALE(ENS,100,12.,XMIN,DX)
      CALL SSWTCH(1,K)
      GØ TØ (43,44    ),K
   43 CALL AXIS(0.,0.,10.,90.,YMIN,DY,45)
      WRITE(16,6)
      CALL AXIS(0.,0.,12.,0.,XMIN,DX,-12)
      WRITE(16,7)
      CALL PLØT(12.,0.,3)
      CALL PLØT(12.,10.,2)
      CALL PLØT(0.,10.,1)
   44 CALL SEIGR(5.,9.,0.,.10)
      WRITE(16,8) RØ,E0
      DØ 45 I=1,190
      YP = CS(I)
      XP = ENS(I)
   45 CALL SYMBOL(XP,YP,0.,.07,4.3)
      CALL PLØT(12.,0.,3)
      READ(1,9) NFIT
      DØ 46 K=NFIT,100
   46 C(J) = C(NFIT)
C
C  LEGENDRE PØLYNØMIAL ANALYSIS ØF DISTØRTED DISTRIBUTIØN
C
      DØ 47 I=1,100
   47 CS(I) = 0.0
      WRITE(5,8) RØ,E0
      DØ 50 N=1,4
      ANG = EN(1)/E0
      ASUBF(N) = C(1)*PLEG(N,ANG)*2.*EN(1)/E0
      DØ 48 J=2,99
      ANG = EN(J)/E0
   48 ASUBF(N) = ASUBF(N) + C(J)*PLEG(N,ANG)*(EN(J+1)-EN(J-1))/(2.*E0)
      ANG = EN(100)/E0
      ASUBF(N) = ASUBF(N) + C(100)*PLEG(N,ANG)*(2.*(E0-EN(100)))/E0
      DØ 49 J=1,100
   49 CS(J) = CS(J) + ASUBF(N)*PLEG(N,EN(J)/E0)
   50 CØNTINUE
      WRITE(5,10)
      TNØRM = ASUBF(1)
      DØ 51 I=1,4
      ASUBF(I) = ASUBF(I)/TNØRM
   51 WRITE(5,11) I,ASUBF(I)
C
C  PLØT FIT TØ DISTRIBUTIØN
C
      FIT = (CS(1) - YMIN)/DY
      CALL PLØT(ENS(1),FIT,3)
      CALL PLTX(16)
      DØ 52 I=2,100
      FIT = (CS(I)-YMIN)/DY
   52 CALL PLØT(ENS(I),FIT,1)
      CALL PLØT(14.,0.,3)
      GØ TØ 22
   99 STØP
      END
      FUNCTIØN PLEG(N,ARG)
      GØ TØ (1,2,3,4),N
    1 PLEG= 1.
      RETURN
    2 PLEG=(2.*ARG - 1.)*1.73205
      RETURN
    3 PLEG=(5.*ARG*(ARG-1.) + 1.)*2.23607
      RETURN
    4 PLEG = (-1.*ARG*(12.-ARG*(30.-ARG*20.)))*2.64575
      RETURN
      END
```

APPENDIX E

THE DOWNSCATTER MATRIX

Above a certain energy determined by the dimensions of a particular counter and its filling gas, all proton-recoil tracks are distorted (see Sec. VIII.C). The neutron spectrum above this energy cannot be determined with this counter. Of course, the neutron spectrum above this energy creates ionization over the range recorded by the counter and must be taken into account if the neutron spectrum below this energy is to be accurately determined. This appendix describes a program that generates the ionization distribution recorded by the counter from an input neutron spectrum extending above the measurement limit. This distribution is used in the downscatter correction section of the data-reduction code for correction of wall-and-end effects in the methane counter (see Sec. XI.B.3).

The asymptotic neutron spectrum above some energy E_c is assumed to have the shape

$$ASNS(E) = \sqrt{E}\, e^{-E/T}, \qquad (E1)$$

where E is the energy and T is a constant characteristic of a particular spectrum. This form has been found to provide a reasonably good fit to calculated fast-reactor spectra above a few MeV. It is interesting to note that this is the same analytical form as that used to describe the prompt-fission neutron energy spectrum [36]. The energy E_c is chosen to be somewhat below the highest energy data point.

The proton-recoil distribution is calculated for this asymptotic neutron spectrum. The neutron spectrum below E_c is zero, and thus the proton-recoil distribution is flat below E_c. This proton-recoil distribution is folded in with the counter response function to produce the downscatter distribution. The counter response function for energies greater than E_c is evaluated with the subroutine RESP(EZERO). The influence of events from the end regions is neglected. Using an input parameterization of $a*N(\ell)$ and a range-energy table and stopping power parameterization (see Appendix D), the distorted part of the response function is evaluated at a hundred equally spaced energy points between zero and E_0. The contained fraction at each E_0 is determined from an input fit to $F(E_0)$ over the energy range from E_c to the energy at which the contained fraction goes to zero. The fit to the contained fraction must join smoothly at E_c to CLEG(1), which is identical to the contained fraction for energies less than E_c. The response function for energies less than E_c is determined from the Legendre polynomial parameterization

TABLE E.I. Input for Program that Determines the Downscatter Matrix

Card	Variable	Format	Description
1	MN	16	Number of methane runs.
2	A(J)	5E12.5	Ionization per channel; same information as on header tape for PSNS programs.
3	RLME	E12.5	An energy cutoff E_c below the highest-energy point. The calculated proton-recoil distribution is normalized to the measured distribution between E_c and highest datum point.
4-8	CPFT	6E12.5	The polynomial expansion for the Legendre coefficients that describe the response function below E_c; same coefficients are used in PSNS 3.
9	T	E12.5	Constant that appears in Eq. E1 which is determined from fit to spectrum above E_c; input in units of keV.
10	EA	E12.5	For energies less than EA, the function EP1 is used to determine dE/dx.
	EB	E12.5	For energies between EA and EB, the function EP2 is used to determine dE/dx. Both EA and EB are entered in MeV.
	P	E12.5	Gas pressure in atm at 15°C.
	DIA	E12.5	Diameter of counter in cm.
	CLEN	E12.5	Sensitive length of counter in cm.
	ELIM	E12.5	Above this energy, all proton-recoil tracks are distorted; input in MeV.
11	CAN	6E12.5	Coefficients of polynomial expansion which approximate $a*N(\ell)$ for ℓ less than the diameter.
12	CLAN	6E12.5	Coefficients of polynomial expansion which approximate $a*N(\ell)$ for ℓ greater than the diameter.
13	CC1	6E12.5	Coefficients of polynomial expansion which specify the contained fraction as a function of energy in MeV for energies greater than E_c.
14-18	E	12F6.4	Energies in MeV in increasing magnitude at which ranges specified.
19-23	RGE	12F6.4	Corresponding proton ranges in cm.

(see Appendix D). The output consists of that part of the downscatter matrix from events above E_C and the complete downscatter matrix. The downscatter matrix is determined in the same format and over the same energy range as the methane data that is to be corrected—i.e., MN sets of data with a hundred energy channels in each set. The normalization at this point is irrelevant; it is determined later when this calculated distribution is normalized to the measured distribution over the energy range from E_C to the top of the measured data.

The input format for the downscatter matrix calculation is listed in Table E.I. A FORTRAN listing of the program for the SEL-840 follows.

```
C     CONNECTION TO MEASURED METHANE PROTON RECOIL DISTRIBUTIONS FOR
C     HIGH ENERGY NEUTRONS ASSUMING THAT THE SPECTRUM OF THESE
C     NEUTRONS IS MAXWELLIAN WITH TEMPERATURE T.
C
      DIMENSION CAN(6),CLAN(6),CC1(6),E(60),RGE(60),C(101),EN(101),
     XRAPS(100,3),A(3),CPFT(6,5),PRD(200),CLEG(5)
      COMMON EA,EB,NN,DIA,CLEN,ELIM,CAN,CLAN,CC1,E,RGE,C,EN
C
      EPRD(M)=DE*FLOAT(M)*RLME
C ENERGY VALUES FOR THE DATA ARRAY DERIVED FROM THE EXPRESSION-
      CHEN(I,J)=A(J)*FLOAT(I*28)
C THE ASYMPTOTIC NEUTRON SPECTRUM IS ASSUMED TO HAVE THE SHAPE-
      ASN3(ENERGY)=SQRT(ENERGY)*EXP(-ENERGY/T)
C
    1 FORMAT(I6)
    2 FORMAT(5E12.5)
    3 FORMAT(6E12.5)
    4 FORMAT(1H0//// 12X,37H  COMPLETED DOWNSCATTER SPECTRUM LIST //)
    5 FORMAT(1H1///4/H  LISTED BELOW ARE RESPONSE LIMIT RLME FOLLOWED
     X/39H  BY THE A(J) VALUES SPECIFYING THE SPECTRUM ENERGY FORMAT. /
     X9H  THEN ARE LISTED VALUES FOR EA,EB,P,DIA,CLEN,ELIM  /
     X 43H  AND FINALLY THE FAST NEUTRON TEMPERATURE.  //)
    6 FORMAT(12F6.4)
    7 FORMAT(1H0//// 12X,36H  DOWNSCATTER FROM EVENTS ABOVE RLME  //)
C
      READ(4,1) MN
      READ(4,2)(A(J),J=1,MN)
C
C     INPUT HIGH ENERGY  CUT-OFF RLME. RLME MUST BE CHOSEN BELOW THE
C     HIGHEST ENERGY DATUM POINT BUT NOT BELOW 2 MEV. ALSO INPUT LEGENDRE
C     EXPANSION COEFFICIENTS WHICH PARAMETRIZE RESPONSE BELOW RLME.
C
      READ(4,3) RLME
      DO12 I=1,5
   12 READ(4,3) (CPFT(J,I),J=1,6)
C
C     INPUT THE MAXWELLIAN TEMPERATURE T FOR NEUTRONS IN THE
C     ASYMPTOTIC ENERGY REGION.  DIMENSION FOR T IS IN KILOVOLTS.
C
      READ(4,3) T
C
C     READ THE GAS AND DETECTOR PARAMETERS NEEDED TO DERIVE THE RESPONSE.
C
      READ(4,3) EA,EB,P,DIA,CLEN,ELIM
      READ(4,3) CAN
      READ(4,3) CLAN
      READ(4,3) CC1
      READ(4,6) E
      READ(4,6) RGE
C
C     LIST THE VARIOUS DATA WHICH HAS BEEN INPUT.
C
      WRITE(5,5)
      WRITE(5,2) RLME
      WRITE(5,3)(A(J),J=1,MN)
      WRITE(5,3) EA,EB,P,DIA,CLEN,ELIM
      WRITE(5,3) T
      PAUSE
C
C     FORM RANGE TABLE FOR COUNTER PRESSURE
C
      DO 23 I = 1,60
   23 RGE(I) = RGE(I)/P
      DO 21 J = 1,90
      NN = 61-J
      IF(RGE(NN)) 21,21,20
   21 CONTINUE
C
C     COMPUTE THE ACTUAL PROTON RECOIL DISTRIBUTION (PRD) ABOVE RLME.
C     THE DISTRIBUTION BELOW RLME WILL BE FLAT.
C
   20 DE=(10000.- RLME)/200.
      PRD(200)=0.0
      I=199
   42 X=EPRD(I)
      T1 =  -1.86*X*(9.415E-05)+X*X*(1.306E-10)
      T2 =  0.4223*X*(1.30E-04)
      SIG =  9.424B/(X*(1.206E-03)+T1*T1)+3.1416/(X*(1.206E-03)+T2*T2)
      PRD(I)=PRD(I+1)+DE*ASN3(X)*SIG/(X*X)
      I=I-1
      IF(I)43,43,42
   43 APD=PRD(1)
C
C     EVALUATE THE DOWN-SCATTER FROM EVENTS ABOVE THE LIMIT RLME.
C     THE RESPONSE SPECTRUM C(I) HAS ALL OF THE CONTAINED FRACTION IN
C     C(101) AND THE REST DISTRIBUTED FROM 1 TO 100.
C
      DO56 J=1,MN
      DO56 I=1,100
   56 RAPS(I,J)=0.0
      K=199
   52 EZERO=EPRD(K)
      CALL RESP(EZERO)
      SPRD(K)=DE/EZERO
      DO60 J=1,MN
      DO60 I=1,100
   62 U=CHEN(I,J)
      IF(U-EZERO)58,58,60
   58 IF(U-EZERO+DE)59,59,61
   61 RAPS(I,J)=RAPS(I,J)+C(101)*PRD(K)
      I=I+1
      IF(I-100)62,62,60
   59 DO54 L=2,100
      IF(EN(L)-U) 54,54,57
   54 CONTINUE
   57 RAPS(I,J)=RAPS(I,J)+S*(C(L)-(EN(L)-U)*(C(L)-C(L-1))/(EN(L)-EN(L-1)
     X))
   60 CONTINUE
      K=K-1
      IF(K)52,52,55
C
C     LIST THE DOWNSCATTER IN RESPONSE ONLY TO WALL EFFECTS ABOVE RLME.
C
   52 WRITE(5,7)
      DO8 J=1,MN
    8 WRITE(5,2)(RAPS(I,J),I=1,100)
C
C     EVALUATE DOWN-SCATTER RESPONSE IN THE ENERGY REGION BELOW RLME
C     WHERE LEGENDRE PARAMETRIZATION IS USED.
C
      M=MN
   80 S=APD*A(M)
      N=1
   79 V=CHEN(N,M)
      X=0.0
      I=1
   90 U=CHEN(I,M)
      IF(U-RLME)91,92,92
   91 IF(I-N)93,95,95
   93 DO97 K=1,5
      CLEG(K)=CPFT(1,K)+U*(CPFT(2,K)+U*(CPFT(3,K)+U*(CPFT(4,K)
     X +U*(CPFT(5,K)+U*CPFT(6,K)))))
      IF(K-2) 97,94,96
   94 UX=CLEG(2)
      GO TO 97
   96 ULEG(K)=CLEG(K)*UX
   97 CONTINUE
      ANG=2.0*V/U-1.0
      TEST=1.5*ANG*ANG
      RS  =CLEG(2)+CLEG(4)*(TEST-0.5)*ARG*(CLEG(3)*CLEG(5)
     X *(1.66667*(TEST-1.5))
      IF(I-N)85,85,86
   85 RAPS(N,M)=RAPS(N,M)+APD*CLEG(1)
      GO TO 93
   86 X=X+RS/U
   93 I=I+1
      GO TO 90
   92 RAPS(N,M)=RAPS(N,M)+S*X
      N=N+1
      IF(N-100)79,79,78
   78 M=M-1
      IF(M)82,82,83
C
C     LIST THE DOWN-SCATTER SPECTRUM. ALSO PUNCH RESULTS IF DESIRED.
C
   82 WRITE(5,4)
      DO71 J=1,MN
   71 WRITE(5,2) (RAPS(I,J),I=1,100)
      PAUSE
      DO75 J=1,MN
   75 WRITE(3,2) (RAPS(I,J),I=1,100)
      STOP
      END
C
C     SUBROUTINE RETURNS A 101 CHANNEL RESPONSE DISTRIBUTION FOR ANY ENERGY
C
      SUBROUTINE RESP(EZERO)
      DIMENSION CAN(6),CLAN(6),CC1(6),E(60),RGE(60),C(101),EN(101)
      COMMON EA,EB,NN,DIA,CLEN,ELIM,CAN,CLAN,CC1,E,RGE,C,EN
C
C     DE/DX DATA FOR PROTONS IN METHANE
C
      EP1(ZZ) = 132.1*(ZZ**0.40)
      GO TO 300 KEV
C     LESS THAN 30 KEV
      EP2(ZY) = 25.85805 + ZY*(555.9812 + ZY*(-6.468577E+3 + ZY*(2.67778
     X1E+4 + ZY*(-4.373533E+4 + ZY*1.756109E+4))))
C     GREATER THAN 300 KEV
      EP3(ZX) = 0.239/ZX*(10.*ALOG(ZX) + 40.0)
C
C     CONVERT ENERGY FROM KEV TO MEV
C
      EU=EZERO/1000.
C
C     DETERMINE RO
C
      DO 3 J = 2,NN
      IF(EU-E(J)) 2,1,3
    1 RO = RGE(J)
      GO TO 4
    2 RATIO = (EU-E(J-1))/(E(J)-E(J-1))
      RO = RGE(J-1) + RATIO*(RGE(J)-RGE(J-1))
      GO TO 4
    3 CONTINUE
C
C     DETERMINE EMAX
C
    4 IF(RO-CLEN) 5,5,6
    5 EMAX = EU
      GO TO 11
    6 RL = RO-CLEN
      DO 10 J = 2,NN
      IF(RL-RGE(J)) 8,7,10
    7 EL = E(J)
      GO TO 9
    8 RATIO = (RL-RGE(J-1))/(RGE(J)-RGE(J-1))
      EL = E(J-1) + RATIO*(E(J)-E(J-1))
```

```
      Y EMAX = E0-EL
        GØ TØ 11
   1Ø CØNTINUE
C
C  CALCULATE UNNØRMALIZED DISTØRTED DISTRIBUTIØN
C
   11 EN(101) = E0
      DE = E0/100.
      DØ 27 I = 1,100
      EN(I) = FLØAT(I-1)*DE + DE/2.
      IF(EN(I)-EMAX)112,112,12
   12 C(I) = 0.
      GØ TØ 27
  112 EØUT = E0-EN(I)
      IF(EØUT-E(1)) 13,16,14
   13 RØUT = EØUT/E(1)*RGE(1)
      GØ TØ 18
   14 DØ 17 J = 2,NN
      IF(EØUT-E(J)) 15,16,17
   15 RATIØ = (EØUT-E(J-1))/(E(J)-E(J-1))
      RØUT = RGE(J-1) + RATIØ*(RGE(J)-RGE(J-1))
      GØ TØ 18
   16 RØUT = RGE(J)
      GØ TØ 18
   17 CØNTINUE
   18 RIN = R0-RØUT
      IF(RIN-DIA) 19,19,20
   19 ANR = CAN(1)+RIN*(CAN(2)+RIN*(CAN(3)+RIN*(CAN(4)+RIN*(CAN(5)+RIN*
     XCAN(6) ))))
      GØ TØ 21
   20 ALNR = CLAN(1)+RIN*(CLAN(2)+RIN*(CLAN(3)+RIN*(CLAN(4)+RIN*(CLAN(5)
     X+RIN*CLAN(6) ))))
      ANR = EXP(ALNR)
   21 IF(EØUT-EA) 22,22,23
   22 DEDC = EP1(EØUT)
      GØ TØ 26
   23 IF(EØUT-EB) 24,24,25
   24 DEDC = EP2(EØUT)
      GØ TØ 26
   25 DEDC = EP3(EØUT)
   26 C(I) = ANR/DEDC
   27 CØNTINUE
C
C  NØRMALIZE THE DISTRIBUTIØN AND CØNVERT ENERGY BACK TØ KEV.
C
      IF(E0-ELIM) 29,28,28
   28 C(101) = 0.
      C1 = 1.0
      GØ TØ 30
   29 C1 = CC1(1) + E0*(CC1(2) + E0*(CC1(3) + E0*(CC1(4) + E0*(CC1(5)
     X+ E0*CC1(6) ))))
      C(101) = 1.-C1
   30 SUM = 0.
      DØ 31 I = 1,100
   31 SUM = SUM + C(I)/100.
      DØ 32 I = 1,100
      EN(I) = EN(I)*1000.
   32 C(I) = C1*C(I)/(SUM*100.)
      EN(101) = EN(101)*1000.
      RETURN
      END
```

APPENDIX F

CODES FOR DATA REDUCTION

The FORTRAN listings of the five codes used in data reduction and described in Sec. XI.B are contained in this appendix. The machine-language data-collection code has been described elsewhere [18].

The Varian-622 computer for which these codes are written has an 18-bit word length with 8k memory. Several peripherals are available. These are a paper-tape system (FORT.DEVICE02) consisting of a 300-character-per-second optical reader and a 60-character-per-second paper-tape punch, a teletype keyboard and paper printer (FORT.DEVICE00), and a storage-type oscilloscope. In many instances, a scope display of data is sufficient; where a high-quality record is needed, results are plotted on a Calcomp digital plotter with a larger computer.

```
C
C  DATA-620 PSNS-1.
C  INITIAL SURVEY OF RAW IONIZATION SPECTRA. SPECTRA CAN BE COMPARED
C  EITHER BY VOLTAGE SETS OR BY ENERGY INTERVAL. PUNCHED RESULTS
C  ARE COMPATIBLE WITH CODES FOR RESPONSE CORRECTION AND FOR
C  SLOPE TAKING.                                        1/24/1970.
C
      DIMENSION RAPS(100,8),A(8),C(8)
      COMMON RAPS,A,C
      CHEN(I,J)=A(J)*FLOAT(I+28)
C
    1 FORMAT(/37H  INPUT INITIAL SET AND LAST SET (I2) )
    2 FORMAT(I2/I2)
    3 FORMAT(/20H  ENERGY LIMITS ARE-   )
   16 FORMAT(5E12.5)
   19 FORMAT(//30H    N    KEV/CHAN     MONITOR      / )
   20 FORMAT(6E12.5)
   21 FORMAT(2F7.0)
   23 FORMAT(/16HRAW DATA SURVEY  /
     X /25H LISTED BELOW ARE MN,NMET  )
   24 FORMAT(F10.2)
   25 FORMAT(/15H MAXIMUM FLUX = / E12.5)
   29 FORMAT(/13H ENERGY RANGE )
   30 FORMAT(14,2E12.5)
C
C  READ HEADER TAPE.
C
      WRITE(0,23)
      READ (2,2) MN,NMET
      WRITE(0,2) MN,NMET
      DO701 J=1,MN
  701 READ(2,16) A(J),C(J)
      WRITE(0,19)
      WRITE(0,30) (J,A(J),C(J),J=1,MN)
      PAUSE
C
C  IF SS3 LIT, READ PRE-PUNCHED SPECTRUM DIRECTLY.
C
      IF(ISNS(3))40,40,41
   40 DO5 J=1,MN
      DO 713 I=1,100
      READ(2,21) DNUM,DOFL
  713 RAPS(I,J) = (DOFL*131071. + DNUM)/(C(J)*A(J))
      PAUSE
    5 CONTINUE
      GO TO 312
   41 DO42 J=1,MN
   42 READ(2,16)(RAPS(I,J),I=1,100)
C
C  ACCORDING TO SENSE LIGHT OPTIONS, DISPLAY PROTON SPECTRA BY
C  SETS (SS1), OR BY INPUT ENERGY RANGE (SS2) . IF NEITHER SS1 OR
C  2 ARE LIT,PUNCH THE SPECTRUM.
C
  312 PAUSE
      IF(ISNS(1))311,311,313
  311 IF(ISNS(2))201,201,202
C
C  INPUT THE SETS TO BE PLOTTED,SCALE TO MAXIMUM,DRAW AXES
C  (UNTIL SS3 IS LIT)  AND THEN PLOT.
C
  313 WRITE(0,1)
      READ(0,2)NLO,NHI
      X=0.0
      DO175 J=NLO,NHI
      DO175 I=1,100
      U=CHEN(I,J)*RAPS(I,J)
      IF(U-X)175,175,176
  176 X=U
  175 CONTINUE
      WRITE(0,25) X
      ELOW=CHEN(1,NHI)
      EUPP=CHEN(100,NLO)
      WRITE(0,3)
      WRITE(0,16)ELOW,EUPP
      CALL AXIS
      SPAN=ALOG(EUPP/ELOW)
      DO205 J=NLO,NHI
      DO205 I=1,100
      U=CHEN(I,J)
      IX=IFIX(131071.*ALOG(U/ELOW)/SPAN)
      IY=IFIX(130000.*U*RAPS(I,J)/X)
      CALL PLOT(IX,IY)
  205 CONTINUE
      GO TO 312
;
;  INPUT AN ENERGY INTERVAL, SCALE, DRAW AXES (UNTIL SS3 LIT) AND PLOT
;
  202 WRITE(0,29)
      READ(0,24)ELOW
      READ(0,24)EUPP
      X=0.0
      DO185 J=1,MN
      DO185 I=1,100
      U = CHEN(I,J)
      IF(U-ELOW)185,165,165
  165 IF(EUPP-U)185,166,166
  166 U=U*RAPS(I,J)
      IF(U-X)185,185,186
  186 X=U
  185 CONTINUE
      WRITE(0,25) X
      CALL AXIS
      SPAN = ALOG(EUPP/ELOW)
      DO209 J=1,MN
      DO209 I=1,100
      U = CHEN(I,J)
      IF(U-ELOW)209,208,208
  208 IF(EUPP-U)209,207,207
  207 IX=IFIX(131071.*ALOG(U/ELOW)/SPAN)
      IY=IFIX(130000.*U*RAPS(I,J)/X)
      CALL PLOT(IX,IY)
  209 CONTINUE
      GO TO 312
C
C  PUNCH SPECTRUM ON PAPER TAPE.
C
  201 DO177 J=1,MN
  177 WRITE(2,16)(RAPS(I,J),I=1,100)
      GO TO 312
      END
      END


C
C  DATA-620 PSNS-2.
C  RESPONSE CORRECTION TO IONIZATION SPECTRA TO ALLOW FOR THE
C  EFFECT OF FIELD DEFINITION AT COUNTER ENDS.
C  MAY ALSO NORMALIZE SPECTRA TO W.                     1/24/1970.
C
      DIMENSION RAPS(100,8),MNOLL(8),A(8),PC(6,8),AREA(8),
     XCWM(6),CWH(6)
      COMMON CWM,CWH,A,NMET,RAPS,TIME,TIHY
      CHEN(I,J)=A(J)*FLOAT(I+28)
C
   16 FORMAT(5E12.5)
   17 FORMAT(//24HTHE RESPONSE DIVIDES AT-  /F10.2)
   18 FORMAT(//31HW IS UNITY FOR ME AND HY ABOVE-  /2F10.2)
   19 FORMAT(//39HW EXPANSION COEFFICIENTS FOR ME AND HY-  /)
   20 FORMAT(6E12.5)
   21 FORMAT(F8.1)
   22 FORMAT(I2/I2)
   23 FORMAT(///10X,37HRESPONSE CORRECTION FOR FIELD EFFECTS  )
   24 FORMAT(//5X,41HPOLYNOMIAL COEFFICIENTS FOR FIELD EFFECTS  /)
   25 FORMAT(15H MAXIMUM FLUX = / E12.5)
   27 FORMAT(///24H   N  CONTAINED FRACTION /)
   28 FORMAT(//40HINTEGRAL CUT-OFF ENERGIES FOR ME AND HY-  /2F10.2)
   29 FORMAT(/21H INPUT ENERGY LIMITS   )
   30 FORMAT(I4,E12.5)
C
C  READ HEADER TAPE.
C
      WRITE(0,23)
      READ (2,22)MN,NMET
      DO 701 J=1,MN
  701 READ(2,16)A(J),X
      PAUSE
C
C  READ ELECTRIC FIELD RESPONSE DATA.
C
      READ(2,20)COME,COHY
      WRITE(0,28)COME,COHY
      WRITE(0,27)
      DO851 I=1,MN
      READ(2,20)AREA(I)
  851 WRITE(0,30)I,AREA(I)
      WRITE(0,24)
      DO31 I=1,MN
      READ (2,20)(PC(J,I),J=1,6)
   31 WRITE(0,20)(PC(J,I),J=1,6)
      DO891 I=1,MN
      DO891 J=1,6
  891 PC(J,I)=(1.0-AREA(I))*PC(J,I)
      READ(2,16) RHI
      WRITE(0,17) RHI
      PAUSE
C
C  READ THE RAW PROTON DISTRIBUTION.
C
      DO5 J=1,MN
    5 READ(2,16)(RAPS(I,J),I=1,100)
C
```

```
C  IF SS1 LIT,DISPLAY DISTRIBUTIONS ON SCOPE.
C  IF SS2 LIT, PUNCH RESULTS. NOT LIT - DO RESPONSE INTEGRATION.
C  IF BOTH SS1 AND 2 ARE LIT - READ W AND NORMALIZE.
C
  210 PAUSE
      IF(ISNS(1))204,204,208
  204 IF(ISNS(2))203,203,201
  208 IF(ISNS(2))202,202,314
C
C  READ PARAMETERS RELATING W TO IONIZATION. THEN NORMALIZE TO W.
C
  314 READ(2,20)X,X,TIME,X,X,TIHY
      READ(2,20)(CWM(J),J=1,6)
      READ(2,20)(CWH(J),J=1,6)
      WRITE(0,18)TIME,TIHY
      WRITE(0,19)
      WRITE(0,20)(CWM(J),J=1,6)
      WRITE(0,20)(CWH(J),J=1,6)
      DO316 J=1,MN
      DO316 I=1,100
  316 RAPS(I,J)=RAPS(I,J)/W(I,J)
      GO TO 210
C
C  DEFINE A MINIMUM NON-OVERLAP LIMIT, MNOLL, FOR EACH SET.
C
  203 DO 68 J=1,MN
      IF(J-1-MN)40,40,62
   40 TEST = CHEN(100,J+1)
      DO 67 K=1,100
      IF(CHEN(K,J)-TEST)67,68,68
   67 CONTINUE
   68 MNOLL(J) = K
   62 MNOLL(MN)=1
C
C  RESPONSE FUNCTION INTEGRATION
C
      DO77 I=1,MN
      IF(I-NMET)52,52,53
   52 CO=COME
      GO TO 54
   53 CO=COHY
   54 N=100
      PC1=PC(1,I)
      PC2=PC(2,I)
      PC3=PC(3,I)
      PC4=PC(4,I)
      PC5=PC(5,I)
      PC6=PC(6,I)
   90 X = 0.0
      SPWT=0.0
      RS=0.0
      V=CHEN(N,I)
      IF(V/RHI-CO)59,50,50
   59 DO 86 J=1,MN
      MNLL = MNOLL(J)
      L=99
   88 U=CHEN(L,J)
      IF(U-CO)56,57,57
   56 ARG=V/U
      SPWT = 0.5*(RAPS(L,J)+RAPS(L+1,J))/U
      S=A(J)*SPWT
      RS=PC1+ARG*(PC2+ARG*(PC3+ARG*(PC4+ARG*(PC5+ARG*(PC6)))))
      IF(ARG-RHI)94,94,95
   95 X=X+S*RS*(CHEN(L+1,J)-V/RHI)/A(J)
      GO TO 51
   94 X = X +S*RS
   57 L = L - 1
      IF(I - J)92,91,92
   92 IF(MNLL-L)88,88,81
   91 IF(N-L)88,88,51
   81 S=(U-CHEN(100,J+1))*SPWT
      X = X+S*RS
   86 CONTINUE
   51 ARG=V/CO
      RSINT=ARG*(PC1+ARG*(PC2/2.+ARG*(PC3/3.+ARG*(PC4/4.+ARG*(PC5/5.+
     XARG*PC6/6.)))))
      Q=AREA(I)+RSINT
      GO TO 89
   50 Q=1.0
   89 RAPS(N,I) = (RAPS(N,I) - X)/Q
      N = N - 1
      IF(N)77,77,90
   77 CONTINUE
      GO TO 210
C
C  SCALE TO MAXIMUM,DRAW AXES UNTIL SS3 LIT, THEN WRITE ON SCOPE.
C
  202 WRITE(0,29)
      READ(0,21)ELOW
      READ(0,21)EUPP
      X=0.0
      DO175 J=1,MN
      DO175 I=1,100
      U = CHEN(I,J)
      IF(U-ELOW)175,165,165
  165 IF(EUPP-U)175,166,166
  166 U=U*RAPS(I,J)
      IF(U-X)175,175,176
  176 X=U
  175 CONTINUE
      WRITE(0,25) X
C
      CALL AXIS
      DO205 J=1,MN
      DO205 I=1,100
      U = CHEN(I,J)
      IF(U-ELOW)205,206,206
  206 IF(EUPP-U)205,207,207
  207 IX=IFIX(13107.*ALOG(U/ELOW)/ALOG(EUPP/ELOW))
      IY=IFIX(130000.*U*RAPS(I,J)/X)
      CALL PLOT(IX,IY)
  205 CONTINUE
      GO TO 210
C
C  PUNCH THE SPECTRUM.
C
  201 DO177 J=1,MN
  177 WRITE(2,16)( RAPS(I,J),I=1,100)
      STOP
      END
      END


C
C  EVALUATE W (DE/DI) FROM THE EXPANSION IN POWERS OF LOG(I).
C
      FUNCTION W(I,J)
      DIMENSION RAPS(100,8),A(8),CWM(6),CWH(6)
      COMMON CWM,CWH,A,NMET,RAPS,TIME,TIHY
C
      X=A(J)*FLOAT(I+28)
      IF(J-NMET)1,1,8
    1 IF(X-TIME)8,7,7
    7 W=1.0
      RETURN
    8 C1=CWM(1)
      C2=CWM(2)
      C3=CWM(3)
      C4=CWM(4)
      C5=CWM(5)
      C6=CWM(6)
      GO TO 3
    2 IF(X-TIHY)5,7,7
    5 C1=CWH(1)
      C2=CWH(2)
      C3=CWH(3)
      C4=CWH(4)
      C5=CWH(5)
      C6=CWH(6)
    3 U=ALOG(X)
      W=C1+U*(C2+U*(C3+U*(C4+U*(C5+U*C6))))
      RETURN
      END
      END


C
C  DATA-620 PSNS-3.
C  WALL AND END (FINITE PROTON RANGE) CORRECTION TO PROTON SPECTRA
C  FROM METHANE COUNTERS. A CORRECTION FOR CARBON RECOILS CAN ALSO
C  BE MADE.                                          4/10/1970.
C
      DIMENSION RAPS(100,3),MNOLL(3),A(3),CEM(6),CPFT(6,5),CLEG(5),
     X COPS(100,3),EDEN(50),FLXL(50)
      COMMON RAPS,COPS,A,CEM,EDEN,FLXL,ELME,BSME,TSME,TIME
C
C  CARBON ELASTIC SCATTERING DETERMINED FROM-
      SIGC(L) = 5520./(EDEN(L)+1150.)
C
   16 FORMAT(5E12.5)
   17 FORMAT(F10.3,E11.4,E10.3,F5.3)
   20 FORMAT(6E12.5)
   21 FORMAT(F8.1)
   22 FORMAT(I2/I2)
   23 FORMAT(//26HMETHANE RESPONSE LIMIT IS-  /F9.2)
   24 FORMAT(/15H WHERE TO NEXT   )
   25 FORMAT(/15H MAXIMUM FLUX =  / E12.5)
   26 FORMAT(//10X,29HCPFT COEFFICIENTS FOR METHANE  )
   28 FORMAT(I2)
   29 FORMAT(/48H INPUT LOWER AND UPPER ENERGY PLOTTING LIMITS
   30 FORMAT(14,E12.5)
C
C  READ HEADER TAPE.
C
      READ (2,22) MN,NMET
      DO701 J=1,NMET
  701 READ(2,16)A(J),X
C
C  READ MATERIAL RELATING ENERGY TO IONIZATION.
C
      PAUSE
      READ(2,20)ELME,X,TIME,X,X,X
      READ(2,20)X,X,X,X,X,X
      READ(2,20)X,X,X,X,X,X
      READ(2,20)BSME,TSME,X,X
      READ(2,20)(CEM(J),J=1,6)
      PAUSE
C
C  INPUT FINITE RANGE RESPONSE FUNCTION. THE UPPER ENERGY CUT OFF
C  (RLME) MUST BE CHOSEN BELOW THE HIGHEST ENERGY DATUM POINT.
C
      READ(2,16)RLME
      WRITE(0,23)RLME
      NHY=MN-NMET
      MN=NMET
      WRITE(0,26)
      DO31 I=1,5
      READ (2,20)(CPFT(J,I),J=1,6)
   31 WRITE(0,20)(CPFT(J,I),J=1,6)
      PAUSE
C
C  INPUT UNCORRECTED PROTON SPECTRA AND SET COPS TO ZERO.
C
      DO4 J=1,MN
    4 READ(2,16)(RAPS(I,J),I=1,100)
      DO5 J=1,MN
      DO5 I=1,100
    5 COPS(I,J)=0.0
C
C  TELETYPE INPUT DETERMINES WHAT IS DONE.
C       0  SCOPE DISPLAY OF BOTH RAPS AND COPS.
C       1  FINITE SIZE CORRECTION MADE.
C       2  CARBON RECOIL CORRECTION.
C       3  OUTPUT COPS RESULTS ON TALLY PUNCH.
C       4  SET RAPS EQUAL TO COPS. DO THIS AFTER C RECOIL CORRECTION
C       5  READ HIGH ENERGY DOWN-SCATTER SPECTRUM. NORMALIZE AND
C          EQUATE TO COPS.
C       6  SUBTRACT COPS FROM RAPS AND SET COPS TO ZERO.
C       7  SET COPS EQUAL TO RAPS.
C
```

```
      WRITE(0,24)
     READ(0,28) IGO
     IF(IGO)289,202,230
230  IF(IGO-1)289,203,231
231  IF(IGO-2)289,350,232
232  IF(IGO-3)289,201,371
371  IF(IGO-4)289,372,390
390  IF(IGO-5)289,391,392
392  IF(IGO-6)289,393,394
394  IF(IGO-7)289,395,289

  SET COPS EQUAL TO RAPS.

395  DO396 J=1,MN
     DO396 I=1,100
396  COPS(I,J)=RAPS(I,J)
     GO TO 289

  SET RAPS EQUAL TO COPS.

372  DO370 J=1,MN
     DO370 I=1,100
370  RAPS(I,J)=COPS(I,J)
     GO TO 289

  INPUT SPECTRA REPRESENTING HIGH-LOW SCATTER AND NORMALIZE
  TO DATA ABOVE THE CUT OFF ENERGY RLME.

391  DO53 J=1,MN
 53  READ(2,16)(COPS(I,J),I=1,100)
     X=0.0
     S=0.0
     DO51 I=1,100
     U=CHEN(I,1)
     IF(U-RLME)51,52,52
 52  X=X+RAPS(I,1)
     S=S+COPS(I,1)
 51  CONTINUE
     DO54 J=1,MN
     DO54 I=1,100
 54  COPS(I,J)=COPS(I,J)*X/S
     GO TO 289

  SUBTRACT COPS FROM RAPS AND SET COPS TO ZERO.

393  DO55 J=1,MN
     DO55 I=1,100
     RAPS(I,J)=RAPS(I,J)-COPS(I,J)
 55  COPS(I,J)=0.0
     GO TO 289

  READ A NEUTRON SPECTRUM AND MAKE A CARBON RECOIL CORRECTION.

350  READ(2,30) NED,DINC
     DO351 I=1,NED
351  READ(2,17) EDEN(I),FLXL(I),X,X
     DO360 J=1,MN
     DO360 I=1,100
     COPS(I,J)=RAPS(I,J)
     U=4.4*CHEN(I,J)
     DO361 L=1,NED
     IF(EDEN(L)-U)362,362,361
361  CONTINUE
362  IF(L-1)360,360,365
365  S=((0.5*(EDEN(L-1)+EDEN(L))-U)*FLXL(L)/(EDEN(L)*EDEN(L)*DINC))
       *SIGC(L)
     L=L-1
     DO363 N=1,L
363  S=S+(FLXL(N)/EDEN(N))*SIGC(N)
     COPS(I,J) = COPS(I,J) - 1.10*DINC*S
360  CONTINUE
     GO TO 289

  DEFINE A MINIMUM NON-OVERLAP LIMIT, MNOLL, FOR EACH SET.

203  DO 68 J=1,MN
     IF(J-1-MN)40,40,62
 40  TEST = CHEN(100,J+1)
     DO 67 K=1,100
     IF(CHEN(K,J)-TEST)67,68,68
 67  CONTINUE
 68  MNOLL(J) = K
 62  MNOLL(MN)=1

  RESPONSE FUNCTION INTEGRATION ALLOWING ENERGY DEPENDENCE.

     DO380 J=1,MN
     DO380 I=1,100
380  COPS(I,J)=RAPS(I,J)
     DO77 I=1,MN
     N=100
 90  X = 0.0
     SPWT=0.0
     RSPF=0.0
     CX=0.0
     V=CHEN(N,I)
     DO 86 J=1,MN
     MNLL = MNOLL(J)
     L=99
 88  U=CHEN(L,J)
     IF(U-RLME)95,95,79
 95  DO97 K=1,5
     CLEG(K)=CPFT(1,K)+U*(CPFT(2,K)+U*(CPFT(3,K)+U*(CPFT(4,K)
    X+U*(CPFT(5,K)+U*(CPFT(6,K))))))
     IF(K-2)97,94,400
 94  CX=CLEG(2)
     GO TO 97
400  CLEG(K)=CLEG(K)*CX
 97  CONTINUE
     SPWT = 0.5*(COPS(L,J)+COPS(L+1,J))/U
     S =A(J)*SPWT
     ARG = 2.*V/U-1.0
     TEST = 1.5*ARG*ARG
     RSPF=CLEG(2) + CLEG(4)*(TEST - 0.5) + ARG*(CLEG(3) + CLEG(5)
    X *(1.66667*TEST - 1.5))
     X = X +S*RSPF
     L=L-1
     IF(I-1)80,93,80
 93  IF(N-100) 80,84,80
 84  X = 0.0
 80  IF(I - J)92,91,92
 92  IF(MNLL-L)88,88,81
 91  IF(N-L)88,88,89
 81  S=(U-CHEN(100,J+1))*SPWT
     X = X+S*RSPF
 86  CONTINUE
 89  COPS(N,I) = (COPS(N,I) - X)/CLEG(1)
     N = N - 1
     IF(N)77,77,90
 77  CONTINUE
     GO TO 289

  SCALE TO MAXIMUM, DRAW AXES AND PLOT ON SCOPE.
  BOTH RAW AND CORRECTED SPECTRA ARE PLOTTED.

202  WRITE(0,29)
     READ(0,21)ELOW
     READ(0,21)EUPP
     X=0.0
     DO175 J=1,MN
     DO175 I=1,100
     U = CHEN(I,J)
     IF(U-ELOW)175,165,165
165  IF(EUPP-U)175,166,166
166  S=U*COPS(I,J)
     U=U*RAPS(I,J)
     IF(U-X)181,181,176
176  X=U
181  IF(S-X)175,175,180
180  X=S
175  CONTINUE
     WRITE(0,25) X

  AN AXIS DRAWN ON SCOPE UNTIL SS3 IS LIT.

     CALL AXIS
     DO205 J=1,MN
     DO205 I=1,100
     U = CHEN(I,J)
     IF(U-ELOW)205,206,206
206  IF(EUPP-U)205,207,207
207  IX=IFIX(131071.*ALOG(U/ELOW)/ALOG(EUPP/ELOW))
     IY=IFIX(130000.*U*RAPS(I,J)/X)
     CALL PLOT(IX,IY)
     IY=IFIX(130000.*U*COPS(I,J)/X)
     CALL PLOT(IX,IY)
205  CONTINUE
     GO TO 289

  PUNCH SPECTRUM ON PAPER TAPE.

201  DO177 J=1,MN
177  WRITE(2,16)(COPS(I,J),I=1,100)

  IF SS2 LIT, CONTINUE METHANE TAPE BY READING IN THE UNCORRECTED
  TAPE AND PUNCHING THE HYDROGEN COMPONENT. THIS IS CONVENIENT IF
  NO FINITE RANGE CORRECTIONS ARE TO BE MADE TO HYDROGEN DATA.

     IF(ISNS(2))229,229,250
250  DO251 J=1,MN
251  READ(2,16)(RAPS(I,J),I=1,100)
     J=NMY
252  READ(2,16)(RAPS(I,1),I=1,100)
     WRITE(2,16)(RAPS(I,1),I=1,100)
     J=J-1
     IF(J)229,229,252
     END
     END



  EVALUATE THE ENERGY FOR GIVEN IONIZATION.

     FUNCTION CHEN(I,J)
     DIMENSION RAPS(100,3),COPS(100,3),A(3),CEM(6),EDEN(50),FLXL(50)
     COMMON RAPS,COPS,A,CEM,EDEN,FLXL,ELME,BSME,TSME,TIME

     X=A(J)*FLOAT(I+28)
     CUT=ELME-BSME
     IF(X-TIME)1,2,2
  2  CHEN=CUT+TSME*X-TIME
     RETURN
  1  U=ALOG(X)
     CHEN=CUT+X*(CEM(1)+U*(CEM(2)+U*(CEM(3)+U*(CEM(4)+U*(CEM(5)
    X+U*CEM(6)))))
     RETURN
     END
     END



  DATA-620 PSNS-4.
  WALL AND END (FINITE PROTON RANGE) RESPONSE CORRECTION TO
  PROTON RECOIL SPECTRA TAKEN WITH HYDROGEN. CORRECTED METHANE
  SPECTRA MAY BE INPUT IF DESIRED.                1/9/70.

     DIMENSION RAPS(100,8),MNOLL(8),A(8),CPFT(6,5),
    XCEM(6),CEN(6),CLEG(5)
     COMMON RAPS,A,CEM,CEN,NMET,ELME,BSME,TSME,TIME,
    XELMY,BSMY,TSMY,TIMY

 16  FORMAT(5E12.5)
 20  FORMAT(6E12.5)
 21  FORMAT(F8.1)
 22  FORMAT(I2/I2)
 23  FORMAT(/17HFOR HYDROGEN DATA   /)
 24  FORMAT(/27HRESPONSE LIMIT FOR HYDROGEN  /F10.2)
 25  FORMAT(/15H MAXIMUM FLUX =  / E12.5)
 26  FORMAT(//10X,30HCPFT COEFFICIENTS FOR HYDROGEN   )
 29  FORMAT(/45H INPUT LOWER AND UPPER ENERGY PLOTTING LIMITS
```

```
C
C  READ HEADER TAPE.
C
      READ (2,22) MN,NMET
      DO701 J=1,MN
  701 READ(2,16)A(J),X
      PAUSE
C
C  READ PARAMETERS RELATING ENERGY TO IONIZATION.
C
      READ(2,20)ELME,X,TIME,ELMY,X,TIMY
      READ(2,20)X,X,X,X,X,X
      READ(2,20)X,X,X,X,X,X
      READ(2,20)BSME,TSME,BSHY,TSHY
      READ(2,20)(CEM(J),J=1,6)
      READ(2,20)(CEH(J),J=1,6)
      PAUSE
C
C  READ FINITE RANGE RESPONSE FUNCTION.
C
      READ(2,16)X
      DO851 I=1,5
  851 READ(2,20)X,X,X,X,X,X
      READ(2,16)RLMY
      WRITE(0,24)RLMY
      WRITE(0,26)
      DO31 I=1,5
      READ (2,20)(CPFT(J,I),J=1,6)
   31 WRITE(0,20)(CPFT(J,I),J=1,6)
      PAUSE
C
C  READ THE UNCORRECTED PROTON SPECTRUM.
C
      DO4 J=1,MN
    4 READ(2,16)(RAPS(I,J),I=1,100)
      PAUSE
C
C  OVER-WRITE METHANE WITH CORRECTED RESULTS IF SS1 IS LIT.
C
      IF(ISNS(1))210,210,858
  858 DO5 J=1,NMET
    5 READ(2,16)(RAPS(I,J),I=1,100)
C
C  IF SS1 LIT DISPLAY DISTRIBUTIONS ON SCOPE.
C  IF SS2 LIT PUNCH RESULTS, NOT LIT-DO RESPONSE INTEGRATION.
C
  210 PAUSE
      IF(ISNS(1))204,204,202
  204 IF(ISNS(2))203,203,201
C
C  DEFINE A MINIMUM NON-OVERLAP LIMIT, MNOLL, FOR EACH SET.
C
  203 DO 68 J=1,MN
      IF(J-1-MN)40,40,62
   40 TEST = CHEN(100,J+1)
      DO 67 K=1,100
      IF(CHEN(K,J)-TEST)67,68,68
   67 CONTINUE
   68 MNOLL(J) = K
   62 MNOLL(MN)=1
C
C  RESPONSE FUNCTION INTEGRATION ALLOWING ENERGY DEPENDENCE.
C
      MM=NMET+1
      DO77 I=MM,MN
      N=100
   90 X = 0.0
      SPWT=0.0
      RSPF=0.0
      CX=0.0
      U=CHEN(N,I)
      DO 86 J=1,MN
      MNLL = MNOLL(J)
      L=99
   88 U=CHEN(L,J)
      IF(U-RLMY)95,95,79
   95 DO97 K=1,5
      CLEG(K)=CPFT(1,K)+U*(CPFT(2,K)+U*(CPFT(3,K)+U*(CPFT(4,K)
     X+U*(CPFT(5,K)+U*(CPFT(6,K))))))
      IF(K-2)97,94,400
   94 CX=CLEG(2)
      GO TO 97
  400 CLEG(K)=CLEG(K)*CX
   97 CONTINUE
      SPWT = 0.5*(RAPS(L,J)+RAPS(L+1,J))/U
      S =A(J)*SPWT
      ARG = 2.*V/U-1.0
      TEST = 1.5*ARG*ARG
      RSPF=CLEG(2) + CLEG(4)*(TEST - 0.5) + ARG*(CLEG(3) + CLEG(5)
     X *(1.66667*TEST - 1.5))
      X = X +S*RSPF
   79 L = L - 1
      IF(I-1)80,93,80
   93 IF(N-100) 80,84,80
   84 X = 0.0
   80 IF( I - J)92,91,92
   92 IF(MNLL-L)88,88,81
   91 IF(N-L)86,86,89
   81 S=(U-CHEN(100,J+1))*SPWT
      X = X+S*RSPF
   86 CONTINUE
   89 RAPS(N,I)=(RAPS(N,I)-X)/CLEG(1)
      N=N-1
      IF(N)77,77,90
   77 CONTINUE
      GO TO 210
C
C  SCALE TO MAXIMUM, DRAW AXES (UNTIL SS3 LIT) AND WRITE ON SCOPE.
C
  202 WRITE(0,29)
      READ(0,21)ELOW
      READ(0,21)EUPP
      X=0.0
      DO175 J=1,MN
      DO175 I=1,100
      U=CHEN(I,J)
      IF(U-ELOW)175,165,165
  165 IF(EUPP-U)175,166,166
  166 U=U*RAPS(I,J)
      IF(U-X)175,175,176
  176 X=U
  175 CONTINUE
      WRITE(0,25)X
C
C  DRAW AXIS.
C
      CALL AXIS
      DO205 J=1,MN
      DO205 I=1,100
      U=CHEN(I,J)
      IF(U-ELOW)205,206,206
  206 IF(EUPP-U)205,207,207
  207 IX=IFIX(131071.*ALOG(U/ELOW)/ALOG(EUPP/ELOW))
      IY=IFIX(130000.*U*RAPS(I,J)/X)
      CALL PLOT(IX,IY)
  205 CONTINUE
      GO TO 210
C
C  PUNCH SPECTRUM ON PAPER TAPE.
C
  201 DO177 J=1,MN
  177 WRITE(2,16)(RAPS(I,J),I=1,100)
      STOP
      END
      END
C
C
C  EVALUATE THE ENERGY FOR ANY VALUE OF IONIZATION.
C
      FUNCTION CHEN(I,J)
      DIMENSION RAPS(100,8),A(8),CEM(6),CEH(6)
      COMMON RAPS,A,CEM,CEH,NMET,ELME,BSME,TSME,TIME,
     XELMY,BSHY,TSHY,TIMY
C
      X=A(J)*FLOAT(I+28)
      IF(J-NMET)1,1,2
    1 CUT=ELME-BSME
      IF(X-TIME)3,3,4
    4 CHEN=CUT+TSME-TIME+X
      RETURN
    3 C1=CEM(1)
      C2=CEM(2)
      C3=CEM(3)
      C4=CEM(4)
      C5=CEM(5)
      C6=CEM(6)
      GO TO 5
    2 CUT=ELHY-BSHY
      IF(X-TIHY)6,6,7
    7 CHEN=CUT+TSHY+X-TIHY
      RETURN
    6 C1=CEH(1)
      C2=CEH(2)
      C3=CEH(3)
      C4=CEH(4)
      C5=CEH(5)
      C6=CEH(6)
    5 U=ALOG(X)
      CHEN=CUT+X*(C1+U*(C2+U*(C3+U*(C4+U*(C5+U*C6)))))
      RETURN
      END
      END


C
C  DATA-620 PSNS-5.
C  CALCULATION WHICH DERIVES THE SPECTRUM OF INCIDENT NEUTRONS
C  FROM A PROTON-RECOIL ENERGY DISTRIBUTION BY SLOPE-TAKING
C  OVER A SPECIFIED ENERGY INTERVAL.          4/10/70.
C
      DIMENSION RAPS(100),EDEN(215),FLXL(215),ERFL(215),
     XCEM(6),CEH(6),A(9),C(9)
      COMMON RAPS,EDEN,FLXL,ERFL,CEM,CEH,A,C,NMET,
     XELME,BSME,TSME,TIME,ELMY,BSHY,TSHY,TIMY
C
C  THE SLOPE-TAKING HALF INTERVAL IS COMPUTED FROM-
C      STHW(E)=SQRT(RA*RA+RB*RB/E)
C  THE INTRINSIC RESOLUTION(FWHM) IS COMPUTED FROM-
C      FWHM(FW,E)=SQRT(FW*FW+0.17/E)
C
   16 FORMAT(/12HSLOPE TAKING ///
     X59HINPUT(F10.5)RA,RB,DINC. INPUT(I2)N1 NON-ZERO FOR METH ONLY. /)
   17 FORMAT(/44HINPUT LOWER AND UPPER ENERGY PLOTTING LIMITS  )
   18 FORMAT(F10.5/F10.5/F10.5/I2)
   19 FORMAT(5E12.5)
   20 FORMAT(6E12.5)
   21 FORMAT(F8.1)
   22 FORMAT(I2/I2)
   23 FORMAT(43HINPUT FWHM FOR METHANE AND HYDROGEN(F10.5/)
     X31HAND RESPONSE LIMIT RLME(F10.2)   /)
   24 FORMAT(F10.3,E11.4,E10.3,F5.3)
   25 FORMAT(F10.5/F10.5/F10.2)
   32 FORMAT(14,E12.5)
C
C  INPUT MATERIAL RELATING TO SLOPE-TAKING INTERVAL, RESOLUTION.
C  LETHARGY INTERVAL, DINC, SHOULD NOT BE LESS THAN .04 FOR FULL SET.
C  NO REASON TO SET RA LESS THAN    FWHM/2. RB MAY BE SET TO ZERO.
C
      WRITE(0,16)
      READ(0,18)RA,RB,DINC,N1
      WRITE(0,23)
      READ(0,25) FWME,FWHY,RLME
C
C  READ HEADER TAPE.
C
      READ(2,22)MN,NMET
      DO701J=1,MN
  701 READ(2,19)A(J),C(J)
```

```
      PAUSE
C
C  READ PARAMETERS RELATING ENERGY TO IONIZATION.
C
      READ(2,20)ELME,X,TIME,ELMY,X,TIMY
      READ(2,20)X,X,X,X,X,X
      READ(2,20)X,X,X,X,X,X
      READ(2,20)BSME,TSME,BSHY,TSHY
      READ(2,20)(CEM(J),J=1,6)
      READ(2,20)(CEH(J),J=1,6)
      IF(N1)2,1,2
    2 MN=NMET
      DINC=0.1
    1 PAUSE
C
C  FORM EDIT ENERGIES HAVING FIXED LOGARITHMIC SPA
C  DO NOT USE DATA ABOVE RESPONSE LIMIT RLME.
C
      DO51 I=3,100
      X=CHEN(I,1)
      IF(RLME-X)52,52,51
   51 CONTINUE
   52 X=CHEN(I-2,1)
      EDEN(1) = X/(1.+STHW(X))
      TEST = CHEN(1,MN)
      DO 50 I=2,215
      FLXL(I)=0.0
      ERFL(I)=0.0
      EDEN(I) = EDEN(I-1)/(1.+ DINC)
      ED = EDEN(I)
      IF(ED-ED*STHW(ED)-TEST)15,15,50
   50 CONTINUE
   15 NED = I-1
      FLXL(1)=0.0
      ERFL(1)=0.0
C
C  READ EACH 100 CHANNEL PROTON SPECTRUM.
C
      DO 28 J=1,MN
      READ(2,19)(RAPS(I),I=1,100)
C
C  DEFINE RANGE OF ENERGY FOR SLOPE TAKING.
C
      CHENJ = CHEN(100,J)
      K = 1
  601 IF(CHENJ - EDEN(K))602,602,603
  602 K = K + 1
      GO TO 601
  604 K = K + 1
  603 EDIT = EDEN(K)
      X = EDIT*STHW(EDIT)
      TEST1 = EDIT + X
      TEST2 = EDIT - X
      IF(CHENJ - TEST1)604,604,605
  605 IF(CHEN(1,J) - TEST2)606,28,28
  606 ITEST = 100
  623 IF(CHEN(ITEST,J) - TEST1)670,669,669
  669 ITEST = ITEST - 1
      GO TO 623
  670 N2 = ITEST + 1
      ITEST = 1
  614 IF(CHEN(ITEST,J) - TEST2)615,615,616
  615 ITEST = ITEST + 1
      GO TO 614
  616 N1 = ITEST - 1
C
C  DETERMINE SLOPES AND ERRORS
C
      L = N1
      T1 = 0.0
      T2 = 0.0
      T3 = 0.0
      T4 = 0.0
      T5 = 0.0
  687 TCHEN = CHEN(L,J)
      T1 = T1 + TCHEN*RAPS(L)
      T2 = T2 + TCHEN
      T3 = T3 +  RAPS(L)
      T4 = T4 + TCHEN*TCHEN
      T5 = T5 + RAPS(L)*TCHEN*TCHEN
      L = L + 1
      IF(N2 - L)688,687,687
  688 T2SQ = T2*T2
      V = FLOAT(N2 - N1 + 1)
      SLOPE = (T1*V - T2*T3)/(T4*V - T2SQ)
      ERSL=SQRT ((T5*V*V+T3*T2SQ-2.*T1*T2*V)/(C(J)*A(J))
     X  /(T4*V-T2SQ)
      T1= -1.86+EDIT*(9.415E-05) +EDIT*EDIT*(1.306E-10)
      T2= 0.4283 + EDIT*(1.30E-04)
      SIGE=9.4248/(EDIT*(1.206E-03)+T1*T1)+
     X 3.1416/(EDIT*(1.206E-03)+T2*T2)
      TEMP = EDIT*EDIT/SIGE
C
C  STORE FLUXES AND ERRORS WITH REGARD TO OVERLAP.
C
      IF(ERFL(K))38,39,38
   38 X = TEMP*ERSL+TEMP*ERSL
      DEN = 1./(ERFL(K)*ERFL(K))+1./X
      FLXL(K)=(FLXL(K)/ (ERFL(K)*ERFL(K))-TEMP*SLOPE/X)/DEN
      ERFL(K) = 1./SQRT (DEN)
      GO TO 604
   39 FLXL(K) = -TEMP*SLOPE
      ERFL(K) = TEMP*ERSL
      GO TO 604
   28 CONTINUE
  245 PAUSE
C
C  SCALE TO MAXIMUM, TRACE AXES (UNTIL 553 LIT) AND PLOT ON SCOPE.
C
      IF(ISNS(1))29,29,203
  203 WRITE(0,17)
      READ(0,21) ELOW
      READ(0,21) EUPP
      X = 0.0
      DO202 I=1,NED
      IF(EDEN(I)-ELOW)202,240,240
  240 IF(EUPP-EDEN(I))202,241,241
  241 IF(X-FLXL(I))201,202,202
  201 X = FLXL(I)
  202 CONTINUE
C
      CALL AXIS
      DO205 I=1,NED
      IF(EDEN(I)-ELOW)205,247,247
  247 IF(EUPP-EDEN(I))205,206,206
  206 IX=IFIX(131071.*ALOG(EDEN(I)/ELOW)/ALOG(EUPP/ELOW))
      IY=IFIX(130000.*FLXL(I)/X)
      CALL PLOT(IX,IY)
  205 CONTINUE
      GO TO 245
C
C  DELETE EMPTY DATA LOCATIONS BEFORE PUNCHING.
C
   29 L = 1
  506 IF(ERFL(L))503,504,503
  503 L = L + 1
      IF(L - NED)506,506,505
  504 NED = NED - 1
      DO 502 K = L,NED
      ERFL(K) = ERFL(K +1)
      FLXL(K) = FLXL(K+1)
  502 EDEN(K) = EDEN(K+1)
      GO TO 29
C
C  DETERMINE OVERALL RESOLUTION (FWHM) AND PUNCH RESULTS.
C
  505 WRITE(2,32)NED,DINC
      TEST=CHEN(1,NMET)
      DO207 I=1,NED
      ED=EDEN(I)
      IF(ED-TEST)401,401,402
  402 V=FWHM(FWME,ED)
      GO TO 403
  401 V=FWHM(FWHY,ED)
  403 X=2.0*STHW(ED)/V
      IF(X-1.0)404,404,405
  404 TEMP=V
      GO TO 207
  405 TEMP=V*(1.0+0.65*(X-1.0))
  207 WRITE(2,24) ED,FLXL(I),ERFL(I),TEMP
      STOP
      END
      END


C
C  EVALUATE THE ENERGY FOR GIVEN IONIZATION.
C
      FUNCTION CHEN(I,J)
      DIMENSION RAPS(100),EDEN(215),FLXL(215),ERFL(215),
     XCEM(6),CEH(6),A(9),C(9)
      COMMON RAPS,EDEN,FLXL,ERFL,CEM,CEH,A,C,NMET,
     XELME,BSME,TSME,TIME,ELMY,BSHY,TSHY,TIMY
C
      X=A(J)*FLOAT(I*28)
      IF(J-NMET)1,1,2
    1 CUT=ELME-BSME
      IF(X-TIME)3,3,4
    4 CHEN=CUT+TSME-TIME+X
      RETURN
    3 C1=CEM(1)
      C2=CEM(2)
      C3=CEM(3)
      C4=CEM(4)
      C5=CEM(5)
      C6=CEM(6)
      GO TO 5
    2 CUT=ELMY-BSHY
      IF(X-TIMY)6,6,7
    7 CHEN=CUT+TSHY+X-TIMY
      RETURN
    6 C1=CEH(1)
      C2=CEH(2)
      C3=CEH(3)
      C4=CEH(4)
      C5=CEH(5)
      C6=CEH(6)
    5 U=ALOG(X)
      CHEN=CUT+X*(C1+U*(C2+U*(C3+U*(C4+U*(C5+U*C6)))))
      RETURN
      END
      END
```

The storage scope is reached through the subroutines AXIS and PLOT. AXIS, when called, traces a rectangular box upon the storage screen. Vertical and horizontal gain adjustments may be made until the box is centered on the scope face, at which time sense switch No. 3 will cause an exit to the main program for plotting. The subroutine PLOT outputs two integer arguments (X and Y coordinates) to the storage scope. The maximum output decoded is $2^{17} - 1$, and scaling is done to maintain the arguments within this limit. The subroutines AXIS and PLOT are described in Ref. 18.

Rather than list the input for each program separately, we have grouped the input in Tables F.I–F.VI according to the subject matter contained. The data in each table are contained on a separate piece of paper tape. Then, depending on the program, various combinations of tapes are used. The order in which the tapes are to be input is contained in the comment statements in the programs.

TABLE F.I. Data on Header Tape for PSNS Data-reduction Codes

Record	Variable	Format	Description[a]
1	MN	I2	Total number of voltage runs. Must not exceed eight.
2	NMET	I2	Number of runs with the methane counter.
3	A(J)	E12.5	Ionization per channel in keV. The input is from the lowest voltage to the highest voltage, starting with the methane values first.
	C(J)	E12.5	Product of the live time and hydrogen atom number in the effective volume.
	Record 3 is repeated for each voltage		

[a]There is a more complete description in Section XI.A.

TABLE F.II. Uncorrected Proton-recoil Data

Record	Variable	Format	Description[a]
1	DNUM DOFL	F7.0 F7.0	The number of events per channel is DOFL*131071. + DNUM.
	The information is input from low channels to high channels. The first record is repeated 100 times for each voltage. The input is from the lowest voltage to the highest voltage, starting with the methane sets first.		

[a]There is a more complete description in Section XI.A.

TABLE F.III. Data for the Electric-field Response Function

Record	Variable	Format	Description[a]
1	COME	E12.5	Cutoff value for field-response integration correction for the methane-filled counter.
	COHY	E12.5	Cutoff value for field-response integration correction for the hydrogen-filled counter.
2	AREA(I)	E12.5	Fractional weight of the contained part of the response function defined to include amplitudes in excess of RHI.
	Record 2 is repeated for each voltage from the lowest voltage to the highest voltage, starting with the methane values first.		
3	PC(J,I)	6E12.5	The coefficients of the fifth-order least-squares polynomial fit to that part of the response function below RHI.
	Record 3 is repeated for each voltage from the lowest voltage to the highest voltage starting with the methane values first.		
4	RHI	E12.5	Fraction separating the response into diagonal and off-diagonal parts. Usually set to 0.7.

[a]There is a more complete description in Section XI.B.2.

TABLE F.IV. Data Relating W and Energy to Ionization

Record	Variable	Format	Description[a]
1	ELME	E12.5	Energy lower limit in keV for methane.
	BIME	E12.5	Ionization lower limit in keV for methane.
	TIME	E12.5	Lowest ionization in keV at which W is assumed constant for methane.
	ELHY	E12.5	Energy lower limit in keV for hydrogen.
	BIHY	E12.5	Ionization lower limit in keV for hydrogen.
	TIHY	E12.5	Lowest ionization in keV at which W is assumed constant for hydrogen.
2	CWM(J)	6E12.5	Expansion coefficients relating W to ionization for methane.
3	CWH(J)	6E12.5	Expansion coefficients relating W to ionization for hydrogen.
4	BSME	E12.5	Constant used in determing energy-to-ionization relationship for methane.[b]
	TSME	E12.5	Constant used in determing energy-to-ionization relationship for hydrogen.
	BSHY	E12.5	Constant used in determing energy-to-ionization relationship for hydrogen.
	TSHY	E12.5	Constant used in determing energy-to-ionization relationship for hydrogen.
5	CEM(J)	6E12.5	Expansion coefficients relating energy to ionization for methane.
6	CEH(J)	6E12.5	Expansion coefficients relating energy to ionization for hydrogen.

[a]There is a more complete description in Section VI.B.
[b]Since the quantities BS, TS, and CE are all derived from the CW coefficients together with EL, BI, and TI, there is some redundancy of data involved. To minimize computer storage, these energy expansion terms, once derived, are included on the tape containing the CW, etc., terms for use in those codes requiring E vs I.

TABLE F.V. Data for Wall-and-End Response Function

Record	Variable	Format	Description[a]
1	RLME	E12.5	The downscatter spectrum is normalized from RLME to the last datum point. It must be within the range of the Legendre polyomial parameterization of the response function.
2-6	CPFT(J,I)	6E12.5	The coefficients of the fifth-order least-squares polynomial fit to CLEG(1) through CLEG(5) for the methane counter.
7	RLHY	E12.5	The limit energy for the use of the response function for the hydrogen counter.
8-12	CPFT(J,I)	6E12.5	The coefficients of the fifth-order least-squares polynomial fit to CLEG(1) through CLEG(5) for the hydrogen counter.

[a]There is a more complete description in Section XI.B.3.

TABLE F.VI. Data Relating to Slope-taking Interval and Resolution

Record	Variable	Format	Description[a]
1	RA	F10.5	RA and RB specify the slope-taking half-interval. It is equal to SQRT(RA*RA + RB*RB/E), where E is in keV. RA should not be set less than half the mechanical resolution of the detector.
2	RB	F10.5	RB may be set equal to zero.
3	DINC	F10.5	The lethargy spacing between energies at which the neutron spectrum is determined. Should not be less than 0.04 if eight voltage sets are used.
4	N1	I2	Greater than zero if only methane data are used. Useful for obtaining neutron spectrum for carbon-recoil correction.
5	FWME	F10.5	The mechanical resolution of the methane counter defined as full width at half maximum. It is assumed to be independent of energy.
6	FWHY	F10.5	The mechanical resolution of the hydrogen counter.
7	RLME	F10.2	The maximum energy in keV at which the neutron spectrum is to be determined.

[a]There is a more complete description in Section XI.B.5.

REFERENCES

1. A. T. G. Ferguson, "Gas-Recoil Counters," J. B. Marion and J. L. Fowler, Eds., *Fast Neutron Physics I,* Interscience Publishers, Inc., New York, p. 179 (1960).

2. E. F. Bennett, *Fast Neutron Spectroscopy by Proton-Recoil Proportional Counters,* Nucl. Sci. Eng. *27*, 16 (1967).

3. P. W. Benjamin, C. D. Kemshall, and J. Redfearn, *The Use of a Gas-Filled Spherical Proportional Counter for Neutron Spectrum Measurements in a Zero Power Fast Reactor*, AWRE NR 2/64 (1964).

4. J. L. Gammel, "The n-p Total and Differential Cross Sections in the Energy Range 0 to 40 MeV," J. B. Marion and J. L. Fowler, Eds., *Fast Neutron Physics II*, Interscience Publishers, Inc., New York, p. 2185 (1960).

5. S. C. Curran, A. L. Cockroft, and J. Angus, *Investigation of Soft Radiation by Proportional Counters-V. Use as a Detector of Ultraviolet Quanta and Analysis of the Gas Multiplication Process*, Phil. Mag. *7*, 929 (1949).

6. H. Werle, G. Fieg, H. Seufert, and D. Stegemann, *Investigation of the Specific Energy Loss of Protons in Hydrogen Above 1 keV with Regard to Neutron Spectrometry*, Nucl. Instr. Methods *72*, 111 (1969).

7. G. C. Hanna, D. H. W. Kirkwood, and D. Pontecorvo, *High Multiplication Proportional Counters for Energy Measurements*, Phys. Rev. *75*, 985 (1949).

8. T. H. R. Skyrme, P. R. Tunnicliffe, and A. G. Ward, *A Proportional Counter for Neutron Flux Measurements in the Energy Range .1 to 1 MeV*, Rev. Sci. Instr. *23*, 204 (1952).

9. R. Batchelor and G. C. Morrison, "Helium-3 Neutron Spectrometers," J. B. Marion and J. L. Fowler, Eds., *Fast Neutron Physics I*, Interscience Publishers, Inc., New York, p. 413 (1960).

10. E. F. Bennett, *Proportional Counter Proton-Recoil Spectrometer with Gamma Discrimination*, Rev. Sci. Instr. *35*, 1153 (1962).

11. R. Gold, *Energy Spectrum of Fast Cosmic Ray Neutrons near Sea Level,* Phys. Rev. *165*, 1406 (1968).

12. J. M. Larson, *A Wide-band Charge-sensitive Preamplifier for Proton-Recoil Proportional Counting*, ANL-7517 (Feb 1969).

13. J. M. Larson and J. E. Powell, *Spectrum Distortion from Amplifier Overloads in Proton-Recoil Proportional Counting,* Nucl. Instr. Methods *71*, 157 (1969).

14. D. H. Wilkinson, *Ionization Chambers and Counters*, Cambridge University Press, London and New York (1950).

15. M. G. Strauss, I. S. Sherman, R. Brenner, S. J. Rudnick, R. N. Larsen, and H. M. Mann, *High Resolution Ge(Li) Spectrometer for High Input Rates*, Rev. Sci. Instr. *38*, 725 (1967).

16. H. H. Bolotin, M. G. Strauss, and D. A. McClure, *Simple Technique for Precise Determinations of Counting Losses in Nuclear Pulse Processing Systems*, Nucl. Instr. Methods *83*, 1 (1970).

17. T. J. Yule and E. F. Bennett, "Use of a Small Computer for Proton-Recoil Proportional Counting," *Reactor Physics Division Annual Report: July 1, 1967 to June 30, 1968,* ANL-7410, pp. 358-360 (Jan 1969).

18. C. E. Cohn, E. F. Bennett, and T. J. Yule, *Hardware and Software for Nuclear Spectroscopy on the Varian Data Machines 622/i Computers*, ANL-7704 (Aug 1970).

19. E. F. Bennett and T. J. Yule, "Fast Neutron Spectra in Uranium Metal," *Reactor Physics Division Annual Report: July 1, 1968 to June 30, 1969,* ANL-7610, pp. 215-216 (Jan 1970).

20. W. Diethorn, *A Methane Proportional Counter System for Natural Radio-Carbon Measurements*, NYO-6628 (1956).

21. H. A. Bethe and J. Ashkin, "Passage of Radiations through Matter," E. Segre, Ed., *Experimental Nuclear Physics I*, John Wiley & Sons, Inc., New York, p. 166 (1953).

22. I. T. Myers, "Ionization," F. H. Attix and W. C. Roesch, Eds., *Radiation Dosimetry*, Academic Press, New York, 2nd Ed., p. 317 (1968).

23. J. W. Rogers, *An Investigation of the Energy Dependence of the Specific Average Energy Loss Per Ion Pair in Methane and Hydrogen with a Proton-Recoil Spectrometer*, Trans. Am. Nucl. Soc. *12*, 936 (1969).

24. B. B. Rossi and H. H. Staub, *Ionization Chambers and Counters*, McGraw-Hill Book Co., Inc., New York, p. 91 (1949).

25. A. Spernol and B. Denecke, *Precise Absolute Measurement of the Activity of Tritium II*, Inter. J. Appl. Rad. Isot. *15*, 195 (1963).

26. E. F. Bennett, R. Gold and I. K. Olson, *Analysis and Reduction of Proton-Recoil Data*, ANL-7394 (Jan 1968).

27. F. B. Hildebrand, *Methods of Applied Mathematics*, Prentice-Hall, Inc., Englewood Cliffs, New Jersey, Chapter 3 (1952).

28. J. B. Parker, P. H. White, and R. J. Webster, *The Interpretation of Recoil Proton Spectra*, Nucl. Instr. Methods *23*, 61 (1962).

29. V. Brandl, *Ein Monte Carlo Programm für Rückstrossprotonenzähler in Zylindergeometrie*, KFK-860, EUR-4154.d (1968).

30. N. L. Snidow and H. D. Warren, *Wall Effect Corrections in Proportional Counter Spectrometers*, Nucl. Instr. Methods *51*, 109 (1967).

31. P. W. Benjamin, C. D. Kemshall, and A. Brickstock, *The Analysis of Recoil Proton Spectra*, AWRE O 9/68 (1968).

32. H. Werle, *Spektrumsmessungen radioaktiver Neutronenquellen im Energiebereich von 10 keV bis 10 MeV mit Protonenrückstoss-Proportionalzählrohren*, Institut für Neutronenphysik und Reaktortechnik INR-4/70-25, Kernforschungszentum Karlsruhe (1970).

33. J. W. Daughtry, R. B. Pond, C. D. Swanson, and R. M. Fleischman, "ZPR-9 Assembly 26, FTR-3," *Applied Physics Divisions Annual Report: July 1, 1969 to June 30, 1970*, ANL-7710, pp. 58-63 (Jan 1971).

34. W. Whaling, "The Energy of Charged Particles in Matter," *Handbuch der Physik*, Vol. XXXIV, p. 193 (1958).

35. L. M. Milne-Thomson, "Elliptic Integrals," *Handbook of Mathematical Functions*, M. Abramowitz and I. A. Stegun, Eds., National Bureau of Standards Applied Mathematics Series 55, p. 587 (1964).

36. *Reactor Physics Constants*, Second Edition, ANL-5800, p. 11 (July 1963).